Remote Sensing of Environment 231 (2019) 111177

Contents lists available at ScienceDirect

Remote Sensing of Environment

journal homepage: www.elsevier.com/locate/rse

Remote sensing of solar-induced chlorophyll fluorescence (SIF) in vegetation: 50 years of progress

Gina H. Mohammed[a,*], Roberto Colombo[b], Elizabeth M. Middleton[c], Uwe Rascher[d], Christiaan van der Tol[e], Ladislav Nedbal[d], Yves Goulas[f], Oscar Pérez-Priego[g], Alexander Damm[h,i], Michele Meroni[j], Joanna Joiner[c], Sergio Cogliati[b], Wouter Verhoef[e], Zbyněk Malenovský[k], Jean-Philippe Gastellu-Etchegorry[l], John R. Miller[m], Luis Guanter[n], Jose Moreno[o], Ismael Moya[f], Joseph A. Berry[p], Christian Frankenberg[q], Pablo J. Zarco-Tejada[j,r,s,t]

[a] P&M Technologies, Sault Ste. Marie, Ontario, Canada
[b] Remote Sensing of Environmental Dynamics Lab, University of Milano - Bicocca, Milan, Italy
[c] NASA/Goddard Space Flight Center, Greenbelt, MD, United States
[d] Forschungszentrum Jülich, Institute of Bio- and Geosciences, IBG-2: Plant Sciences, Jülich, Germany
[e] University of Twente, Faculty of Geo-Information Science and Earth Observation, Enschede, the Netherlands
[f] CNRS, Laboratoire de Météorologie Dynamique (LMD), Ecole Polytechnique, Palaiseau, France
[g] Department of Biogeochemical Integration, Max Planck Institute for Biogeochemistry, Jena, Germany
[h] Department of Geography, University of Zurich, Zurich, Switzerland
[i] Eawag, Swiss Federal Institute of Aquatic Science and Technology, Duebendorf, Switzerland
[j] European Commission, Joint Research Centre (JRC), Ispra, VA, Italy
[k] Department of Geography and Spatial Sciences, School of Technology, Environments and Design, College of Sciences and Engineering, University of Tasmania, Hobart, Australia
[l] Centre d'Etudes Spatiales de la BIOsphère – UPS, CNES, CNRS, IRD, Université de Toulouse, Toulouse, France
[m] Department of Earth and Space Science and Engineering, York University, Toronto, Canada
[n] German Research Center for Geosciences (GFZ), Remote Sensing Section, Potsdam, Germany
[o] Department of Earth Physics and Thermodynamics, University of Valencia, Valencia, Spain
[p] Department of Global Ecology, Carnegie Institution of Washington, Stanford, CA, United States
[q] Jet Propulsion Laboratory, California Institute of Technology, Pasadena, CA, United States
[r] Instituto de Agriculture Sostenible (IAS), Consejo Superior de Investigaciones Científicas (CSIC), Córdoba, Spain
[s] Department of Infrastructure Engineering, Melbourne School of Engineering, University of Melbourne, Melbourne, Victoria, Australia
[t] School of Agriculture and Food, Faculty of Veterinary and Agricultural Sciences, University of Melbourne, Melbourne, Victoria, Australia

ARTICLE INFO

Edited by Jing M. Chen

Keywords:
Sun-induced fluorescence
Steady-state photosynthesis
Stress detection
Radiative transfer modelling
SIF retrieval methods
Satellite sensors
Airborne instruments
Applications
Terrestrial vegetation
Passive optical techniques
Review

ABSTRACT

Remote sensing of solar-induced chlorophyll fluorescence (SIF) is a rapidly advancing front in terrestrial vegetation science, with emerging capability in space-based methodologies and diverse application prospects. Although remote sensing of SIF – especially from space – is seen as a contemporary new specialty for terrestrial plants, it is founded upon a multi-decadal history of research, applications, and sensor developments in active and passive sensing of chlorophyll fluorescence. Current technical capabilities allow SIF to be measured across a range of biological, spatial, and temporal scales. As an optical signal, SIF may be assessed remotely using high-resolution spectral sensors in tandem with state-of-the-art algorithms to distinguish the emission from reflected and/or scattered ambient light. Because the red to far-red SIF emission is detectable non-invasively, it may be sampled repeatedly to acquire spatio-temporally explicit information about photosynthetic light responses and steady-state behaviour in vegetation. Progress in this field is accelerating with innovative sensor developments, retrieval methods, and modelling advances. This review distills the historical and current developments spanning the last several decades. It highlights SIF heritage and complementarity within the broader field of fluorescence science, the maturation of physiological and radiative transfer modelling, SIF signal retrieval strategies, techniques for field and airborne sensing, advances in satellite-based systems, and applications of these capabilities in evaluation of photosynthesis and stress effects. Progress, challenges, and future directions are considered for this unique avenue of remote sensing.

* Corresponding author.
E-mail address: gina.mohammed@pmtech.ca (G.H. Mohammed).

https://doi.org/10.1016/j.rse.2019.04.030
Received 27 October 2018; Received in revised form 13 February 2019; Accepted 27 April 2019

1. Introduction

The first recorded observation of solar-induced fluorescence (SIF) was made almost two centuries ago when Sir David Brewster, a Scottish preacher, discovered that a beam of sunlight striking a green alcoholic extract of laurel leaves elicited a brilliant red light (Brewster, 1834). He also noted that, as the light passed through successive 'thicknesses' of the extract, the emission changed colour from red to orange to yellow – this transition possibly being the first evidence of re-absorption by chlorophyll (Govindjee, 1995). Professor G.G. Stokes (1852) later coined the term 'fluorescence' to describe the emission. The likelihood of a link between the emission and photosynthetic assimilation was suggested by Müller (1874), and this idea was confirmed in the seminal work of Kautsky and Hirsch (1931), who revealed the kinetics of chlorophyll-*a* fluorescence (CF) emission in dark-adapted, suddenly illuminated leaves. Using only their eyes to track the initial fluorescence peak and its prompt decay to a lower steady-state level, they correlated this signature with the time course of CO_2 assimilation.

The theme of covariation between CF and photosynthesis was studied by McAlister and Myers (1940), who described two processes – one involving an inverse relation between rate of CO_2 uptake and intensity of fluorescence, the other a direct relationship. The key to this dual response was offered by Duysens and Sweers (1963), who pioneered the use of modulated excitation light – as is used in modern-day pulse-amplitude modulation (PAM) fluorimetry – and were the first to describe the active regulation of fluorescence yield by the process we now call "non-photochemical quenching" (Krause and Weis, 1991; Weis and Berry, 1987). The Duysens and Sweers (1963) approach was used to establish a quantitative relationship between fluorescence yield and the rate of electron transport (Genty et al., 1989; Weis and Berry, 1987).

These pioneers prepared the stage for analysis of CF to become an established protocol in photosynthesis research and applications in forestry, crop science, horticulture, and ecophysiology (reviews by Baker and Rosenqvist, 2004; DeEll and Toivonen, 2003; Govindjee, 2004; Krause and Weis, 1991, 1984; Lichtenthaler, 1989; Lichtenthaler and Rinderle, 1988; Mohammed et al., 1995; Papageorgiou and Govindjee, 2004; Tremblay et al., 2012). PAM fluorimetry is now used routinely to monitor photosynthetic responses. CF is informative about the light reactions of Photosystem II (PSII) especially, and is non-invasive, rapidly performed, and field-portable (Duysens, 1963; Franck and Herzfeld, 1941; Franck et al., 1941; Papageorgiou and Govindjee, 2004; Porcar-Castell et al., 2014; Schreiber, 2004; Schreiber et al., 1986). The catch is that PAM requires active manipulation of the light environment, limiting the approach to small scale (i.e., mostly single leaf) applications.

As an optical signal, CF can be remotely sensed. This generally relies on passive measurement of SIF instead of active techniques using artificial excitation light. Remote sensing of fluorescence, already well-established in aquatic science since the early 1960s (reviews by Blondeau-Patissier et al., 2014; Gower, 2016), is a more recent endeavour in terrestrial science (reviews by Frankenberg and Berry, 2018; Malenovský et al., 2009; Meroni et al., 2009; Middleton et al., 2018; Moya and Cerovic, 2004; Moya et al., 1992; Zhang et al., 2009). Passive airborne sensors for fluorescence assessment include hyperspectral imaging systems able to retrieve discrete emission bands and potentially the full SIF emission spectrum, with high spatial granularity for field applications (e.g., Damm et al., 2011; Frankenberg et al., 2018; Meroni et al., 2009; Rascher et al., 2015; Zarco-Tejada et al., 2018, 2013b).

Atmospheric satellite sensors from several missions have been used to measure far-red SIF in terrestrial vegetation. They include: the Greenhouse gases Observing SATellite (GOSAT) – Thermal And Near-infrared Sensor for carbon Observation Fourier Transform Spectrometer (TANSO-FTS); the Meteorological Operational satellite (MetOp) – Global Ozone Monitoring Experiment-2 (GOME-2) sensor; the Environmental Satellite (EnviSat) – SCanning Imaging Absorption spectroMeter for Atmospheric CHartographY (SCIAMACHY), and MEdium Resolution Imaging Spectrometer (MERIS); the Orbiting Carbon Observatory (OCO-2) (Frankenberg et al., 2014); the Sentinel-5 Precursor (S-5P) – TROPOspheric Monitoring Instrument (TROPOMI); and the Carbon Dioxide Observation Satellite (TanSat) – Atmospheric Carbon dioxide Grating Spectrometer (ACGS) (Du et al., 2018; Frankenberg et al., 2011b; Guanter et al., 2007; Joiner et al., 2012, 2011; Köhler et al., 2018a; Sun et al., 2018). Applications of this satellite data are being studied for estimation of photosynthesis and stress effects (e.g., He et al., 2017; Köhler et al., 2018b; Li et al., 2018b; MacBean et al., 2018; Middleton et al., 2018; Qiu et al., 2018; Smith et al., 2018; Verma et al., 2017). None of those satellite systems were intended originally for measuring SIF, and only recently was the first global mission approved that is designed specifically for SIF measurement of terrestrial vegetation – the FLuorescence EXplorer (FLEX) (Drusch et al., 2017).

The vision to utilize remotely-detected fluorescence for ecological purposes is not entirely new. Almost 30 years ago, Krause and Weis (1991) presciently speculated that "…extension of fluorescence measurements to large-scale spectroscopy may be useful in basic and applied environmental research, such as mapping of the photosynthetic activity of terrestrial and marine vegetation." Progress in that direction was realized when chlorophyll fluorescence was shown experimentally and analytically to be a signal superimposed upon apparent reflectance spectra in leaves and canopies (Zarco-Tejada et al., 2000a, 2000b). Later, Moya and Cerovic (2004) commented that "…it is surprising that, even after a quarter of a century of research on satellite detection of chlorophyll fluorescence, no operational system has yet even been developed" (a situation they considered true to some extent for airborne systems as well). Today, there are exceptional breakthroughs on these fronts – in SIF sensor technologies, retrieval algorithms, and the modelling of leaf and canopy fluorescence and photosynthesis (Cogliati et al., 2015b; Damm et al., 2014; Frankenberg et al., 2012; Gastellu-Etchegorry et al., 2017; Hernández-Clemente et al., 2017; Joiner et al., 2016; Pedrós et al., 2010; Van der Tol et al., 2014, 2009a, 2009b; Verhoef et al., 2018; Vilfan et al., 2016; Zarco-Tejada et al., 2013b, 2006; Zhao et al., 2016). Much has occurred in fluorescence science since Brewster recorded that first observation! Now, fluorescence may be 'viewed' at multiple and complementary scales – and even from space.

This review synthesizes developments in terrestrial SIF remote sensing over the last 50 years. It covers essential fluorescence basics, historical progress delineating fluorescence effects upon leaf and canopy reflectance spectra, advances in modelling, SIF retrieval methods, remote sensing technologies, and applications. As a synoptic overview, it complements recent reviews focused more specifically on fluorescence-photosynthesis linkages, SIF retrieval methods, applications, or instrumentation (Ač et al., 2015; Frankenberg and Berry, 2018; Garbulsky et al., 2014a, 2014b; Malenovský et al., 2009; Meroni et al., 2009; Middleton et al., 2018; Porcar-Castell et al., 2014; Zhang et al., 2009).

Our paper is dedicated to Dr. Marvin Bauer, who was pivotal for the communication of scientific advances in remote sensing of chlorophyll fluorescence during his tenure as Senior Editor of *Remote Sensing of Environment*. Dr. Bauer engaged this emerging specialty with a balance of curiosity and caution, weighing its application and relevance to the field of remote sensing. Subsequent reporting of fluorescence science in this journal (and others) over the decades attests to his willingness to debut many advances in this field.

2. Steady-state chlorophyll fluorescence and vegetation physiology

2.1. Fluorescence basics

The CF spectral emission spans approximately 650–800 nm in intact

leaves, with two maxima (under normal ambient temperatures) – one in the red spectral region around 685–690 nm (F_{685}) and the other as a shoulder in the far-red (near-infrared) around 730–740 nm (F_{740}). Two photosystems are involved: PSII, which emits in both the red and far-red regions of the spectrum, and PSI, which emits mainly in the far-red (Boardman et al., 1966; Govindjee, 1995; Murata et al., 1966; Pfündel, 1998) (Fig. 1). Emission of CF is one of the pathways by which plants dissipate excitation energy absorbed from Photosynthetically Active Radiation (PAR), the others being photochemical electron transport and two types of thermal energy dissipation – constitutive (i.e., internal conversions at the level of the chlorophyll molecule that change over extended timeframes or seasonally), and regulated (i.e., photosystem and molecular processes that respond rapidly to short-term changes in light intensity) (Hendrickson et al., 2004; Kitajima and Butler, 1975; Krause and Weis, 1991; Lichtenthaler and Rinderle, 1988; Papageorgiou and Govindjee, 2004; Porcar-Castell et al., 2014).

The dynamic nature of fluorescence emission from plants – evident under varying light intensity or, in the extreme, to sudden dark-to-light transition – is due to changing photochemical and non-photochemical quenching in the photosystem. The term 'quenching' may be used to represent all processes that reduce fluorescence emission (Krause and Weis, 1991). Photochemical quenching (PQ) indicates the availability of open PSII reaction centres for photochemistry. In dark-adapted foliage that is suddenly exposed to strong light, PQ is quickly saturated, causing fluorescence to rise to a maximum (F_{max}); concomitantly, non-photochemical processes are triggered to harmlessly dissipate absorbed excessive light energy until PQ is re-established, allowing fluorescence to decline to a 'steady-state' level after a few minutes of illumination (Bradbury and Baker, 1981; Demmig-Adams et al., 2012; Genty et al., 1990). Outdoors, steady-state fluorescence is dynamically tuned by the balance of photochemical and non-photochemical processes responding to light intensities and other environmental conditions. CF quantum yield in vivo usually is < 10%, with typical values of 0.5–3% under steady-state illumination and unimpaired electron transport (Porcar-Castell et al., 2014); CF lifetimes are also extremely short (on the order of tens to hundreds of picoseconds) (Schmuck and Moya, 1994).

Steady-state fluorescence is sometimes called terminal or stationary fluorescence (in Kautsky induction kinetics) and denoted as F_T, Ft, or F_S (Maxwell and Johnson, 2000; Van Kooten and Snel, 1990). Specific metrics quantify F_T, Ft, or F_S (Toivonen and Vidaver, 1984; Schreiber et al., 1986; Soukupová et al., 2008); PSII maximal or effective quantum yield (Genty et al., 1989); amplitude of the individual emission peaks, or their ratio (Agati et al., 1995; Campbell et al., 2007; Kuckenberg et al., 2009; Lichtenthaler and Rinderle, 1988); fluorescence lifetime (Cerovic et al., 1996); spectral wavelength position of the peaks (Kancheva et al., 2007); fluorescence band width (Subhash and Mohanan, 1997); area under the spectral emission curve (Srivastava and Pandey, 2012; Subhash, 1995); and fluorescence spatial patterns (Lichtenthaler and Rinderle, 1988).

Sensitivity of PSII reactions to abiotic and biotic stresses results in impairments of photochemical electron transport capacity, often readily echoed in changes to the fluorescence emission (Ač et al., 2015), and reflecting a complex relationship between CF and carbon assimilation (Ireland et al., 1984). Although photochemical electron transport enables CO_2 assimilation, the two processes are not always tightly coupled because electron fluxes can take alternative routes (e.g., photorespiration), especially in the presence of stress (Takahashi and Badger, 2011). Strategies for photoprotection involve multiple mechanisms in addition to thermal dissipation. These include: avoidance of light absorption via leaf or chloroplast movements; screening of

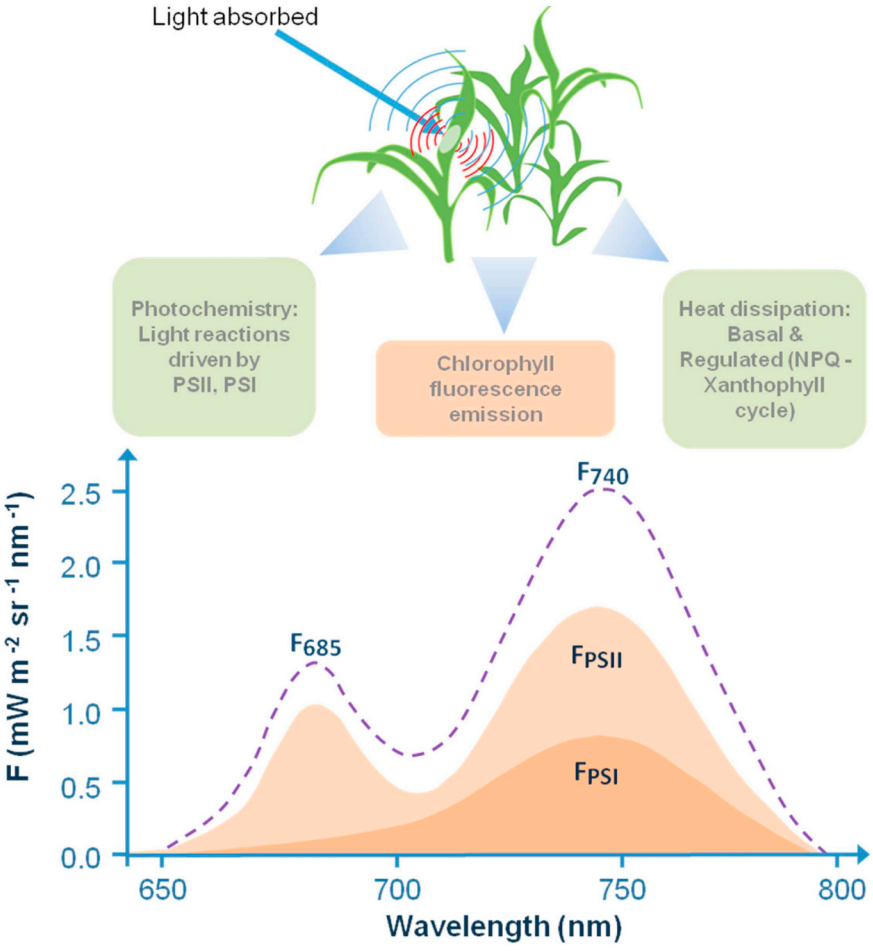

Fig. 1. Distribution of absorbed light energy in leaves under steady-state conditions. Absorbed light may be used for photochemistry, dissipated thermally, or re-emitted as chlorophyll fluorescence. Lower graph: Conceptual figure of leaf fluorescence emission, with maxima in the red and far-red spectral regions, and arising from photosystems PSII and PSI. PSII contributes to both red and far-red emissions, and PSI mainly to the far-red region. In healthy green leaves the red peak typically is lower than the far-red one, due to greater re-absorption of red fluorescence by chlorophyll during the transit of fluorescence to the leaf surface. (Plant drawing courtesy of C. van der Tol; lower graph courtesy of U. Rascher, and adapted.) (For interpretation of the references to colour in this figure legend, the reader is referred to the web version of this article.)

photoradiation; scavenging of reactive oxygen species; photorespiration; cyclic electron flow around PSI; redistribution of light energy between PSII and PSI via state transitions (migration of light harvesting complexes); and adjustments in photosystem stoichiometry (relative amounts of PSII and PSI) (Brugnoli and Björkman, 1992; Dall'Osto et al., 2014; Demmig-Adams et al., 2012; Krause and Weis, 1991; Takahashi and Badger, 2011). Although these are 'non-photochemical' in a generic sense, the more specific, regulated thermal dissipation is usually intended by the term 'non-photochemical quenching' (NPQ), which is assessed by active fluorescence sensors (albeit imperfectly as they cannot exclude all the other forms of photoprotection during measurement). The NPQ mechanism that is most ubiquitous among plants involves interconversion of the xanthophyll carotenoids violaxanthin, antheraxanthin, and zeaxanthin (Demmig-Adams, 1990; Demmig-Adams et al., 2012, 1990; Goss and Lepetit, 2015). A complementary xanthophyll mechanism is the lutein-epoxide cycle, which is more restricted taxonomically (e.g., shade-tolerant or woody species) (García-Plazaola et al., 2012; Matsubara et al., 2007).

By the time fluorescence emission reaches a remote sensor, it has been subjected to the influences of diverse drivers in the vegetation, environment, and atmosphere, which can affect quenching, light absorption, re-absorption and scattering of fluorescence signals [see also Sections 4 and 8]. Disentangling the effects and importance of the various factors in a given situation is a focus of mechanistic interpretation of fluorescence data [Section 4] and is relevant to the effective usage of fluorescence as an optical proxy for photosynthesis and associated stress effects (Ač et al., 2015; Paul-Limoges et al., 2018; Verrelst et al., 2016, 2015b).

2.2. Methodological advances in measuring steady-state fluorescence under controlled conditions

Fluorescence assessment in the laboratory, growth chamber, or greenhouse has utilized a suite of measurement devices, including fluorescence microscopes, spectroscopic or spectrofluorimetric devices, portable fluorometers, and imaging tools (Kalaji et al., 2012; Mohammed et al., 1995). These have allowed study of fluorescence induction kinetics and steady-state behaviour at scales ranging from isolated photosystems to small vegetation canopies (Table 1) (reviews by Bolhàr-Nordenkampf et al., 1989; Fernandez-Jaramillo et al., 2012; Kalaji et al., 2012; Mohammed et al., 1995). They have enabled the study of leaf ultrastructural influences on light absorption, scattering, transmission, and fluorescence re-absorption (Kalaji et al., 2012), and of non-chlorophyll fluorophores and absorbers in leaf tissues (Bornman et al., 1991; Buschmann et al., 2000; Chappelle and Williams, 1987; Kalaji et al., 2012; Vogelmann and Evans, 2002).

Imaging of CF reveals spatial and temporal heterogeneities on leaf or plant surfaces due to biotic and abiotic stress factors (Barón et al., 2016; Buschmann et al., 2009; Donaldson and Williams, 2018; Gorbe and Calatayud, 2012; Lang et al., 1996; Middleton et al., 2005; Nedbal and Whitmarsh, 2004; Nedbal et al., 2000; Oxborough, 2004; Rascher and Lüttge, 2002; Rascher et al., 2001).

Imaging techniques have been combined with other methods like gas exchange or infrared thermography to investigate the spatial distribution of photosynthetic variables, stomatal function, and water use efficiency (Chaerle et al., 2007; Lawson, 2009; Murchie and Lawson, 2013).

Laboratory spectroscopic methods have been used to examine fluorescence induction and decay kinetics, derive excitation-emission matrices (Louis et al., 2006), and discriminate PSII and PSI fluorescence (Franck et al., 2002; Palombi et al., 2011; Papageorgiou, 1975; Vácha et al., 2007). They also have supported the development of leaf and canopy fluorescence models (Pedrós et al., 2010, 2008; Van der Tol et al., 2009a, 2009b). Combinations and special configurations of devices have been used as well – such as a PAM fluorometer with a spectroradiometer to probe changes in the green spectral region related

Table 1
Laboratory technologies to measure steady-state fluorescence. Symbols: ✓ standard feature, ◉ requires specialized configuration, ◇ provides mainly qualitative information.

Technology type	Steady-state CF feature							
	Location within leaf	Amplitude (intensity)	Quenching analysis	Life-time	Red, far-red, full emission	Integrated CF over branch/plant	Effective PSII quantum yield	Heterogeneity of CF over leaf/plant
Fluorescence microscopes [1]	✓	◇	–	–	–	–	–	✓
Cryo-F-microscopes [2]	✓	✓	◉	–	◉	–	◉	–
Confocal & two-photon microscopes [3]	✓	◇	◉	–	–	–	–	–
Fiber-optic microprobes [4]	✓	✓	–	–	–	–	–	–
Imaging systems (PAM etc.) [5]	–	✓	✓	–	–	✓	✓	✓
High-resolution spectrometers (spectro-radiometers) [6]	–	✓	–	–	–	–	–	–
Spectro-fluorimeters [7]	–	✓	–	–	✓	–	–	✓
Continuous excitation fluorometers [8]	–	✓	–	–	–	–	–	–
Integrating-sphere fluorometer [9]	–	✓	–	–	–	✓	–	–
Laser-induced fluorescence (LIF) systems [10]	✓	✓	✓	–	✓	–	–	✓
τ-LIDARs [11]	–	–	–	✓	–	–	–	–
PAM systems (excluding imaging) [12]	–	✓	✓	–	–	–	✓	–
Laser-induced fluorometers measuring fluorescence transients and PSII effective antenna size [13]	–	–	–	–	–	–	✓	–

[1] Buurman et al., 1992; Kalaji et al., 2012; Murchie and Lawson, 2013. **[2]** Vácha et al., 2007. **[3]** Benediktyová and Nedbal, 2009; Osmond et al., 1999. **[4]** Bornman et al., 1991. **[5]** Aldea et al., 2006; Calatayud et al., 2006; Genty and Meyer, 1995; Gorbe and Calatayud, 2012; Nedbal et al., 2000; Oxborough, 2004. **[6]** Dobrowski et al., 2005; Julitta et al., 2016; Magney et al., 2017; Zarco-Tejada et al., 2003, 2001, 2000a, 2000b. **[7]** Boardman et al., 1966; Gitelson et al., 1998; Govindjee, 1995; Mohanty et al., 1972; Papageorgiou, 1975. **[8]** Bolhàr-Nordenkampf et al., 1989*; Mohammed et al., 1995*; Öquist and Wass, 1988; Strasser et al., 1995. **[9]** Toivonen and Vidaver, 1984. **[10]** Buschmann and Lichtenthaler, 1998; Buschmann et al., 2000; Cecchi et al., 1994; Lichtenthaler and Rinderle, 1988*; Omasa et al., 2007; Ounis et al., 2001; Rosema et al., 1991; Stober et al., 1994; Szabó et al., 1992. **[11]** Cerovic et al., 1996; Moya et al., 1995. **[12]** Magney et al., 2017; Schreiber, 2004; Schreiber et al., 1986. **[13]** Keller et al., 2019; Kolber and Falkowski, 1993; Kolber et al., 1998; Nedbal et al., 1999.

* Review.

to NPQ (Gamon et al., 1997, 1992, 1990; Wong and Gamon, 2015); a fluorescence spectrometer and an integrating sphere to quantify fluorescence re-absorption by chlorophyll (Gitelson et al., 1998); an integrating sphere with spectral detectors to study CF in whole plants or branches (Toivonen and Vidaver, 1984), or fluorescence effects on apparent reflectance (Zarco-Tejada et al., 2003, 2000a, 2000b); and passive with active sensors to follow induction kinetics (Moya et al., 2004), spectrally-resolved fluorescence emission signatures, quenching parameters, and other photosynthetic variables (Magney et al., 2017; Meroni et al., 2008; Wyber et al., 2017).

2.3. Transitioning from lab to field

Since the late 1980s, portable devices increasingly have dominated laboratory and field-based CF science. The PAM systems have been used extensively for leaf-level work (Schreiber, 2004; Schreiber et al., 1986) (e.g., from Heinz Walz GmbH, Germany; Hansatech Instruments Ltd., UK; Photon Systems Instruments, Czech Republic; Opti-Sciences, USA). Some systems also measure gas exchange, chlorophyll content, and other spectral characteristics (e.g., from PP Systems, USA; LI-COR, USA; PhotosynQ, USA). Fluorescence lifetime has been analyzed, as it is correlated with CF yield and is feasible for short-distance assessments (e.g., a few meters) (Cerovic et al., 1996; Moya and Cerovic, 2004; Moya et al., 1995; Terjung, 1998). Micro-lidars have been used in short-range work (1–10 m) (Flexas et al., 2000; Ounis et al., 2001), but delivering high intensity light pulses from great distances in order to saturate photosynthesis has been technically challenging. The LIFT method (Kolber et al., 2005) uses fast repetition of high-power laser diode or LED pulses to partially reduce the plastoquinone pool and can allow distances up to 50 m. A recent version is smaller and still allows a full suite of active fluorescence parameters and canopy reflectance in a fast scanning mode (Keller et al., 2019).

Airborne lasers for excitation of fluorescence generally require high-peak-power sources (Chekalyuk et al., 2000; Hoge and Swift, 1981; Kim, 1973) that can pose risks to eye safety. However, Ounis et al. (2016) found that eye safety is achievable with appropriate operational conditions using an airborne platform for laser-induced fluorescence (LIF), SIF, reflectance, and waveform analysis of the backscattered laser signal – thereby safely deriving a multiple set of vegetation variables to help disentangle the effects of different SIF drivers.

2.4. Lessons for remote sensing of SIF

Research into fluorescence-photosynthesis relationships, stress effects, and confounding factors has been greatly facilitated by the variety of measurement tools and the use of controlled studies. Such studies have been helpful for development and refinement of models representing fluorescence-photosynthesis linkages in different vegetation types, radiative transfer of fluorescence in leaves and small canopies, and fluorescence superimpositional effects upon reflectance [Sections 3 and 4]. Key messages have emerged from such research. First, steady-state fluorescence is influenced by a range of factors, including environmental conditions, structural traits, stress effects, and light absorption by chlorophyll (Buschmann, 2007; Cecchi et al., 1994; Chappelle and Williams, 1987; Strand and Öquist, 1988; Stober et al., 1994; Valentini et al., 1994; Vogelmann et al., 1996). Therefore, ancillary information is needed to reduce sources of error in interpretation of fluorescence changes and for parameterization of models (Mohammed et al., 2016, 2003, 1995). Second, since re-absorption reduces the visible fluorescence below that initially produced by the photosystems (e.g., Gitelson et al., 1998; Lichtenthaler and Rinderle, 1988), quantification of the re-absorption effect requires radiative transfer theory [Section 4] and understanding of leaf anatomical effects on light penetration, scattering, transmission, and re-absorption. Third, it can be advantageous to measure more than one fluorescence variable. Having both red and far-red fluorescence has been shown empirically to be advantageous for studying fluorescence-photosynthesis associations, stress effects, and influences due to vegetation type (Chappelle and Williams, 1987; Middleton et al., 1996; Valentini et al., 1994). Atherton et al. (2016) concluded that the selection of optimal fluorescence wavelengths requires further experimental work to fully characterize the spectral properties and controlling factors of the signal across relevant scales. Several steady-state fluorescence indicators have been identified from fundamental studies and are relevant for the design of future remote sensors and associated ground-based activities (Drusch et al., 2017; Fernandez-Jaramillo et al., 2012; Maxwell and Johnson, 2000; Mohammed et al., 2003, 1995; Roháček et al., 2008).

Transferability of lab-based fluorescence results to field situations, and likewise that of active to passive methods, is subject to caveats. Laboratory results might not mirror in-situ behaviour due to differences in growing environments, sampling protocols, and sensor operating conditions (Maxwell and Johnson, 2000; Stober et al., 1994). Data from active and passive techniques might not be consistently comparable (Goulas et al., 2017; Porcar-Castell et al., 2014; Rascher et al., 2009), and this continues to be investigated (Ač et al., 2015; Cecchi et al., 1994; Magney et al., 2017; Wyber et al., 2017). Artificial excitation light sources differ from sunlight in spectral composition, intensity and directionality (affecting light penetration, emission wavelength, and re-absorption) (Cerovic et al., 1999). Portable fluorometers using red excitation light can be biased toward the far-red region of the emission (to avoid overlap between excitation and emitted light) (Kalaji et al., 2014; Porcar-Castell et al., 2014), whereas blue light stimulates the full CF emission but mainly from superficial leaf layers. A helpful approach is to analyze excitation-emission matrices to reveal illumination effects (Corp et al., 2003; Louis et al., 2006; Middleton et al., 2008). Further comparative work is warranted, and assumptions must be well understood (Porcar-Castell et al., 2014).

Recognizing the above caveats, future lab-scale or controlled-environment trials can support SIF remote sensing activities in several ways: (i) creation of spectral-fluorescence-physiology databases and libraries to support calibration, modelling and interpretation of remotely sensed SIF; (ii) elucidation of confounding factors for interpretation of SIF changes; (iii) identification of ancillary data types needed for airborne or space-based missions; (iv) prototyping and refinement of remote sensor specifications and spatio-temporal sampling protocols; (v) testing of field sensors to be used in ground-truthing and validation; and (vi) determination of confidence margins and constraints for applications, based on vegetational and environmental variables.

3. Early evidence of steady-state chlorophyll fluorescence effects on leaf and canopy spectra

Before the year 2000, measurement technology was limited in its capacity to provide convincing evidence that for vegetation in natural light the very small upwelling fluorescence signal could be reliably distinguished in the presence of the dominant reflected radiance signal.

Consequently, first references on the topic were qualitative or tentative. Buschmann and Lichtenthaler (1988) inspected reflectance and fluorescence signatures using the Visible Infrared Reflectance Absorbance Fluorescence (VIRAF) spectrometer and concluded that the fluorescence emission could probably influence the red edge spectral region – in particular around 750 nm. McFarlane et al. (1980) and Carter et al. (1996, 1990) used a Fraunhofer Line Radiometer and the Fraunhofer Line Depth (FLD) measurement principle to study fluorescence in the Hα line (656 nm) and the O_2-B absorption band (687 nm), revealing changes in SIF from leaves or canopies with treatments of herbicide, water stress, or light regime. Later, other studies evaluated

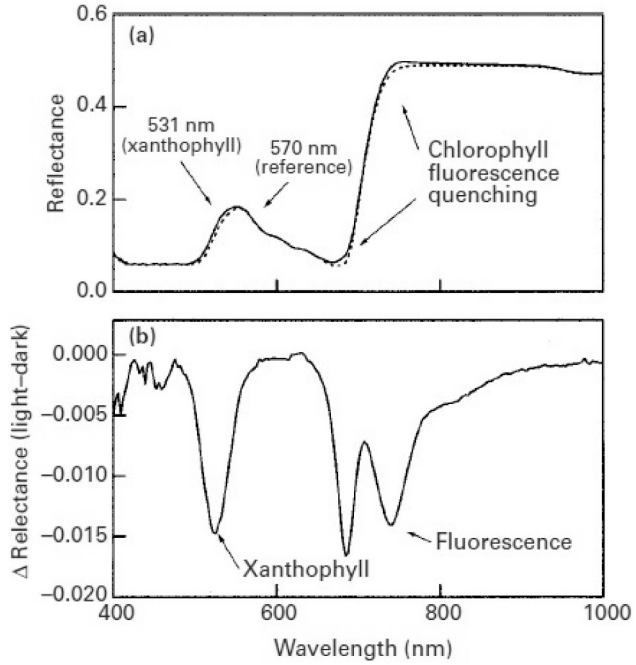

Fig. 2. Leaf reflectance spectra of *Helianthus annuus* (sunflower), (a) in the dark state (solid line) and after 10 min of exposure to light (dotted line); (b) reflectance-difference calculation (dark-state minus light-state), showing the effects due to xanthophyll pigment de-epoxidation in the green region, and chlorophyll fluorescence quenching in the red-edge region. (Source: Gamon and Surfus, 1999.)

relationships between reflectance indices and fluorescence, especially trends between the Photochemical Reflectance Index (PRI) and fluorescence-based indicators of PSII photochemical efficiency in the context of radiation-use-efficiency estimations (Gamon et al., 1997; Peñuelas et al., 1998, 1997). Using calculations of reflectance-difference spectra between dark-adapted and light-adapted leaves, Gamon and Surfus (1999) showed that xanthophyll pigment de-epoxidation and CF emission affected the reflectance signatures of vegetation after exposure to white light (Fig. 2). Nevertheless, the main focus of this work was on the PRI, and particularly its relative increment (ΔPRI) as a direct indicator of xanthophyll cycle pigment activity. As yet, no quantitative assessments were carried out to demonstrate the reliability of the fluorescence emission extracted from the leaf spectral radiance or apparent spectral reflectance.

After these first qualitative demonstrations of the potential effects of chlorophyll fluorescence superimposed on the apparent reflectance, a series of laboratory-based experiments were undertaken aimed at its quantitative assessment both at the leaf level (Zarco-Tejada et al., 2000a, 1999a) and at the canopy level using the Compact Airborne Spectrographic Imager (CASI) (Zarco-Tejada et al., 2000b, 1999b). Experiments were conducted with an integrating sphere to examine the leaf optical properties with and without a cut-off bandpass filter (< 695 nm), allowing leaves to be illuminated thereby without and with fluorescence-exciting radiation (Fig. 3, left). These experiments were also carried out with the CASI to acquire imagery over plant seedlings (Fig. 3, centre), which enabled the quantitative demonstration at the image level (i.e., canopy level) of a fluorescence signal superimposed upon the apparent reflectance. These results were further validated via the development of a leaf radiative transfer model (RTM), named the Fluorescence–Reflectance–Transmittance (FRT) model, based on the doubling method that accounted for the within-leaf fluorescence signal (Zarco-Tejada et al., 2000a) (Fig. 3, right). These leaf- and canopy-level experiments, along with the physical modelling approach, served as a quantitative demonstration that the fluorescence emission could be extracted and, more importantly, that the observed fluorescence signal effects on the apparent reflectance agreed with independently acquired fluorescence data using the PAM-2000 instrument. It was further demonstrated that the experimental protocols used to extract the fluorescence signal from the leaf reflectance spectra were consistent with basic radiative transfer theory.

Those experiments and the modelling work proved that the SIF emission was superimposed upon the apparent reflectance acquired by the *"narrow-band"* imaging spectrometers of that time (i.e., imagers with spectral resolution, SR, in the range of 2.5 to 10 nm full-width-at-half-maximum, FWHM). Further efforts attempted to quantify the fluorescence signal under natural illumination (Zarco-Tejada et al., 2002, 2001) using CASI imagery acquired over *Acer saccharum* M. (sugar maple) sites in Canada. Flights conducted over the course of diurnal experiments under natural light conditions and over forest sites with different levels of stress demonstrated that the SIF signal could be extracted by reflectance subtraction methods. Reflectance differences calculated between early and midday imagery acquired by CASI showed spectral differences that at the time were associated with the diminution of the fluorescence emission as a function of stress over the course of the diurnal cycle. Moreover, the derivative reflectance calculated from canopy-level CASI airborne imagery showed a peak at the 700–730 nm region which was experimentally shown to relate to stress conditions and potentially to be caused by fluorescence emission and chlorophyll content changes in vegetation under stress.

The derivative-based peak feature discussed in Zarco-Tejada et al. (2002), which responded as a function of forest health condition, was further investigated in a series of laboratory experiments (Dobrowski et al., 2005; Zarco-Tejada et al., 2003). The studies of this feature, observed on the derivative reflectance with heat- and light-induced stress in growth chambers, demonstrated that the diurnal dynamics of the chlorophyll fluorescence emission could be tracked at the canopy level, mimicking the dynamics of the steady-state fluorescence measured concurrently and corresponding with induced stress levels. Dobrowski et al. (2005) successfully extracted the fluorescence signal in diurnal experiments designed to induce stress, analyzing the dynamics

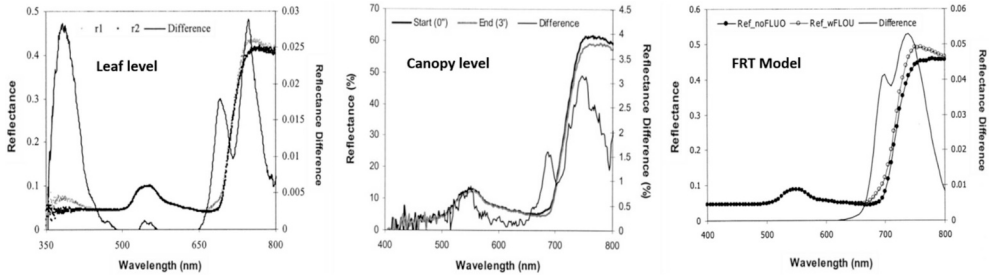

Fig. 3. Reflectance differences between a dark-adapted and light-adapted leaf of *Acer saccharum* (sugar maple) showing the spectral differences in the blue region, in the green region due to the xanthophyll pigment dynamics, and in the red edge region due to the fluorescence emission (**left**). Canopy level reflectance of dark-adapted seedlings after illumination with white light, showing the fluorescence signal extracted by spectral subtraction using the CASI imager after three minutes (**centre**). First attempts of fluorescence simulation by radiative transfer with the Fluorescence–Reflectance–Transmittance model to simulate leaf reflectance accounting for the fluorescence emission (**right**). (Source: Zarco-Tejada et al., 2000a, 2000b.

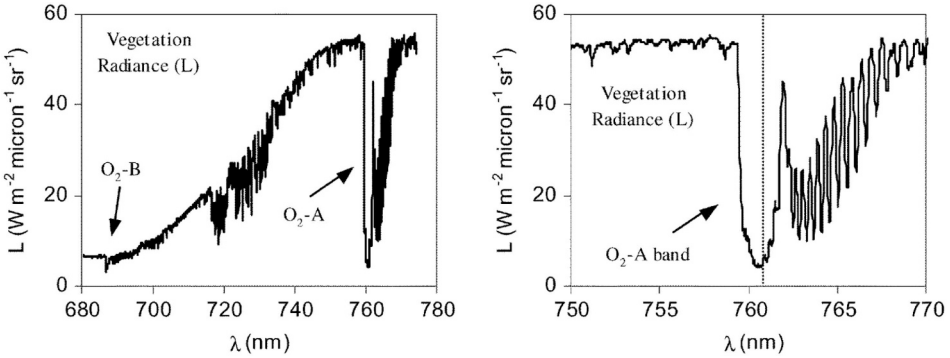

Fig. 4. Canopy radiance measured from *Olea europea* (olive) trees under water stress levels using a sub-nanometer spectrometer covering the O_2-B and O_2-A regions (left) and the detailed absorption features observed (right). (Source: Pérez-Priego et al., 2005.)

of the recovery from stress in the reflectance spectra. They proved the link between the fluorescence variables extracted from canopy reflectance and plant photosynthesis measured at the same time. Later, Campbell et al. (2008) showed the contribution of CF to the apparent reflectance of corn leaves in time-resolved laboratory measurements using a solar simulator and blocking filters (which blocked incoming light in the PAR region to prevent fluorescence excitation, similarly to what was done by Zarco-Tejada et al., 2000a). This concept was extended to leaf-based assessments under ambient field conditions using a spectroradiometer coupled with a simple leaf clip (the FluoWat) having blocking filters; this approach has enabled the separation of spectral reflectance and fluorescence across the full emission spectrum for a number of species and physiological conditions (Van Wittenberghe et al., 2014, 2013).

New experiments to extract chlorophyll fluorescence signals using the FLD principle with the oxygen absorption feature became possible with spectrometers able to provide sub-nanometer resolutions [Section 5] (Meroni and Colombo, 2006; Pérez-Priego et al., 2005). In water stress experiments conducted under natural light and field conditions, Pérez-Priego et al. (2005) demonstrated that the radiance in-filling within the O_2-A feature was related to steady-state fluorescence, an indicator of the water stress dynamics over the course of diurnal experiments. More importantly, they proved experimentally that sub-nanometer spectrometers could be used to understand the radiance variations embedded in the O_2-B and O_2-A absorption bands (Fig. 4). This approach would be used several years later, along with narrow-band spectrometers, as standard protocols for validation of fluorescence results. The FLD principle has been successfully applied to leaf radiance spectra to track changes in the photosynthetic apparatus of herbicide-treated vegetation (Meroni and Colombo, 2006), demonstrating the feasibility of the oxygen features for fluorescence quantification using high-resolution spectrometers [Section 5].

The experiments described here were critical for the understanding of the fluorescence emission effects on apparent reflectance and for convincing the scientific community of the feasibility of measuring fluorescence from passive reflectance spectra. (Although now widely accepted, doubts still existed until the late 1990s.) The initial qualitative descriptions by Buschmann and Lichtenthaler (1988) followed by Gamon and Surfus (1999) served to encourage further progress on the quantitative assessments as part of detailed experiments carried out in the laboratory and under natural light conditions, both at the leaf and at the canopy levels (Zarco-Tejada et al., 2000a, 2000b). The conclusions of these studies seeded the development of the first robust RTMs to account for the fluorescence emission at both the leaf and canopy levels, and stimulated an in-depth analysis of more advanced methodologies for the retrieval of chlorophyll fluorescence using the FLD principle – widely used currently, but poorly understood at the beginning of the millennium.

4. Modelling the effects of chlorophyll fluorescence through the canopy

4.1. Fundamentals of chlorophyll fluorescence modelling

The development of technologies and retrieval algorithms to evaluate fluorescence has progressed hand in hand with model developments. Measurement of active chlorophyll fluorescence in plant leaves, often combined with analysis of gas exchange [Section 2], has supported the development of mathematical models for leaf photosynthesis (Farquhar et al., 1980). These models have been implemented in global land surface models (LSMs) for climate research (for a review, see Pitman, 2003), which has entailed upscaling of modelled photosynthetic processes from the leaf to the stand level (or 'vegetation canopy') and differentiation between sunlit and shaded leaves (De Pury and Farquhar, 1997). Two-stream RTMs (simulating direct and diffuse fluxes) have been implemented in dynamic vegetation models such as the Boreal Ecosystems Productivity Simulator (BEPS) (Liu et al., 1997), Biome-BGC (Chen et al., 1999), and LSMs such as CLM2 (Dai et al., 2004), CLM4 (Bonan et al., 2011), and the Breathing Earth System Simulator (BESS) (Ryu et al., 2011).

Contemporary analyses of airborne and satellite fluorescence have further stimulated the development of models as scaling tools. In contrast to measurements conducted on individual leaves, SIF retrieved from Top-of-Canopy (TOC) data is subject to many drivers [Sections 2 and 8] (Fournier et al., 2012; Malenovský et al., 2009; Middleton et al., 2018; Porcar-Castell et al., 2014; Rosema et al., 1991). Quantitative modelling of such effects allows a way to integrate them and to use SIF in parameterizing terrestrial vegetation traits in LSMs (Lee et al., 2015; Norton et al., 2018).

A canopy-level model for fluorescence describes three key processes: (i) absorption of incident radiation; (ii) subsequent emission as fluorescence; and (iii) scattering and re-absorption of fluorescence throughout the canopy after emission. While plant physiological models describe the emission of fluorescence and its relation with electron transport and photochemistry in leaves (e.g., Schreiber et al., 1995), RTMs describe the effects of canopy structure on absorption and scattering (Jacquemoud et al., 2009). During the last two decades, that work has resulted in models that quantify the key processes and their

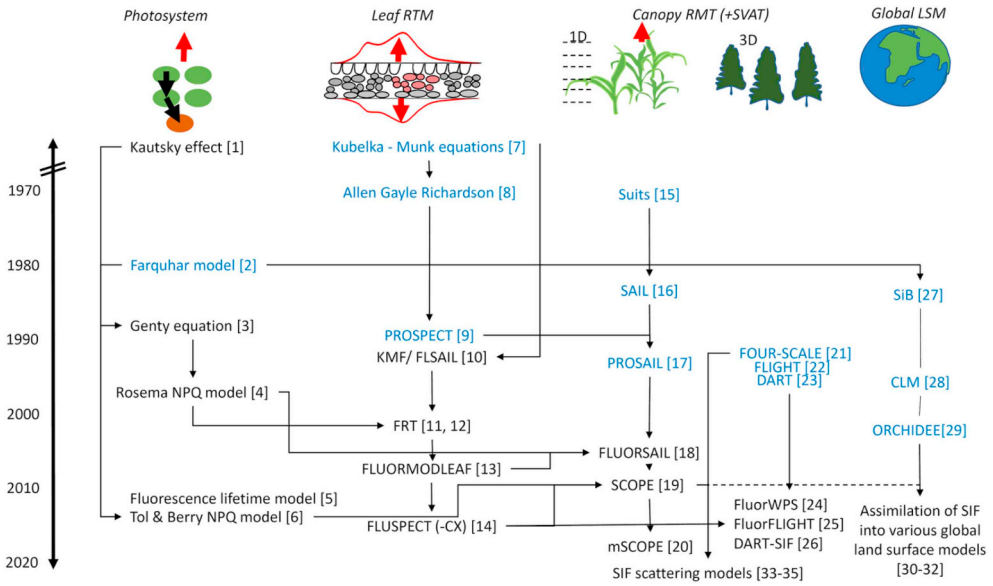

Fig. 5. History of leaf physiological and radiative transfer models of leaves and canopy for fluorescence. Relevant models that do not include fluorescence are shown in blue. **[1]** Kautsky and Hirsch, 1931. **[2]** Farquhar et al., 1980. **[3]** Genty et al., 1989. **[4]** Rosema et al., 1998. **[5]** Zaks et al., 2012. **[6]** Van der Tol et al., 2014. **[7]** Kubelka and Munk, 1931. **[8]** Allen et al., 1970. **[9]** Jacquemoud and Baret, 1990. **[10]** Rosema et al., 1991. **[11]** Zarco-Tejada et al., 2000a. **[12]** Zarco-Tejada et al., 2000b. **[13]** Pedrós et al., 2010. **[14]** Vilfan et al., 2016. **[15]** Suits, 1972. **[16]** Verhoef, 1984. **[17]** Jacquemoud, 1993. **[18]** Miller et al., 2005. **[19]** Van der Tol et al., 2009b. **[20]** Yang et al., 2017. **[21]** Chen and Leblanc, 1997. **[22]** North, 1996. **[23]** Gastellu-Etchegorry et al., 1996. **[24]** Zhao et al., 2016. **[25]** Hernández-Clemente et al., 2017. **[26]** Gastellu-Etchegorry et al., 2017. **[27]** Sellers et al., 1996. **[28]** Bonan, 1996. **[29]** Krinner et al., 2005. **[30]** Lee et al., 2015. **[31]** MacBean et al., 2018. **[32]** Norton et al., 2018. **[33]** He et al., 2017. **[34]** Yang and Van der Tol, 2018. **[35]** Liu et al., 2018. (For interpretation of the references to colour in this figure legend, the reader is referred to the web version of this article.)

interdependencies (Fig. 5).

4.2. Leaf physiological models of steady-state fluorescence

Leaf physiological models have aimed to quantify the partitioning of absorbed radiation to the pathways of PQ and NPQ [Section 2]. Andries Rosema and co-workers developed the Laser Environmental Active Fluorosensor (LEAF-NL), which they used to acquire active and passive fluorescence and to develop a quantitative model for steady-state fluorescence that describes NPQ as a function of irradiance with two empirical parameters (Rosema et al., 1998). Their measurements on poplar seedlings and their modelling showed that NPQ causes a positive relationship between fluorescence emission and photochemistry efficiency at high light intensities. The values of the fitting parameters in Rosema's model appeared to depend not only on irradiance, but also on the temperature and water stress status of the plants. This was consistent with studies using PAM fluorescence showing positive correlation of steady-state fluorescence with actual photosynthesis rate, as assessed via gas exchange (Flexas et al., 2002), and with the presence of feedback mechanisms between actual photosynthesis and NPQ (Bilger and Björkman, 1990). Van der Tol et al. (2009a) modelled this feedback by introducing the fluorescence emission, the pH-gradient across the thylakoid membrane, and NPQ, into the photosynthesis model of Farquhar et al. (1980). Later Lee et al. (2013) and Van der Tol et al. (2014), on the initiative of Joe Berry, parameterized a simpler model for this feedback, using a calibrated non-linear relationship between NPQ and the relative light saturation of photosynthesis (i.e., the ratio of actual to theoretical maximum electron transport).

These simple models can easily be implemented in canopy-level or global-scale models, but they still rely on empirical coefficients and lack a mechanistic process description of the feedback mechanism. Zaks et al. (2012), Bennett et al. (2018), and Morris and Fleming (2018) developed a dynamic (time-resolved) model that simulates the pools of excited chlorophyll and the concentrations of the quenchers, zeaxanthin and antheraxanthin, using the rate coefficients of the involved processes in a more mechanistic way. Such mechanistic representations could be used in remote sensing models for satellite fluorescence as well.

All of the models for fluorescence, photochemistry and NPQ quantify the initial emission of fluorescence after incident photons have been captured by photosystems. They do not answer the questions of 'how much light is absorbed by the photosystems in the first place?', nor 'what happens to the fluorescence after emission by the photosystems?'. These questions have been addressed with RTMs, for both individual leaves and vegetation canopies.

4.3. Leaf radiative transfer models for fluorescence

The absorption of incident light and the (re-)absorption of emitted fluorescence inside leaves has been described in detail by Gitelson et al. (1999, 1998) and Buschmann (2007). A part of the incident light is reflected by the leaf surface, while the remaining light penetrates into the leaf, where it may be absorbed by different pigments, including chlorophyll, or scattered. When fluorescence is produced, a certain part is (re-)absorbed by pigments on its way out of the leaf, owing to the overlap of the fluorescence emission spectrum (~650–800 nm) with the absorption spectrum of chlorophyll (~400–720 nm). Absorption by chlorophyll is strong in the red region, thus red fluorescence quickly saturates and then decreases with increase in leaf chlorophyll content. As the leaf is far less absorbent in the far-red region, the saturation of fluorescence is much lower there. Gitelson et al. (1999) showed that for this reason, the fluorescence peak ratio, i.e., the ratio of far-red to red fluorescence is correlated with chlorophyll content. Due to re-absorption, only a little red fluorescence (~690 nm) escapes from the shaded (usually abaxial) side of the leaf compared to the illuminated (usually adaxial) leaf side, resulting in different spectral shapes (Louis et al., 2006; Van Wittenberghe et al., 2013).

For modelling of fluorescence, it was necessary to describe these processes mathematically. Several leaf RTMs (without fluorescence) emerged in the 1960s. Most prominent was one by Allen et al. (1970, 1969), using the analogy of a pile of glass plates. An improved successor is the widely used PROSPECT (from the French PROpriétés SPECTrales) model, created by Jacquemoud and Baret (1990), which relaxed the number of plates to be a non-integer to gain more control over the variability of mesophyll scattering properties of the modelled leaves.

To support the interpretation of fluorescence data from Rosema's work in the early 1990s, an early attempt was made to incorporate fluorescence in RTMs for single leaves as well as vegetation canopies, resulting in the FLSAIL model (Rosema et al., 1991) – also called KMF ('Kubelka-Munk Fluorescence'), since it included fluorescence by using the two-stream approach of Kubelka and Munk (1931). This model solved the radiative transfer equations numerically using an efficient

layer doubling algorithm, a variant of the adding algorithm of Van de Hulst (1957, cited in Van de Hulst, 1981). The doubling algorithm, which scales from an extremely thin layer to an optically thick layer by repeated stacking of identical layers, was used also in the FRT leaf RTM to provide theoretical support for fluorescence contribution to apparent reflectance (Zarco-Tejada et al., 2000a, 2000b; see also Section 3). Subsequent leaf fluorescence models were FluorMODleaf (Pedrós et al., 2010), based on PROSPECT; and Fluspect (Vilfan et al., 2016), which uses the doubling algorithm for fluorescence calculation, but the rest of its algorithm is based on PROSPECT.

4.4. Canopy radiative transfer models for fluorescence

To study vegetation canopy fluorescence in relation with in-situ (i.e., Bottom Of Atmosphere, BOA), airborne, and satellite (i.e., Top Of Atmosphere, TOA) observations, a canopy fluorescence model should simulate two types of products: (i) canopy spectral radiative budget, including fluorescence emission; and (ii) fluorescence signal measured at any altitude. Calculation of the three-dimensional (3D) radiative budget can be very demanding in terms of computer time and memory, especially for reverse ray tracing Monte Carlo models (Disney et al., 2000) that trace sample photon paths from the sensor to the illumination sources. A common solution is to couple a canopy model and an atmospheric RTM [e.g., the MODerate resolution atmospheric TRANsmission, MODTRAN) (Berk et al., 2014), or 6-S (Kotchenova et al., 2008)]. However, this solution cannot accurately simulate the complex neighboring effects due to the 3D Earth-Atmosphere radiative coupling.

Canopy fluorescence modelling relies on embedding a leaf fluorescence model into a canopy reflectance model (Disney, 2016). One-dimensional (1D) models, simulating the vegetation canopy as homogeneous layers (e.g., the canopy FLSAIL model, Rosema et al., 1991), appeared first. FLSAIL and its successors FluorSAIL (Miller et al., 2005) and the Soil-Canopy-Observation of Photosynthesis and Energy fluxes (SCOPE) (Van der Tol et al., 2009b) models are all based on the 'Scattering of Arbitrarily Inclined Leaves' (SAIL) model (Verhoef, 1985, 1984), which, in turn is based on the models of Allen et al. (1970) and Suits (1972). SAIL treats the vegetation as identical leaves with stochastically described orientation that scatter the four streams of incident solar light, the diffuse upward and downward fluxes and the radiance in the observation direction. The 1D models do not simulate the effects of spatial and structural heterogeneity of vegetation in the horizontal plane (e.g., crown shadows or row culture effects), nor do they capture vertical variability of leaf types, leaf orientation angles or leaf pigment concentrations, as might be present in a real forest stand with an understory and overstory. Although approaches exist to handle clumping in RTMs (Ni-Meister et al., 2010), the effect of clumping on SIF has received little attention. Modifications to the four-stream radiative transfer concept have been made to overcome these limitations. For example, the FluorFLIM model (Zarco-Tejada et al., 2013a), based on FluorSAIL and FLIM (Rosema et al., 1992), simulates vegetation clumping (crowns), while mSCOPE (Yang et al., 2017) simulates fluorescence emanating from vertically heterogeneous canopies. He et al. (2017) derived a relatively simple correction for the solar-viewing geometry, in which the observed signal of SIF is decomposed into contributions from sunlit and shaded fractions of the canopy. Since it is based on radiative transfer for discrete objects with internal structures ('4-scale'), such as forest stands (Chen and Leblanc, 1997), it also simulates a clumped vegetation. Recent models that derive the scattering of SIF directly from reflectance take effects of clumping on SIF implicitly into account via the reflectance (Liu et al., 2018; Yang and Van der Tol, 2018).

3D photon and flux tracing RTMs can work with realistic descriptions of actual vegetation canopies, either by representing all plant parts as facets or by discretizing canopies into 3D pixels called voxels, i.e., small spatially distinct volumes filled with a turbid medium of leaves, possibly with different optical properties. Several 3D models have been extended to include simulation of passive fluorescence, notably FluorFLIGHT for forest canopies (Hernández-Clemente et al., 2017), the Fluorescence model with Weight Photon Spread (FluorWPS) for row crops (Zhao et al., 2016), and the Discrete Anisotropic Radiative Transfer (DART) model for any 3D explicit vegetation architecture (Gastellu-Etchegorry et al., 2017). All three models simulate leaf-emitted fluorescence with Fluspect, after which within-canopy radiation propagation is tracked with ray or flux tracing algorithms. Their spatially detailed simulations can potentially provide a deep insight into interactions of fluorescence fluxes within structurally complex canopies.

The DART model (Gastellu-Etchegorry et al., 2017, 2015, 1996) was designed to simulate both the 3D radiative budget and remote sensing observations of any urban and natural landscape with a 3D topography. The 3D SIF emission is simulated using Fluspect. The vegetation may be considered as facets or turbid voxels, and foliage can be divided into sunlit and shaded by simulating instantaneous leaf irradiance, and into sun- and shade-adapted classes by simulating time series of scene diurnal radiative budgets.

3D models like DART do not include an energy balance and do not work with the environmental parameters (e.g., air temperature) driving apparent leaf fluorescence. At this time, SCOPE is the only canopy model that includes the energy balance at the leaf level. DART can, however, import values pre-computed in SCOPE to include in its computation of the SIF emission modulation by photosystems and quenching mechanisms. DART chlorophyll fluorescence products, namely BOA and TOA canopy SIF radiance and reflectance images and the 3D leaf radiative budget (i.e., PSI and PSII fluorescence exitance and sun-scattered exitance per triangular facet), allow computation of advanced outputs, such as the canopy fluorescence escape factor (Guanter et al., 2014). An advantage of the ray or flux tracing models is the possibility to not only quantify but also visualize processes leading to modelled canopy fluorescence.

Fig. 6 shows an example of a 3D DART-simulated BOA chlorophyll

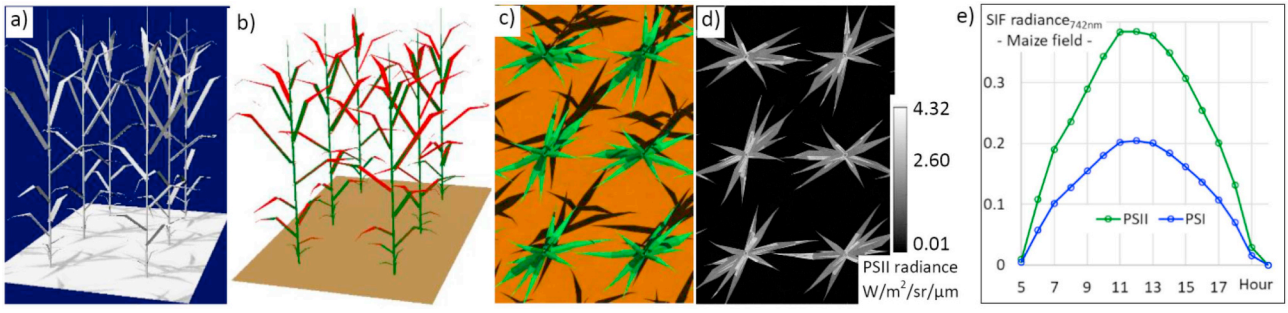

Fig. 6. Simulation of BOA fluorescence in maize by DART: (a) Intensity of solar irradiance for a maize field in an early growth stage (39°N, 76.8°E; June 21, 2015; 13 h local time); (b) 3D representation of sun- (red) and shade-adapted (blue) leaves; (c) DART true colour composite of the nadir reflectance image; (d) DART simulated PSII fluorescence radiance image; and (e) hourly evolution of the maize canopy BOA PSI and PSII fluorescence radiance at the wavelength of 742.5 nm for clear sky conditions (atmosphere characterized using models based on MODTRAN gas and aerosol databases, see Berk et al., 2014). (For interpretation of the references to colour in this figure legend, the reader is referred to the web version of this article.)

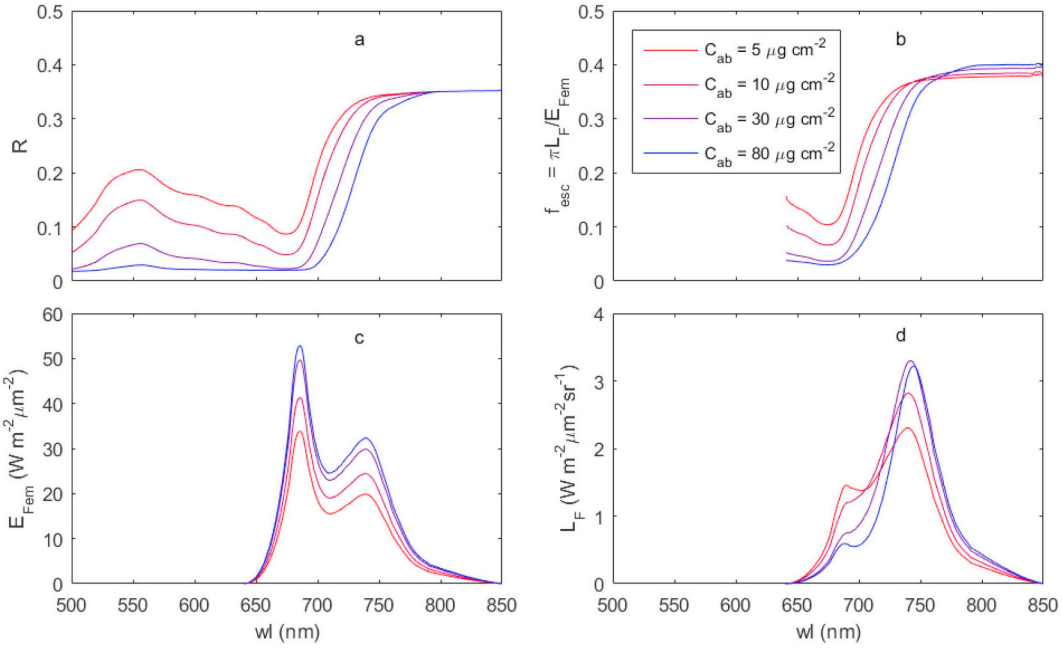

Fig. 7. SCOPE model simulation of (a) reflectance R, (b) fluorescence escape probability f_{esc}, (c) fluorescence irradiance emitted by all photosystems E_{Fem}, and (d) fluorescence radiance in nadir direction L_F – for four values of leaf chlorophyll content and a leaf area index of 3. Note the changes in fluorescence spectral shape as chlorophyll(a + b) mass per unit leaf surface (C_{ab}) increases, and the similarity between the fluorescence escape probability and the reflectance. (For interpretation of the references to colour in this figure legend, the reader is referred to the web version of this article.)

fluorescence for a maize field at an early growth stage. Simulation of diurnal radiative budgets of solar irradiation (Fig. 6a) allowed for classification of the stand into sun- and shade-adapted parts (Fig. 6b), further used to simulate canopy reflectance (Fig. 6c) and fluorescence images (Figs. 6d & e). Although producing more accurate results, the use of triangular facets is computationally more demanding than the use of turbid voxels representing a large set of foliar elements.

4.5. Integrated canopy fluorescence and photosynthesis models

Interpreting canopy SIF in terms of photosynthesis and stress requires modelling of both the radiative fluxes and the non-radiative energy fluxes. Non-radiative fluxes are not commonly taken into account in remote sensing observation models, but they are an important component of LSMs (Anderson, 1963; Kalma et al., 2008). Non-radiative fluxes include the energy used in metabolism (photosynthesis and respiration), the turbulent exchange of latent and sensible heat flux, and the conduction of heat into biomass and soil. These fluxes eventually determine leaf temperature and the humidity in vegetation canopies, both of which are crucial variables for stomatal aperture (Ball et al., 1987; Leuning, 1995), photosynthesis (Collatz et al., 1991) and fluorescence quenching (Bilger and Björkman, 1990). For a complete modelling of fluorescence, it was therefore considered necessary to include these processes in canopy fluorescence models.

Integration of radiative with non-radiative energy fluxes and photosynthesis has been studied since the 1960s (De Wit, 1965; Goudriaan, 1977). Norman (1979) presented Cupid, a comprehensive model for the soil-plant-atmosphere continuum that also simulates visible, near infrared and thermal radiation. The model SCOPE (Van der Tol et al., 2009b) builds on the heritage of these energy budget models on the one hand, and the radiative transfer of the FluorMOD model (Miller et al., 2005) on the other hand.

4.6. Lessons learned using these models

As Porcar-Castell et al. (2014) pointed out, scaling from leaf to canopy is not just a matter of applying existing models to a larger area. Rather, it requires description of all SIF-relevant processes: absorption, emission, scattering, and re-absorption. With the present knowledge, we are able to describe these processes with models and quantify the effects of leaf chlorophyll (Fig. 7) and other vegetation properties on reflectance, SIF and GPP. The challenges of scaling from leaf to canopy therefore also present opportunities to improve understanding of photosynthesis at the canopy scale.

Various papers have reported a close correlation between far-red SIF and GPP (Cui et al., 2017a; Frankenberg et al., 2011b; Goulas et al., 2017; Guanter et al., 2012; Joiner et al., 2011; Rossini et al., 2010; Verma et al., 2017; Wagle et al., 2016; Yang et al., 2015). It is now clear this correlation is mostly due to the fact that both SIF and GPP rely on the incident radiation and the absorption of light by chlorophyll in the whole canopy leaf area (Goulas et al., 2017; Joiner et al., 2014; Yang et al., 2018b, 2015). The dominance of total chlorophyll absorption is confirmed by sensitivity analyses of the SCOPE model (Koffi et al., 2015; Verrelst et al., 2015b).

Furthermore, Migliavacca et al. (2017b) in their study of grassland vegetation were able to differentiate effects of canopy structure on scattering from photosynthetic effects on fluorescence emission. They showed that the relative abundance of species affects canopy structure and the scattering of fluorescence, and that these changes in canopy structure dominate the variations in observed SIF among the vegetation communities studied. This confirms model sensitivity analyses demonstrating that leaf area index and leaf inclination have a significant effect on SIF (Verrelst et al., 2015b), and also that scattering and re-absorption can cause substantial differences in SIF among various vegetation communities. Romero et al. (2018) developed a quantitative model for re-absorption in the canopy and confirmed with canopy-level fluorescence measurements the change in spectral shape (the relative reduction of red fluorescence) when scaling from the leaf to the canopy, as found earlier with SCOPE.

Because scattering depends on the geometry of illumination and observation directions, quantification of fluorescence scattering in the canopy is needed for meaningful comparisons between fluorescence observations taken under different solar and observation angles. One route is to invert quantitative RTMs and retrieve from reflectance the

parameters necessary to quantify the scattering (Van der Tol et al., 2016). Köhler et al. (2018b) analyzed the directional scattering of fluorescence in the canopy, and showed that the seasonality in SIF observed by GOME-2 is affected by the angular anisotropy of the canopy fluorescence and that correction for this effect is needed. Subsequently, Liu et al. (2018) used SCOPE and DART SIF simulations of vegetation canopies combined with the spectral invariant theory, in the random forest machine-learning algorithm to devise a new means for scaling a canopy SIF signal down to the level of single photosystems. Downscaling of SIF by correcting for scattering and re-absorption appeared to be an efficient way to obtain a solar-view geometry-independent measure, and a measure for the fluorescence emission at leaf level before re-absorption. Yang and Van der Tol (2018) analytically compared the radiative transfer of incident radiation to that of scattered fluorescence radiation and showed that far-red fluorescence scattering in a 1D canopy is proportional to far-red reflectance normalized by the leaf albedo and canopy interceptance. With this simple equation, far-red SIF can be corrected for illumination and observation geometry and for re-absorption within the canopy at the same time, using reflectance along with SIF.

4.7. Challenges and future directions in modelling

Challenges and opportunities still lie ahead for modellers in the fields of remote sensing of fluorescence and plant physiology. An issue with current models of passive fluorescence is the empirical parameterization of NPQ and the lack of quantitative mechanistic parameterizations for NPQ as a function of measurable quantities. A possible approach is to use reflectance in the region of 500–600 nm, as leaf optical properties in this spectral region are affected by a number of pigments, including those involved in photoprotection and non-photochemical heat dissipation (e.g., zeaxanthin). Spectral changes in this region are the basis of the PRI (Gamon et al., 1997). The leaf RTM, Fluspect, was refined recently to more precisely simulate the reflectance and transmittance between 500 and 600 nm, by including spectral changes associated with NPQ (Vilfan et al., 2018). Including these effects in other RTMs and SCOPE could help to retrieve a measure of NPQ and constrain the modelled fluorescence–photosynthesis relationship. Spectrally contiguous reflectance of the far-red (red edge) shoulder (700–800 nm) is also being investigated for spectral absorbance features related to the pigment-pigment excitation interactions and xanthophyll conversion, as possible indication of NPQ manifestation (S. van Wittenberghe, personal communication).

Laboratory and field experiments continue to provide new insights [Section 2.4], based on joint acquisition of active and passive SIF and gas exchange information to examine fluorescence-photosynthesis linkages, stress effects, and diurnal and seasonal relationships between SIF and other photosynthetic parameters (Magney et al., 2017; Wyber et al., 2017). These data may be combined with those of e.g. fluorescence lifetime (Sylak-Glassman et al., 2016) to better understand PSI and PSII fluorescence dynamics and interdependence, and possibly lead to methods for differentiating fluorescence from the two photosystems using retrieved SIF spectra corrected for re-absorption. High-spatial-resolution fluorescence imagery is another promising tool, as shown by Pinto et al. (2016), who set a hyperspectral camera above a vegetation canopy to retrieve fluorescence images and to differentiate contributions from individual leaves with different insolation and orientation; this is an excellent data source for model validation.

Advances in computational power facilitate application of 3D ray and flux tracing models to explore canopy structural effects (e.g., for row crops or savannah-type vegetation) on fluorescence, with realistic vegetation parameterizations obtained from LiDAR or orthophoto data (Fawcett et al., 2018). Also the influence of landscape spatial heterogeneity – originating from topographical gradients and landcover variability – on large-scale space-based SIF observations is anticipated in upcoming versions of 3D RTMs. Significant progress in the use of machine learning, neural networks and emulation of models (Rivera et al., 2015; Verrelst and Rivera, 2017), and the development of end-to-end simulators for satellite missions (Vicent et al., 2016), will bring the operational use of more complex RTMs at large spatial scales within

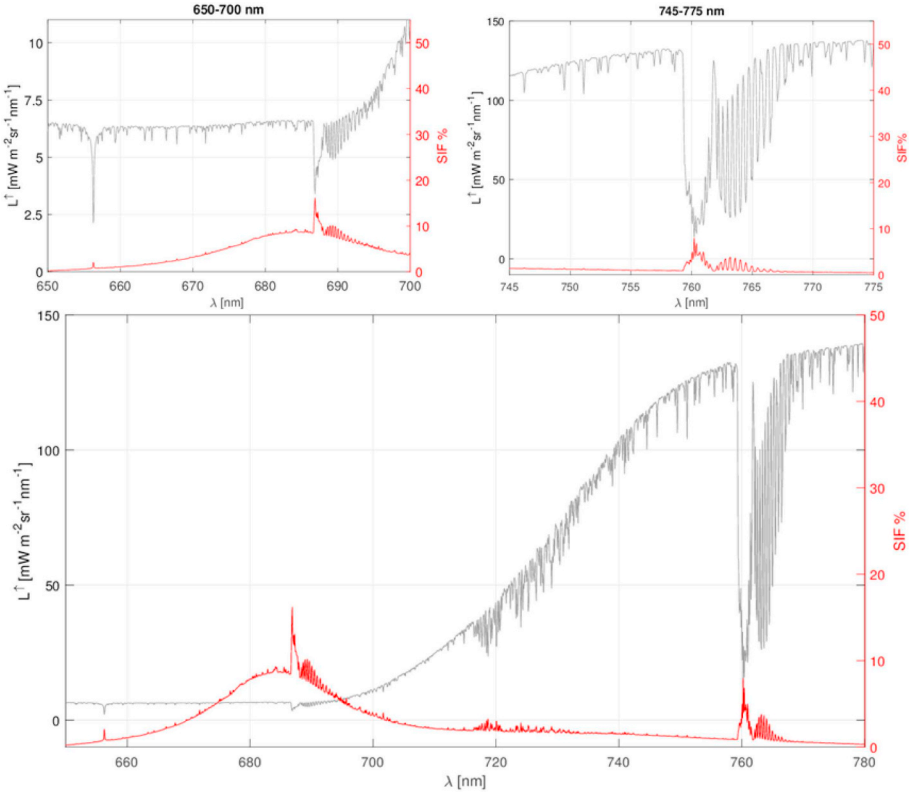

Fig. 8. Relative contribution of solar-induced fluorescence (red curves and right axes) with respect to the total emerging radiance at top-of-canopy (grey curves and left axes) at spectral resolution of 0.1 nm, considering typical dense vegetation during summer conditions. The figure on the bottom shows the spectral range of fluorescence emission; whereas the figures on top show O_2-B (left) and O_2-A (right) details. Note the difference in radiance scales for plots. (For interpretation of the references to colour in this figure legend, the reader is referred to the web version of this article.)

Table 2
Current SIF retrieval methods and their characteristics.

	Absorption band	Method	Reference	Target SIF (R = red; FR = far-red; F = full spectrum)	Scale of design (F = field; A = airborne; S = satellite; ms = model simulations)	Spectral channels (M = multispectral; H = hyperspectral)	Retrieval Spectral Range (nm)	Retrieved SIF	Assumed SIF spectral shape	Assumed r spectral shape	Model solution (A = analytical; N = numerical)	Atmospheric correction (E = empirical; D = data driven; P = physical)
Selected absorption bands	*O_2 bands*											
		FLD	Plascyk, 1975	R	A	M	486.1; 589.0; 656.3	Scalar	Constant	Constant	A	(No correction)
		3FLD	Maier et al., 2003	FR	A	M	760	Scalar	Linear	Linear	A	Single-step (E)
		SFM	Meroni and Colombo, 2006	R, FR	F (leaf)	H	686.5–690.0; 759.0–764.0	Restricted	Linear	Linear	N	–
		cFLD	Gómez-Chova et al., 2006	R, FR	F (leaf)	H	687; 760	Scalar	Adjusted with correction factor	From apparent R	A	–
		iFLD	Alonso et al., 2008	FR	F (canopy), ms	H	750–780	Scalar	Adjusted with correction factor	Adjusted with correction factor	A	–
		SFM	Mazzoni et al., 2008	R	F (leaf)	H	686.3–691.6	Restricted	Polynomial	Polynomial	N	–
		FLD/ SFM	Guanter et al., 2010	R, FR	ms	H	677–697; 750–770	Restricted	Reference spectrum	Linear combination of end-members	A/N	Single-step (P)
		SFM	Meroni et al., 2010	R, FR	F (canopy), ms	H	686.7–691.2; 755.6–765.5	Restricted	Linear, polynomial, gaussian	Linear, polynomial	N	–
		nFLD	Daumard et al., 2010	R, FR	F (canopy)	M	683.1–697.1; 757.9–770.5	Scalar	Reference spectrum	Polynomial	A	–
		SFM	Mazzoni et al., 2010	R, FR	ms	H	677.0–697.0; 750.0–770.0	Restricted	Voigt	Cubic spline	N	Two-step (P)
		SFM	Mazzoni et al., 2012	FR	F (canopy), ms	H	750–770	Restricted	Voigt, legendre polynomial	Polynomials, cubic-spline, legendre polynomial	N	–
		3FLD	Damm et al., 2014	FR	A	M	753–771	Scalar	Linear	Linear	A	Two-step (E)
		SFM	Cogliati et al., 2015a	R, FR	ms	H	750–770	Restricted	Gaussian, lorentzian, voigt	Polynomial, cubic spline	N	Two-step (P)
		iFLD	Wieneke et al., 2016	R, FR	A	M	–	Scalar	adjusted with correction factor	Adjusted with correction factor	A	Two-step (E)
	Fraunhofer lines											
		–	Frankenberg et al., 2011a	FR	S, ms	H	769.5–775; 770.1 (K_I)	Scalar	Constant	Polynomial	N	Single-step (P)
		–	Joiner et al., 2011/2012	FR	S, ms	H	769.90–770.25 (K_I)	Scalar	Constant	Constant	N	Single-step (P)
		SVD	Guanter et al., 2012	FR	F, ms	H	755.8–759.3; 769.2–775.2	Scalar	Constant	Singular vectors	N	Single-step (D)
		PCA	Joiner et al., 2014	FR	S, ms	H	712–747; 747–783	Scalar	Gaussian	Polynomial	N	Single-step (D)
		–	Köhler et al., 2015	FR	S, ms	H	720–758	Scalar	Constant/ normalized fluorescence spectrum	Linear	N	Single-step (D)
		DOAS	Wolanin et al., 2015	R	S	H	681.8–685.5	Scalar	Reference spectrum	Polynomial	N	single-step (P)
		–		R, FR	S, ms	H		Scalar	Gaussian	Polynomial	N	Single-step (D)

(*continued on next page*)

Table 2 (*continued*)

	Absorption band	Method	Reference	Target SIF (R = red; FR = far-red; F = full spectrum)	Scale of design (F = field; A = airborne; S = satellite; ms = model simulations)	Spectral channels (M = multispectral; H = hyperspectral)	Retrieval Spectral Range (nm)	Retrieved SIF	Assumed SIF spectral shape	Assumed r spectral shape	Model solution (A = analytical; N = numerical)	Atmospheric correction (E = empirical; D = data driven; P = physical)
			Joiner et al., 2016				622–640; 682–692					
		two step linearized	Grossmann et al., 2018	R, FR	F (canopy)	H	680–686; 745–758	Scalar	Reference spectrum	Polynomial	N	–
Full Spectrum	*Spectrum fitting*											
		FSR	Zhao et al., 2014/2018	F	F (canopy), ms	H	640–850	Spectrum	Linear combination of basis spectra	–	N	–
		F-SFM	Liu et al., 2015	F	F (canopy), ms	H	645–805	Spectrum	Linear combination of basis spectra	Linear combination of basis spectra	N	–
		SpecFit	Cogliati et al., 2015b	F	ms	H	670–780	Spectrum	Pseudo-voigt	Piecewise cubic spline	N	two-step (P)
		Model inversion										
		–	Verhoef et al., 2018	F	ms	H	400–2255	Spectrum	Singular vectors from SVD	Physically based (RTMo)	N	two-step (P)
		–	Celesti et al., 2018	F	F (canopy), ms	H	400–900	Spectrum	Physically based (RTMf)	Physically based (RTMo)	N	–

reach. This would expedite assimilation of fluorescence data into global LSMs, as initiated by Lee et al. (2015) for the Community Land Model, Norton et al. (2018) for BETHY, and MacBean et al. (2018) for the ORganising Carbon and Hydrology In Dynamic EcosystEms (ORCHIDEE) model.

5. SIF estimation methods

5.1. General strategies

Approaches used to quantify SIF emission from vegetation TOC radiance are anchored by a simple equation describing the additive contributions of solar-reflected (r) and SIF radiance to the total TOC radiance $L(\lambda)$ (assuming isotropic surface reflectance and neglecting canopy-sensor atmospheric effects and adjacency):

$$L(\lambda) = r(\lambda)\, E(\lambda)/\pi + SIF(\lambda) \quad (1)$$

where λ is wavelength and $E(\lambda)$ the known (measured or modelled) incident irradiance at the surface (direct and diffuse). All the terms of Eq. (1) are spectrally variable, making retrieval of the two unknowns challenging. Fluorescence retrieval algorithms are built mostly on the key assumption that prior knowledge of the spectral shape of all terms of the equation can be leveraged to estimate the unknown terms. Specifically, unlike L and E, r and SIF are smooth functions of wavelength and this knowledge is exploited to retrieve SIF at specific spectral absorption bands by assuming that these two variables are either constant or vary linearly over a narrow wavelength range (a few nm), or vary in a more complex way over larger spectral ranges (e.g., the full SIF emission spectrum).

Retrieval methods further exploit the larger relative contribution of SIF to the total TOC radiance at selected absorption bands as compared to over the whole spectrum (Fig. 8). The proportional contribution of SIF to total TOC radiance is larger for red wavelengths because, despite the red fluorescence being strongly re-absorbed by chlorophyll, the canopy reflected radiance is very low for the same reason. Conversely, the SIF contribution is proportionally lower in the far-red where the reflected radiance is dominated mainly by canopy scattering. Besides the overall effect of fluorescence in these spectral regions, it is the specific in-filling effect within absorption bands that is key for retrieving SIF in most approaches. When observed at high SR, the fluorescence in-filling effect within the terrestrial oxygen absorption bands (i.e., O_2-A and O_2-B at 760 nm and 687 nm, respectively) can exceed 10% (Fig. 8). A similar effect occurs in the Fraunhofer Lines (FLs), but here the fluorescence proportional contribution is generally smaller as these absorption bands are less dark than oxygen bands for a given SR. In contrast to the O_2 bands, absorption in the FLs does not occur in the terrestrial atmosphere, an advantage in that modelling of atmospheric influence is much easier (as detailed in this section).

The depth of the absorption bands varies greatly over very narrow spectral ranges, hence, sensor capability to accurately detect such radiance variations through fine SR and high signal-to-noise ratio (SNR) is essential for SIF retrieval. Recent technological developments have produced a number of high-performance spectrometers (ground, airborne, and satellite) providing sufficiently high SRs and SNR for SIF retrieval [Sections 6 and 7]. For satellite instruments, these features also must be balanced with spatial resolution and, in some cases, a coarse resolution of several (or more) kilometers is necessary to achieve the required SNR.

Most retrieval algorithms can quantify fluorescence at selected absorption bands, but a novel group of approaches allows derivation of the full fluorescence emission spectrum (Zhao et al., 2018). This capability affords new opportunities for better understanding SIF with respect to leaf composition, canopy structure and plant functional status (Verrelst et al., 2016, 2015b). Herein, the methods are grouped into two main classes based on whether they allow retrieval within restricted absorption bands or over the full SIF emission region

(Table 2). Within the first class, we can distinguish methods based on O_2 bands and those for FLs, and in the second class methods based on parametric functions to describe $r(\lambda)$ and $SIF(\lambda)$ (i.e., spectrum fitting) are distinguished from those using a full radiative transfer approach (i.e., model inversion). Most retrieve SIF at different scales, from ground to satellite, using different acquisition techniques.

For airborne and satellite observations, different physically-based or empirical approaches have been explored to account for atmospheric effects. Table 2 also summarizes characteristics of the methods such as: capability of retrieving red, far-red, or full fluorescence; number of spectral bands employed (e.g., multispectral, hyperspectral); spectral range used in the retrieval; main assumptions; use of parametric expressions vs. model-based functions; and treatment of the atmospheric effect. We focus mainly on developments subsequent to the review of Meroni et al. (2009), with a few earlier ones included for historical context and completeness.

5.2. Retrieval of SIF at selected absorption bands

The first class of retrieval methods targets restricted spectral regions associated with strong absorption from gases in the terrestrial or solar atmosphere (i.e., O_2 bands or FLs, respectively). Retrieval at selected wavelengths exploits the contrast between (i) spectral wavelengths where the radiance signal is mostly dominated by the reflected solar flux, and (ii) narrow spectral regions where the solar incident flux is largely attenuated.

5.2.1. Oxygen absorption bands

A classical strategy to disentangle reflected radiance and SIF contributions is to compare the radiance outside and inside the O_2 absorption bands. The approach is an extension of a technique originally developed for FLs, the FLD principle (Plascyk, 1975; Plascyk and Gabriel, 1975), which relies on two radiance measurements – one inside and one outside the absorption feature – to solve Eq. (1). A refinement particularly relevant for red fluorescence uses more spectral bands to introduce a spectral dependency of reflectance and fluorescence, as exemplified by the 3FLD (Maier, 2002), cFLD (Gómez-Chova et al., 2006), and iFLD (Alonso et al., 2008), reviewed by Meroni et al. (2009).

Spectral Fitting Methods (SFMs) are a more sophisticated approach that uses all available (hyper)spectral bands to quantify the spectrally variable fluorescence and reflectance contribution over a restricted spectral range. The upwelling radiance spectrum is modelled over a broader spectral window (i.e., ~tens of nm) including multiple absorption lines (i.e., O_2 bands and FLs), with fluorescence and reflectance as continuous parametric functions. The resulting mathematical system (one equation per spectral wavelength considered) is solved to retrieve the underlying unknown function parameters. Several types of functions have been proposed to approximate the reflectance and fluorescence spectral behaviour within spectral windows around the main oxygen absorption bands (Table 2). Because SFMs use all of the high-resolution spectral information along the absorption region – theoretically hundreds of bands – the impact of instrument noise is reduced.

5.2.2. Fraunhofer lines

In contrast to methods using oxygen absorption bands, those using solar absorption features do not require complex atmospheric modelling, hence, they have been extensively applied to current space-based SIF retrievals. This family of algorithms may be categorized into two main groups: (i) simplified physically-based schemes applied to specific FLs, and (ii) data-driven statistical approaches involving Principal Component Analysis (PCA) or Singular Value Decomposition (SVD) analysis. When the retrieval is fitting only FLs (e.g., spectral windows 745–758 nm, as in GOSAT, OCO-2 or S-5P), both simple physically-based (e.g., Frankenberg et al., 2011a) and data-driven (e.g., Guanter et al., 2012) methods can be used. When the fitting window is wider and includes atmospheric bands, as in SIF retrievals from GOME-2 data, spanning either water vapour around 740 nm or O_2 in 760 nm, then data-driven approaches are the only way to avoid the complex explicit modelling of atmospheric radiative transfer (e.g., Joiner et al., 2013; Köhler et al., 2015). Several methods have been proposed and all these strategies have allowed determination of the far-red fluorescence (Table 2).

Terrestrial SIF in the red spectral region is more difficult to detect from space using FLs as the lines in the red region are not as wide, nor as deep, as those in the far-red. Also, red SIF signal levels are typically lower overall than those in the far-red for healthy vegetation, because of re-absorption by chlorophyll *a*nd also because the emitted red fluorescence by leaves within a canopy conceivably can add to the directly emitted far-red fluorescence (i.e., the re-emission phenomenon). The sharp upturn of the red edge also complicates retrievals and may necessitate smaller fitting windows. Quantification of the red SIF emission was reported by Wolanin et al. (2015) using SCIAMACHY and GOME-2 data and by Joiner et al. (2016).

Recently, FL-based methods developed for satellite sensors also are being used for ground-based and airborne spectrometers operating at high SR (Grossmann et al., 2018; Frankenberg et al., 2018).

5.3. Retrieval of the full SIF spectrum

Two main approaches have been developed to retrieve the continuous SIF emission spectrum (Table 2).

5.3.1. Spectrum fitting

Spectral fitting techniques are an evolution of SFMs to encompass the broader spectral region where fluorescence emission occurs. Methods such as the Fluorescence Spectrum Reconstruction (FSR) (Zhao et al., 2014), the Full-spectrum Spectral Fitting (F-SFM) (Liu et al., 2015), and the advanced FSR (aFSR) (Zhao et al., 2018) are examples that use linear combinations of basis spectra to model the SIF spectrum at TOC. The basis spectra are derived from PCA (Liu et al., 2015) or SVD (Zhao et al., 2014) on a large dataset of SIF spectra simulated by the canopy RT model SCOPE. In general, these methods are structured as follows: first, SIF is retrieved at selected absorption bands (i.e., O_2 bands, Hα FL, etc.) by means of a modified version of SFM; then, the SIF spectrum is reconstructed as a linear combination of the basis spectra matching the SIF SFM retrievals. Alternatively, the full SIF spectrum is estimated by considering simultaneously all the wavelengths in the spectral window where fluorescence occurs, as in the SpecFit model and using piecewise cubic spline to fit the reflectance (Cogliati et al., 2015b).

5.3.2. Model-inversion methods

An emerging approach for quantifying SIF is based on numerical inversion of canopy RTMs. This route permits retrieval also of relevant biophysical parameters (e.g., chlorophyll content, leaf area index, etc.), and related variables (e.g., fraction of photosynthetically active radiation absorbed, fAPAR), as side-products of the fluorescence retrieval. This additional information is crucial for interpretation of SIF with respect to plant photosynthetic activity.

An inversion approach was first developed by Verhoef et al. (2018) and is suited to the spectral and directional outputs of the tandem mission of FLEX and Sentinel-3 (S-3). The method is based on model inversion of simulated TOA radiance where the SIF and canopy parameters are retrieved simultaneously and in a consistent manner. It employs a 'light' version of SCOPE to generate the canopy reflectance signature; then SIF is modelled as an additional source of radiance using a linear combination of principal components (PCs). Actually, this approach represents a hybrid solution between model inversion (reflectance modelling) and the spectrum fitting methods (fluorescence modelling).

A more complete canopy model-inversion procedure was recently

proposed by Celesti et al. (2018) based on simulations and experimental TOC observations collected during controlled stress induction experiments. It employs both the fluorescence and reflectance SCOPE subroutines. These routines are used to forward model the TOC apparent reflectance to be matched with spectral observations. The use of the fluorescence routine allows quantification of the fluorescence quantum yield, one of the key variables for understanding fluorescence and its link to photosynthesis. Because the work of Celesti et al. (2018) involved extreme contrasts in vegetation properties induced by a chemical treatment, the operational applicability of their approach to natural vegetation canopies or TOA satellite data remains to be studied.

In the model inversion approach, Visible and Near-Infrared (VNIR) information are needed for adjusting the canopy reflectance model parameters. Unfortunately, due to current technological constraints, wide-spectral-range high-resolution spectra cannot be collected by the same spectrometer, potentially giving rise to some inconsistencies between spectral datasets with respect to spatial co-registration, radiometric intercalibration, etc. For this reason, accurate co-registration and intercalibration methods must be applied prior to fluorescence determination whenever more than one sensor is used.

5.4. Atmospheric correction, illumination, and surface anisotropy

Some of the retrieval methods require atmospheric correction before SIF retrieval (two-steps), whereas others explicitly include atmospheric correction in the design of the algorithm in a complete TOA scheme (one-step). Atmospheric effects depend on the type of absorption feature used (terrestrial vs. solar). Satellite-based FL methods explicitly include the atmospheric effect directly in a single-step algorithm design facilitated by the relatively simple behaviour of the atmosphere at these wavelengths. The assumption is that the atmospheric interference is caused mainly by scattering that, within the narrow FLs, can be considered spectrally invariant or varying as linear or polynomial functions. Thus, the simplified physically-based methods and the data-driven approaches working with FLs correct for this scattering but do not require characterization of the atmospheric status (such as aerosol optical depth or height distribution) which can strongly impact the O_2-A feature (Frankenberg et al., 2011a). By contrast, retrieval at the O_2 bands requires very accurate atmospheric modelling. High-resolution atmospheric RT codes are used to compute the spectrally-resolved atmospheric RT functions (i.e., two-way direct and diffuse transmittance, bidirectional reflectance and spherical albedo) to represent accurately the TOA reflected radiance in addition to SIF. Verhoef et al. (2018, 2014) proposed a means to couple atmospheric and surface RT at high SR based on the so-called T-18 system of atmospheric transfer functions – a method specifically designed to accommodate the finite spectral band effect. This effect concerns the fact that the atmospheric transmittance of absorption lines does not follow Beer's Law when there are large variations of the spectral absorption within the interval (spectral band), therefore the product of two atmospheric functions (e.g., downward and upward transmittance) is not equivalent to the product of these functions convolved. This strategy has been employed in several schemes based on FLD, spectral fitting, and model inversion (Cogliati et al., 2015b; Damm et al., 2014; Mazzoni et al., 2010; Wieneke et al., 2016).

The atmospheric correction at the O_2 bands may be performed either as a two-step or one-step procedure. Cogliati et al. (2015a) used a two-step approach where the TOA spectrum is converted to TOC followed by decoupling of the SIF and reflectance, based on SFM and SpecFit. A two-step approach including a more realistic atmospheric correction was presented in Sabater et al. (2017, 2015) and implemented within the FLEX End-to-End simulator (Vicent et al., 2016). A direct TOA radiance optimization approach has instead been introduced by Verhoef et al. (2018), in which at-sensor spectra are calculated by coupling a canopy model with an atmospheric RT model. The procedures described here for satellite instruments also have been adapted for airborne imaging spectrometers. For example, FL approaches have been used with the *HyPlant* airborne sensor (Colombo et al., 2018; Rossini et al., 2015) and with the novel Chlorophyll Fluorescence Imaging Spectrometer (CFIS) (Frankenberg et al., 2018) [Section 6]. The physical methods at the O_2 bands were adapted for *HyPlant* by Cogliati et al. (2018) and a semi-empirical technique making use of fluorescence-free reference pixels (i.e., bare soils) was shown to improve characterization of the atmospheric transfer functions (Damm et al., 2014; Wieneke et al., 2016).

Retrievals that rely on O_2 absorption bands are sensitive to the direct-to-diffuse ratio of the incident light and its coupled effect with canopy anisotropy. To reach the sensor, diffuse light traverses a longer pathway compared to direct light, making the depth of the absorption sensitive to the fraction of diffuse light. This effect might be confused with in-filling by fluorescence, leading to over/under-estimation of fluorescence. Evidence of such effects based on RT simulations has been reported in Fournier et al. (2014), Cogliati et al. (2015b), and Verhoef et al. (2018). Liu and Liu (2018) considered in more detail the impact of direct/diffuse radiation on the in-filling effect and SIF retrieval using simulated data. They found that this effect can have a marked impact on estimated SIF (up to 20% at the O_2-A band). These studies have been developed mainly with turbid-medium canopy RTMs, but the fluorescence angular distribution is also affected significantly by the structural arrangement of the canopy – with respect to sun and sensor viewing angles – which determines the actual fraction of illuminated and shaded leaves observed by the instrument. This is commonly observed from diurnal continuous measurements of fluorescence using ground-based and tower-mounted instruments viewing a fixed spot of the canopy. Understanding whether changes in fluorescence are related to canopy self-shadowing or to more relevant physiological processes is not trivial and still a challenge. Detailed consideration of anisotropic effects and the impact on retrieval accuracy of fluorescence was provided in Damm et al. (2015b) and Yang et al. (in press). Sensor technical characteristics (e.g., spatial resolution, spectral range and resolution, and SNR) are relevant to such aspects and play an important role in determining the accuracy of SIF retrieval.

5.5. Assessment of SIF retrieval accuracy

Validation of SIF retrieval methods, especially for satellite-based acquisitions, is still a challenge due to issues such as large footprint sizes and instrument errors [Section 7]. Also, until recently there has been a lack of direct ways to observe SIF independently; however, this situation is changing with the advent of new portable sensors for leaf/canopy-scale work, platform-mounted devices, drones, and other airborne sensors for SIF detection [Section 6].

So far, retrieval accuracy has been evaluated mainly through numerical experiments in which RT simulations – ones that consider comprehensive variability of reflectance, fluorescence and atmospheric conditions – are performed according to specific instrument characteristics (sampling interval, FWHM, SNR, etc.). But the reliability of accuracy statistics obtained in this way depends on the overall assumptions included in the canopy and atmospheric RT models and how accurately the models are coupled. Most numerical simulations are based on homogeneous 1D surfaces and Lambertian assumption (e.g., Damm et al., 2011; Liu et al., 2015; Meroni et al., 2010; Zhao et al., 2014), and in only a few cases has a full bidirectional reflectance distribution function (BRDF) scenario been included in the forward model (Cogliati et al., 2015b; Liu and Liu, 2018; Mazzoni et al., 2010; Verhoef et al., 2018). More recently, full 3D RT models incorporating fluorescence (e.g., FluorWPS, FluorFLIGHT, and DART) [Section 4] were developed, offering more complex strategies to calculate retrieval accuracy in heterogeneous canopies and landscapes.

A more direct evaluation of SIF retrieval accuracies from airborne and satellite sensors is possible using direct comparisons with ground-based data. These data can provide more reliable estimations of

fluorescence because surface irradiance is measured, and atmospheric effects may be neglected. This has been used successfully for airborne observations from the *HyPlant* sensor, operating at spatial resolution of one meter (Rascher et al., 2015; Rossini et al., 2015). However, since ground-based methods (e.g., from towers) sample a footprint of only a few square meters, it presents difficulties for validation of medium and coarse-spatial-resolution data. Validation of SIF retrievals from medium-resolution satellite missions such as FLEX ($300 \times 300\ m^2$) could be feasible by combining data from field spectroscopy instruments – to get continuous temporal data – with less frequent acquisitions over larger spatial areas using robotic systems, UAVs, or other airborne sensors in selected sites.

5.6. Challenges and future directions in SIF retrieval

Main novelties in retrieval strategies include protocols for satellites using FLs and derivation of the full SIF spectrum. A recent shift from the use of terrestrial oxygen absorption bands – nearly all papers reviewed by Meroni et al. (2009) – to FLs alone, or in parallel with O_2 bands, is seen also in applications using atmospheric satellite sensors. Development of FL procedures was prompted by the convenient availability of atmospheric chemistry satellites, which allowed researchers to capitalize on the simplified modelling of atmospheric effects in the solar absorption bands to quantify SIF at coarse spatial resolution [Section 7]. However, such results have suffered from the fact that the sensors employed were not specifically designed for SIF. Therefore, the instantaneous retrievals are aggregated to improve their quality at the cost of spatio-temporal resolution. However, improved observational capabilities and better SNR are offered by new atmospheric sensors (e.g., TROPOMI aboard the S-5P satellite) (Guanter et al., 2015).

Retrieval methods that use O_2 absorption features have their pros and cons. On the one hand, they have access to features where the fluorescence contribution is more prominent, but on the other hand they require much more complex modelling to correct for atmospheric absorption and scattering inside the O_2 bands. The particular design of the tandem FLEX/S-3 mission concept, aimed at SIF retrieval using the O_2 bands, was developed specifically to address requirements for an accurate atmospheric correction and SIF detection. The broad spectral coverage (from visible to IR wavelengths), the high-spectral resolution in the red and far-red region, and the dual-view (nadir and oblique) offered by the tandem mission provide the spectral and directional information for an accurate atmospheric characterization (Drusch et al., 2017; ESA, 2015; Sabater et al., 2017).

Most methods emphasize selected absorption bands at both O_2 and FLs to provide independent fluorescence values, neglecting the possible functional relationship between red and far-red fluorescence emission peaks. Only the new generation of methods – full SIF spectrum and model-based inversion – offers a broader spectral characterization of SIF, and makes consistent use of the spectral detail available from the two fluorescence emission regions. The perspective of exploiting the full SIF spectrum is relevant for future work on fluorescence in relation to different canopy species, chemical/physical variables, and physiology. Knowledge of the entire fluorescence spectrum may be helpful to better quantify canopy re-absorption, as well as for deriving the respective PSI/PSII contributions and the fluorescence quantum efficiency. However, the full SIF spectrum is influenced at leaf and canopy levels by diverse factors which are not necessarily related directly to the photosynthetic activity of the plants [Sections 2 and 8]. To further help understanding of all these combined effects, model inversion methods have the additional advantage of offering physiologically consistent estimates of canopy parameters that are essential to better interpretation of fluorescence. Nonetheless, in the model inversion approach VNIR information is needed for adjusting the canopy reflectance model parameters. Given that two spectrometers will likely be needed to acquire such data, accurate co-registration and intercalibration methods will be critical.

6. SIF measurement technologies – Field and airborne systems

6.1. Technological overview

A range of field sensors have been developed over the years, from hand-held and clip-on devices to TOC sensors deployable from stationary or mobile ground-based platforms, unmanned aerial vehicles (UAVs), and traditional aircraft. These technologies provide complementary capacity for measuring and interpreting fluorescence in the context of physiological processes. Airborne imaging allows mapping of fluorescence over plant canopies and derivation of indicators of photosynthetic functionality and pre-visual stress at ecological and management-relevant scales. Field and airborne systems also support satellite-based measurements through validation, interpretation, and provision of data inputs to models. The types of field systems are compared in Fig. 9, indicating relative merits with respect to operational and biological considerations.

6.2. Hand-held leaf instrumentation

Portability is a priority for passive SIF field devices. But unlike the availability of active fluorometers that detect steady-state fluorescence in leaves – for which there are multiple commercial devices –

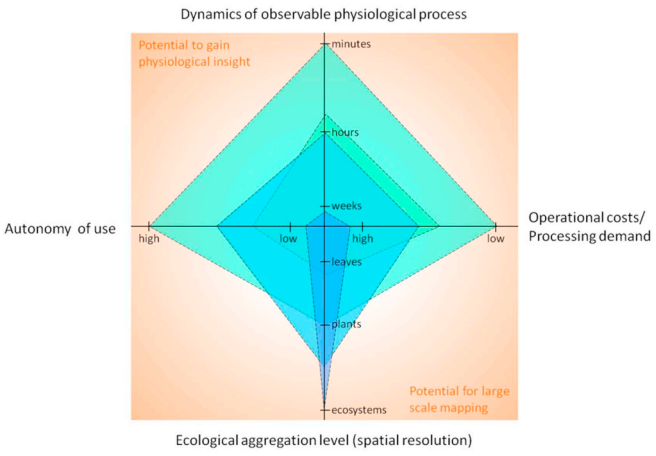

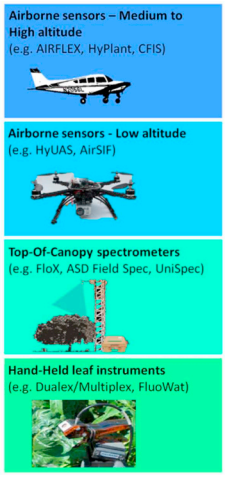

Fig. 9. Comparison and complementarity of hand-held, top-of-canopy, and airborne instrumentation to gain insight into the information content of fluorescence and facilitate mapping. (Colours on the left panel correspond to those on the right.) (For interpretation of the references to colour in this figure legend, the reader is referred to the web version of this article.)

instruments designed specifically for SIF are still rare. One such device is FluoWat, a hand-held leaf clip designed for use in natural sunlight. When coupled to a field-portable spectrometer, the device allows quantification of the full SIF emission and also reflectance and transmittance. FluoWat uses a short-pass filter (< 650 nm) to control incoming light, so only the fluorescence emission is measured when the filter is in place. Its fiber-optic probe may be positioned to measure upward- or downward-directed fluorescence (typically from adaxial or abaxial leaf surfaces, respectively), thereby allowing study of the interplay among vertical pigment gradients, re-absorption, scattering properties, and leaf fluorescence emission. The instrument has been used to facilitate linking of canopy and leaf-level SIF data, and for stress detection (Cendrero-Mateo et al., 2016; Van Wittenberghe et al., 2015, 2014, 2013).

6.3. Top-of-canopy spectrometers

Early work in passive detection of TOC fluorescence was inspired by the development of the MKII Fraunhofer line discriminator, an airborne instrument for remote sensing of solar-induced 'luminescence' (Hemphill et al., 1977; Plascyk, 1975). It was used with leaves and canopies to reveal subtle changes at the Hα FL (656.3 nm). The method was applied successfully by McFarlane et al. (1980) to identify water stress in citrus crops, and by Carter et al. (1990) to relate SIF to carbon assimilation in field vegetation. But limitations to using the Hα band were its distance from the fluorescence peaks and its narrow width (~0.1 nm FWHM) which necessitated very high SNR.

Detection of SIF in the O_2 bands has been researched intensively in the last twenty years [Section 5], and assorted instruments have emerged (Meroni et al., 2009). Kebabian et al. (1999) introduced a plant fluorescence sensor to detect photons re-emitted after absorption of fluorescence by oxygen contained in a low-pressure cell, which was used to measure effects of nitrogen deficiency on the red to far-red peak ratio (Freedman et al., 2002). Carter et al. (1996) used a Fraunhofer Line Radiometer measuring in the O_2-B band to study herbicide effects on leaf fluorescence. Moya et al. (2004) invented an instrument using narrow-band interference filters to derive fluorescence in the O_2-A band. And Evain et al. (2001) introduced a Passive Multi-wavelength Fluorescence Detector (PMFD) to measure fluorescence and reflectance at 760 nm and at 687 nm. Quantification of SIF in the O_2-B and O_2-A bands also was done by Fournier et al. (2012) using their SpectroFLEX canopy instrument, able to perform continuous and automatic measurements over several weeks. Finally, Pérez-Priego et al. (2005) illustrated the sensitivity of fluorescence (in-filling) at the O_2-A band to water stress by using a high-resolution spectrometer housed in a temperature-controlled box and connected to a 15-m-long fiber-optic cable for acquisition of reflectance from single tree crowns.

Developments in sensor technologies have sought to harness the combined information of reflectance and fluorescence (Burkart et al., 2015; Cheng et al., 2013; Migliavacca et al., 2017a; Panigada et al., 2014; Pérez-Priego et al., 2015, 2005; Yang et al., 2015). Well-calibrated ASD FieldSpec devices, for example, which have high SNR (even though the O_2 absorption bands are not well resolved), have been used to capture diurnal courses of canopy SIF and reflectance (Damm et al., 2014, 2010; Liu et al., 2005), an approach also tested with some success from low-flying research aircraft (Damm et al., 2014; Schickling et al., 2016).

Sophisticated apparatus have emerged to better resolve absorption features and leverage the availability of low-cost miniaturized spectrometers. A fully automatic system, consisting of three miniature high-resolution HR2000+ spectrometers (Ocean Optics, Florida, USA) enclosed in a temperature-stabilized box and connected to collimated optic fibers, was installed atop a crane to continuously monitor SIF and reflectance spectra at a high repetition rate (1 Hz) (Daumard et al., 2012, 2010; Goulas et al., 2017). Two inter-calibrated spectrometers allowed almost simultaneous determinations of incoming and reflected radiation, with an automated routine continuously adjusting integration time to the intensity of incoming radiation to optimize SNR.

New instrument architectures introduced by researchers at the University of Milano and their colleagues combined high-resolution spectrometers in a temperature-stabilized box, with optical multiplexers and a dedicated intercalibration routine, creating a stable TOC measurement system (Cogliati et al., 2015a). In ecosystem studies, this apparatus provided the first concise comparison of fluorescence emissions across different plant functional types (Rossini et al., 2016). The Milano system, known commercially under the name 'FloX' (Julitta et al., 2017), houses two spectrometers (one broadband, one high-resolution) with bifurcated fibers to allow almost simultaneous measurements of incoming and reflected irradiance. Precise calibration of the integrated system and automated data retrieval algorithms permit estimation of red and far-red fluorescence. The systems have been installed on about a dozen observation towers internationally to date.

An automated, tower-based canopy system called FUSION, developed by NASA-GSFC, integrates multi-directional spectral, thermal, and SIF observations (Middleton et al., 2018). Its two dual-channel systems (upward- and downward-looking spectrometers) simultaneously collect high-spectral-resolution data of reflected light and fluorescence and can operate continuously during daylight hours to capture diurnal and seasonal dynamics. Data products include VNIR surface reflectance spectra from ~350–1100 nm, red and far-red SIF, and surface temperature.

Other tower-based examples include FluoSpec, PhotoSpec, and AutoSIF. FluoSpec (Yang et al., 2018c, 2015) is an automated system that provides high SR (~0.13 nm FWHM) between 680 and 775 nm for red and far-red SIF; it has been used since 2012 in a site network called FluoNet. PhotoSpec assesses the red (670–732 nm) and far-red (729–784 nm) wavelength ranges and also canopy reflectance (400–900 nm); it has a high SNR and SR to allow FL retrievals and has been used successfully for continuous daytime monitoring of SIF (Grossmann et al., 2018). AutoSIF (Zhou et al., 2016; Xu et al., 2018) uses a single spectrometer to capture a spectral range of ~480–850 nm, with a spectral resolution of 0.9 nm, SNR of 1000:1, and spectral sampling interval of 0.4 nm; it has been used to quantify red and far-red SIF (Xu et al., 2018).

6.4. Airborne systems

6.4.1. Low-altitude systems – Unmanned aerial vehicles

UAVs, also called unmanned aircraft systems (UAS), provide observations of vegetation optical properties at the intermediate scales between ground-based and higher-altitude airborne systems. The appeal of this approach is the flexibility to provide on-demand imaging spectroscopy at high spatial and temporal resolutions (Berni et al., 2009; Garzonio et al., 2017; Lucieer et al., 2014; Malenovský et al., 2017; Zarco-Tejada et al., 2012, 2009). UAV deployments over vegetation is a fairly recent undertaking, with first prototypes developed in the early 2000s used in agricultural applications (e.g., Herwitz et al., 2004; Johnson et al., 2003). Subsequent trials were restricted primarily to multispectral and broad-band thermal imagery acquisition (e.g., Turner et al., 2014) – but in the last decade UAV systems suitable for SIF retrieval have emerged.

UAV capability to retrieve SIF has been demonstrated in several investigations. Some early experiments used a fixed-wing type of unmanned aircraft equipped with a micro-hyperspectral imager and thermal camera (Fig. 10) (Zarco-Tejada et al., 2013b, 2012). SIF emission (O_2-A) derived from the extracted spectral radiance of pure-crown 30-cm or 40-cm pixels showed, along with independent ground observations and models, that SIF signals from individual trees with different water stress status could be discriminated (using the 3FLD method with a 6-nm FWHM and 1.85 nm sampling spectra). Other systems of a higher spectral resolution and sampling followed. For instance, the HyUAS (Garzonio et al., 2017) is a non-imaging multi-rotor-

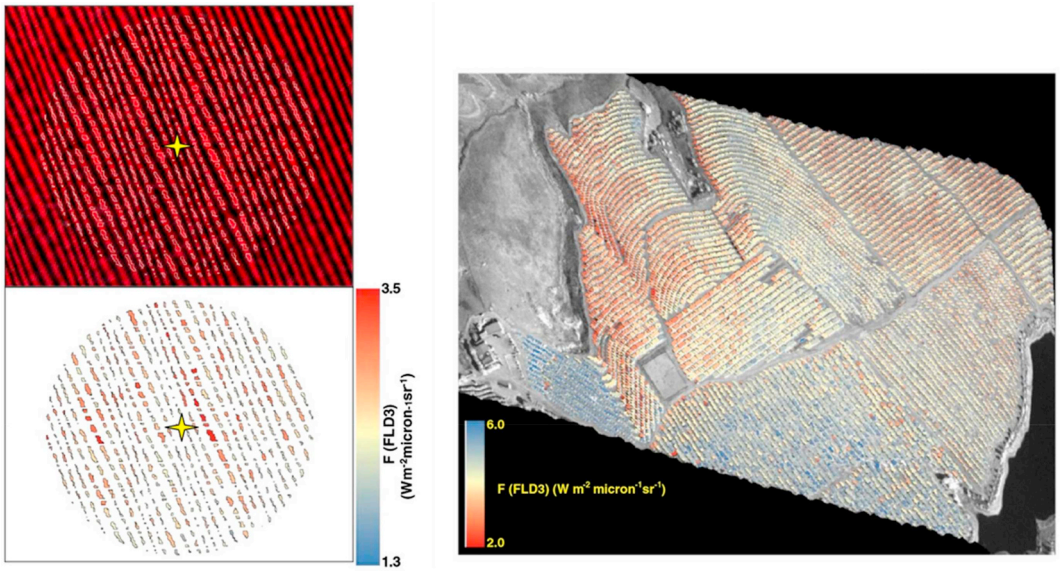

Fig. 10. High (30- or 40-cm) resolution SIF retrievals from hyperspectral imagery acquired from an unmanned aerial vehicle flown over an eddy covariance flux tower in an olive orchard (left, false colour composite) (Source: Zarco-Tejada et al., 2013b), and over a citrus field subjected to water stress treatments (right) (Source: Zarco-Tejada et al., 2012). The high resolution imagery acquired by the micro-hyperspectral camera enabled the quantification of SIF (O_2-A band) on pure tree crowns, removing the large effects caused by shadows and background in heterogeneous canopies. (For interpretation of the references to colour in this figure legend, the reader is referred to the web version of this article.)

platform apparatus designed to optimize optical data acquisition under changing meteorological conditions (Cogliati et al., 2015a) and for provision of a more homogeneous footprint at a given flight height. Another development is the Piccolo doppio (Mac Arthur et al., 2014), which incorporates two fiber-optic-based spectrometers and allows near-simultaneous measurements of reflectance and fluorescence in the oxygen bands. Finally, the AirSIF sensor mounted on a multi-rotor UAV uses a QE PRO spectrometer (Ocean Optics) with bifurcated two-channel optical fibers. It was designed to achieve accurate ground localization and shape reconstruction of the SIF and reflectance measurement footprints by considering exact UAV posture, geographic position, and detailed digital surface modelling of the vegetation canopy (Bendig et al., 2018).

Technical advantages of UAVs include the capability for highly customized deployments (e.g., low and slow flights allowing for high spatial resolutions and long integration times) and quick response and turn-around for planning and investigation. Although UAV systems must be miniaturized and lightweight, they must also provide a stable high-resolution spectral performance with sufficient SNR and precision to measure SIF with a required accuracy. On the other hand, for some applications, the primary value might be a high spatial resolution with an accurate geolocation rather than precise SIF estimates (Gautam et al., 2018) allowing e.g., mapping of SIF spatial variability in stressed vegetation. In controlled studies, high spatial resolution can also help to discriminate the many confounding influences on SIF magnitude (e.g., shadows, vegetated background with different structure, pigment contents, etc.), thereby complementing medium- and high-altitude airborne and satellite systems.

6.4.2. Medium- or high-altitude systems

6.4.2.1. Line scanners. Over 30 years ago, it was shown that, despite the low emission of SIF in natural environments, it was detectable using airborne sensors in marine systems. Using the fluorescence line height feature, the fluorescence peak at 685 nm emitted by phytoplankton was clearly discriminated from background radiance of the sea surface (Gower and Borstad, 1990; Neville and Gower, 1977). But this differential technique was not applicable to terrestrial vegetation owing to its very different spectral properties such as higher reflectance – the shape of which is controlled mainly by photosynthetic pigment content and strong re-absorption of the red fluorescence (Zarco-Tejada et al., 2000b). Instead, passive detection of vegetation SIF using airborne systems came to rely on narrow absorption features of the incident radiation. To the best of our knowledge, the first reported airborne test over vegetation was performed with the MKII Fraunhofer Line Discriminator deployed onboard a helicopter (Watson and Hemphill, 1976). Later, using the enhanced sensitivity provided by the oxygen bands, the AIRFLEX line scanner became the first dedicated airborne instrument for measuring SIF in terrestrial vegetation (Moya et al., 2006). AIRFLEX is a multichannel radiometer that uses narrowband interference filters (FWHM between 0.5 and 1 nm, depending on the channel) to sample the in-band and out-of-band radiances at 687 nm and 760 nm. Interference filters allow for the detection of a high flux, enhancing SNR (albeit at the expense of spectral resolution). AIRFLEX was first tested in campaigns of the SENtinel-2 and FLuorescence EXperiment (SEN2FLEX) program, and it demonstrated clearly the feasibility of analysis in the O_2 bands (Moya et al., 2006). These early experiments were crucial in proving the distinctive nature of the fluorescence signal compared to conventional reflectance (Rascher et al., 2009).

6.4.2.2. Airborne imaging spectrometers. Until airborne imaging sensors specialized for measuring SIF became available, spectrometers with lower SR were used. They included, for example, the Reflective Optics System Imaging Spectrometer (ROSIS) (Maier et al., 2003), the CASI (Zarco-Tejada et al., 2002, 2001), and the Airborne Prism Experiment (APEX) (Damm et al., 2015a) – to retrieve SIF in the wider O_2-A band. From today's perspective, such instruments are considered sub-optimal due to their low SR (e.g., 2.2 nm for CASI-1500, 5.7 nm for APEX, and 7 nm for ROSIS), which allows fluorescence maps only in relative units, but some of these imagers (e.g., APEX) benefited from a high SNR, partly compensating for the lower SR (Damm et al., 2011). These case studies propelled the entire field by providing relevant and interesting insight into the spatial and temporal variability of SIF. They demonstrated the value of the 3FLD technique (Maier et al., 2003), the feasibility of using airborne data to validate maps of SIF retrieved from satellite sensors (Guanter et al., 2007), and the possibility to

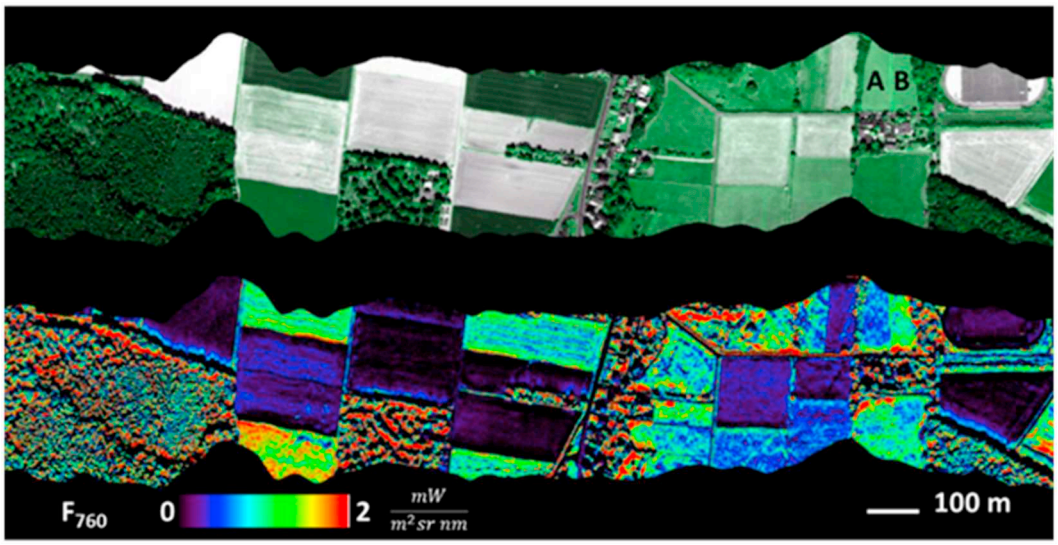

Fig. 11. Reflectance (upper panel) and canopy SIF (lower panel) maps obtained with the *HyPlant* airborne sensor over an agricultural research site in Klein Altendorf, Germany. Lower SIF is evident in forests (left in lower panel) and higher SIF in dense agricultural fields (middle and right in lower panel). Fluorescence emission reveals information on vegetation status which is not visible in the reflectance domain. For example, the two fields denoted as A and B display almost identical reflectance (upper panel), whereas their fluorescence emission is very different (lower panel). (Source: U. Rascher/Forschungszentrum Jülich). (For interpretation of the references to colour in this figure legend, the reader is referred to the web version of this article.)

derive multi-year data to study relationships between SIF and ecosystem GPP (Damm et al., 2015a).

After some attempts to use existing imaging spectrometers in a re-programmed mode (Rascher et al., 2009), the *HyPlant* airborne imaging spectrometer was developed as a cooperative endeavour between Germany's Forschungszentrum Jülich and the Finnish company SPECIM. As the core reference instrument and demonstrator for the FLEX satellite mission, *HyPlant* was the first airborne sensor optimized optically for full-spectrum SIF retrieval, taking advantage of the oxygen absorption and FLs near 685 and 760 nm. *HyPlant*'s core module operates with high SR (0.25 nm) and a spectral sampling interval of 0.11 nm to resolve the spectral window between 670 and 780 nm (Rascher et al., 2015). Initial tests starting in 2012 confirmed that SIF could be retrieved successfully in the O_2-A band from such an airborne platform to provide information not discernible from reflectance (Fig. 11) (Rascher et al., 2015; Rossini et al., 2015; Simmer et al., 2015). While the first version of the instrument had an imperfect point-spread function and limited SNR, subsequent improvements have increased SNR and pointing accuracy. The optical path of the fluorescence module has been redesigned and upgraded to achieve a stable optical performance of the detector, also helping retrieval of both fluorescence peaks using the O_2-A and the O_2-B absorption features (Wieneke et al., 2016; Middleton et al., 2017; Colombo et al., 2018; Gerhards et al., 2018; Liu et al., 2018; Von Hebel et al., 2018; Yang et al., in press).

Two airborne imaging spectrometers were developed recently in the US. One is the NASA/JPL CFIS, an imaging system developed for validation of OCO-2 SIF retrievals. CFIS has a high SR (< 0.1 nm) and spectral coverage between 737 and 772 nm for estimation of far-red SIF (Frankenberg et al., 2018; Sun et al., 2017). It has been used in airborne campaigns to under-fly orbital tracks of the OCO-2 satellite, revealing strong agreement between SIF retrieved from OCO-2 and CFIS along latitudinal gradients (Sun et al., 2017). A second imager, the Hyperspec High Resolution Chlorophyll Fluorescence Sensor, is a lightweight sensor developed by Headwall Photonics, Inc. (Bolton, Massachusetts) in partnership with NASA/Goddard to capture the spectral range of 670–780 nm (~0.2 nm SR), allowing retrieval of both red and far-red SIF. This sensor has been integrated into NASA/Goddard's G-LiHT airborne package which also collects lidar, thermal, and hyperspectral visible-NIR optical data (Middleton et al., 2017).

6.5. Adapting theory to the 'real world'

The study of fluorescence in natural field conditions and at different biological and spatial scales requires consideration of multiple factors to acquire coherent measurements, to avoid retrieval artefacts, and to correctly interpret results. Sensor technologies, retrieval strategies, and the specific influential factors in a given situation can all affect robustness and reliability of fluorescence results. Aspects that change between proximal and remote sensing with implications for fluorescence retrievals include (i) non-uniformities and instabilities of the detectors, (ii) spatial footprint of the instrumentation, and (iii) impact of atmospheric effects. Also important are the appropriate use and the relative height placement of canopy versus reference sensors for accurate SIF measurements (Sabater et al., 2018).

With field spectrometers positioned within a short distance of the surface target, information on atmospheric functions (including atmospheric transmittances, path-scattered radiance, and spherical albedo) can be provided by measuring reference panels. But with increasing distances (i.e., using tower, airborne or satellite sensors), a combination of measured and modelled atmospheric functions is required, necessitating accurate dynamic calibration status of the sensors during operation (i.e., SR, centre wavelength position, stray light, etc.). It is common for spectrometers to change their spectral and radiometric performance due to pressure or temperature variations during operations. As a result, spectral non-uniformities associated with changing centre wavelength position or SR during operations eventually impact the point spread function of the spectral detector element. Radiometric non-uniformities are associated with, for instance, temperature-dependent changes in dark noise (D'Odorico et al., 2010; Schlapfer et al., 2007). In situations where sensors deviate during operations from their nominal lab performance, or where they were imperfectly calibrated, the combination of modelled atmospheric functions with measured radiances is prone to error and even substantial uncertainties in retrieved fluorescence (Damm et al., 2011; Moreno et al., 2014).

The spatial footprint measured by instrumentation can have implications for the validity of assumptions used in atmospheric correction [Section 5]. For example, SIF retrievals using tower-based or airborne instrumentation with very small pixels (e.g., < 2 m) may be subject to artefacts due to greater dominance of geometric optical

scattering by canopy components and higher likelihood of measuring (partly) shaded surfaces (i.e., a reduced fraction of direct irradiance) (Damm et al., 2015b). This could violate atmospheric correction tools that assume fully illuminated, homogeneous, and Lambertian reflecting surfaces, with isotropic and volumetric scattering being the dominant scattering processes.

While the emphasis here is on passive sensing of SIF, the broader context of fluorescence evaluation includes active sensors and other spectral technologies helpful for studying fluorescence characteristics and the influence of multiple factors [Sections 2 and 8]. Active technologies tend to allow better control of excitation conditions and are well suited to measurement of parameters such as fluorescence yield (the metric often associated to plant physiology). They can be an important complement to passive devices for proximal field work.

6.6. Challenges and future directions in field and airborne sensing of SIF

Substantial progress has been achieved in measuring SIF in field settings using ground-based and airborne systems, with noteworthy prospects for applications [Section 8]. Airborne SIF sensors, for example, have been used to reveal pre-visual stress effects from a bacterial pathogen (*Xylella fastidiosa*) currently infecting economically vital crops worldwide (Zarco-Tejada et al., 2018) or were applied to early signs of photosynthetic down regulation during drought stress in various crop species (Yang et al., in press). Such applications will be supported by an expanding choice of available instruments which allows analysis of SIF across spatial scales. We expect that UAV-based sensors will become more available in the near future and that a next generation of *HyPlant*-like instruments will be developed. In light of the recommendations from Section 5 – for improved spatio-temporal capacity; flexibility to measure both red and far-red fluorescence (including the full emission spectrum of SIF); sufficiently high SR and SNR to allow accurate SIF retrieval; and the provision of surface reflectance VNIR spectra to support model inversion – it is evident that modern options are well on the way to realizing those objectives.

Some of the required techniques and corrections are well established for high-performance airborne systems, and they are being refined for miniaturized or lightweight sensors so as to avoid instrument and retrieval artefacts. Priorities for improvements include the correction of sensor stray light, non-linearity, and point-spread-function artefacts. [Straylight aspects have been covered by Coppo et al., 2017 in their discussion of the FLEX sensors, and it is instructive for sensors in general.] Overcoming the problem of illumination artefacts originating from geometric optical scattering in high-spatial-resolution data (i.e., individual scattering elements dominate the sensor's field-of-view; Kückenbrink et al., 2019) is still an open issue. With controlled field observations, it appears to be of smaller impact, but when airborne spectrometers with high spatial resolution are used, retrieval artefacts are possible and new retrieval concepts accounting for varying fractions of direct and diffuse irradiance components must be developed (Damm et al., 2015b). We expect that technical advances in ground-, tractor-, UAV-, and aircraft-based instruments will facilitate realization of the full potential of SIF techniques for applications in vegetation and crop management, and in validation and interpretation of SIF retrievals from satellite spectrometers. In this context, these sensors will complement satellite-based measurements and will provide SIF data at higher spatial and temporal scales, necessary for local mapping of natural ecosystems and in agriculture.

7. SIF measurement technologies – Satellite systems

7.1. Technological overview

Breakthroughs in understanding the effects of fluorescence on apparent reflectance, coupled with advances in modelling, SIF retrieval approaches, and sensor capabilities, have contributed to the realization of satellite-based SIF detection. In 1999, Marc-Philippe Stoll and colleagues proposed to the European Space Agency that a satellite mission, FLEX, be developed to measure SIF from terrestrial vegetation to support science and applications in agriculture, forestry and global change issues (Stoll et al., 1999). This concept was developed, evaluated, and refined over the ensuing years (ESA, 2015; Moreno et al., 2006; Rascher et al., 2008), and in 2015 FLEX was approved to be ESA's 8th Earth Explorer, with a projected launch date of 2022 (Drusch et al., 2017).

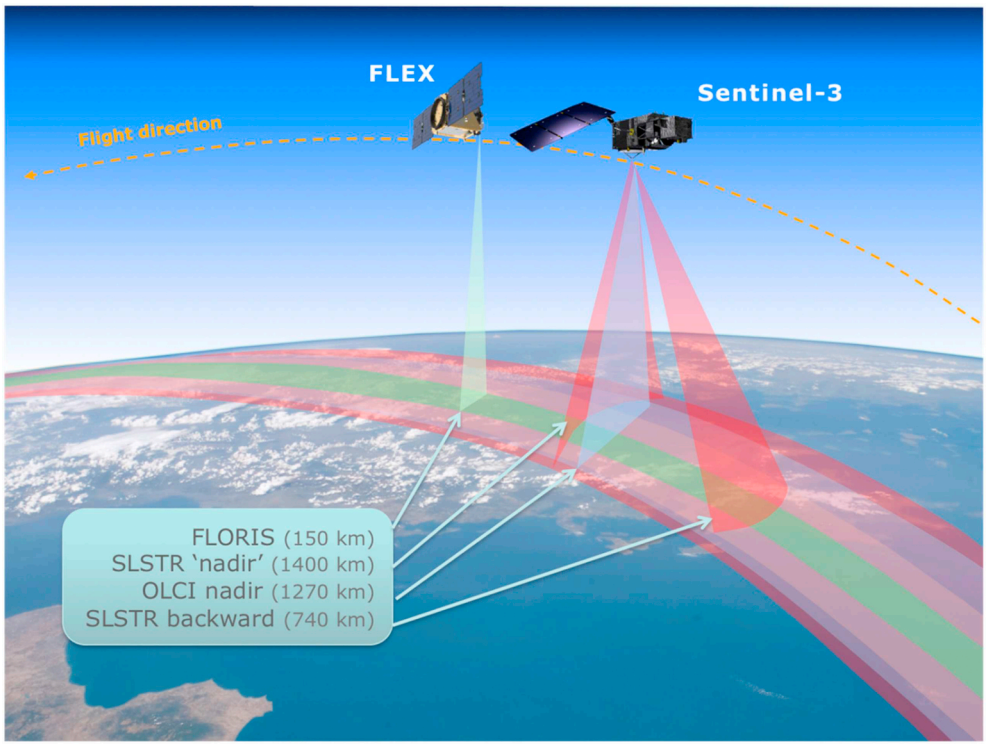

Fig. 12. Schematic of the FLEX two-satellite tandem mission combining the FLORIS free-flyer with an operational Sentinel-3 satellite having a 10:00 am equatorial overpass time. FLEX's 150 km nadir swath (green track) lies within the wider swath of the nadir OLCI camera (blue track, 1270 km). The SLSTR (red tracks) has a back-looking swath (740 km, 500 × 500 m^2 pixels) and a nadir swath (1400 km, 1000 × 1000 m^2 pixels). (Source: European Space Agency.) (For interpretation of the references to colour in this figure legend, the reader is referred to the web version of this article.)

During the preparatory activities, ESA commissioned scientific studies, field and airborne campaigns with prototype sensors, and modelling developments foundational to satellite-based SIF science (e.g., Ač et al., 2015; Magnani et al., 2009; Miller et al., 2005; Mohammed et al., 2016, 2014; Moreno et al., 2014; Pedrós et al., 2010; Rascher et al., 2015, 2009; Van der Tol et al., 2014, 2009b; Verhoef et al., 2018; Verrelst et al., 2016, 2015a; Zarco-Tejada et al., 2006).

Meanwhile, researchers independently working with the atmospheric chemistry satellite GOSAT reported that chlorophyll fluorescence could indeed be retrieved in the very narrow far-red wavelengths adjacent to the O_2-A band, albeit at very coarse spatial resolution ($\geq 0.5^{\circ}$), from which global maps could be produced (Frankenberg et al., 2011a, 2011b; Joiner et al., 2011). This exciting finding affirmed the earlier work of Guanter et al. (2007) who had shown that far-red SIF could be discriminated in terrestrial vegetation using the MERIS satellite sensor onboard EnviSat. Several satellite sensors designed primarily for measurement of atmospheric trace gases (e.g., CO_2, methane, and cloud parameters) have since been used to quantify SIF regionally and globally at coarse spatial scales. Retrievals from almost all of these missions have been of far-red SIF.

7.2. The FLuorescence EXplorer (FLEX): A tandem mission with Sentinel-3

FLEX is the first satellite mission designed specifically for SIF measurement. It will obtain the suite of SIF features and ancillary data types considered necessary for quantification and interpretation of vegetation parameters related to photosynthetic function (Drusch et al., 2017). The overarching scientific objective of FLEX is to achieve an improved understanding of global seasonally variable photosynthetic functioning and efficiency of vegetation, including physiological indicators of plant stress. The five-year global mission will cover terrestrial vegetation and coastal regions, including land areas between 75°N and 56°S, islands > 100 km^2, and coastal zones within 50 km of coastlines. FLEX will produce imagery and maps at 300 × 300 m^2 spatial resolution, intended for the monitoring of vegetation at scales of local to landscape-level management units and ecosystems (Drusch et al., 2017).

FLEX will be deployed in a tandem mission with Sentinel-3 (Fig. 12), a European operational satellite carrying the Ocean and Land Colour Imager (OLCI) and the Sea and Land Surface Temperature Radiometer (SLSTR) sensors. The FLEX mission will carry a single payload, the FLuORescence Imaging Spectrometer (FLORIS), which is a dual-spectrometer imaging system consisting of narrow-band (high SR)

Table 3
Current and future satellite missions. Instruments in space or planned for launch that have SIF measurement capability (red SIF wavelengths ~680–690 nm, and far-red ~730–780 nm). A few of these also capture PRI wavelengths (between 520 and 580 nm). This list is not exhaustive; e.g., follow-on missions such as OCO-3 and GOSAT-2 are not included. Pixel quality refers to the combined utility of data products for uses based on influences of sensor specifications (spectral range and parameters retrieved, FWHM, SNR), spatial resolution, temporal collections, and Level 2–4 mission product support. (For interpretation of the references to colour in this table, the reader is referred to the web version of this article.)

Mission / Sensor	Status / Launch	Coverage	Footprint (km^2)	Equatorial Overpass Time	Repeat Cycle	Spectral Range (nm)	FWHM (nm) (SIF)	SIF & PRI meas.	SNR	SIF Pixel Quality	Adequate Support meas.
FLEX / FLORIS	Selected/ ~2022	56°S-75°N	0.3 x 0.3	10:00	27 day	500-780	0.3-2.0	FR, R, full, PRI			
Sentinel-5P/ TROPOMI	In Orbit	Global	7 x 7	13:30	16 day	270-500 675-775 2305-2385	0.5	FR, full, (R)			
MetOp / GOME-2	In Orbit	Global	40 x 40 40 x 80	09:30	29 day	270-790	0.5	FR, full, (R), PRI			
TEMPO	Selected/ ~2019	CONUS	4 x 5	GEO	1 hour	290-490 540-740	0.6	(FR), PRI			
OCO-2	In Orbit	Global**	1.3 x 2.2	13:30	16 day	757-775	0.04	FR			
GOSAT / TANSO-FTS	In Orbit	Global**	10 x 10	13:00	3 day	758-775 1560-1720 1920-2080 5550-14300	0.025	FR			
MTG-S / Sentinel-4	Selected/ 2019	Europe	8 x 8	GEO	1 hour	290-500 750-775	0.12	FR			
GeoCARB	Selected/ 2021	N & S America	~3 x 3	GEO	8 hour	757-772 1591-1621 2045-2085 2300-2345	0.05	FR	N/A	N/A	N/A
TanSat / ACGS	In Orbit	Global**	2 x 2	13:30	16 day	758-778 1594-1624 2042-2082	0.04	FR			

References:
FLEX: Drusch et al. (2017)
TROPOMI: Guanter et al. (2015)
GOME-2: Joiner et al. (2016, 2013)
TEMPO: Zoogman et al. (2016)
OCO-2: Frankenberg et al. (2014)
GOSAT: Joiner et al. (2011); Frankenberg et al. (2011b)
Sentinel-4: Meijer et al. (2014)
GeoCARB: O'Brien et al. (2016)
TanSat: Du et al. (2018)

Excellent Very Good Good Fair Poor

** = Global coverage, discontinuous
GEO = Geo-Synchronous Orbit
FR = Far-Red SIF
R = Red SIF
Full = 650-780 nm
(FR), (R) = retrieval possible
PRI = Reflectance @ 530nm, and reference wavelength (usually 570nm)

and wide-band (low SR) sensors, measuring the spectral range of 500–780 nm to capture the full SIF emission as well as reflectance for vegetation indices. Instruments from S-3 will provide atmospheric and thermal data, geolocation, and other ancillary data (ESA, 2018).

Unique products from the FLEX/S-3 tandem mission include: (i) total fluorescence emission (F_{tot}, 650–780 nm); (ii) red and far-red fluorescence at the peaks (F_{685}, F_{740}) and at the O_2-B and O_2-A features (F_{687}, F_{760}); (iii) photosynthetic activity estimates; and (iv) biophysical variables and indices derived from reflectance (e.g., surface fractional vegetation cover; canopy chlorophyll content; LAI; the fraction of photosynthetically active radiation absorbed by chlorophyll, $fAPAR_{chl}$; and PRI) (ESA, 2018). These products will be derived from harmonized TOA synergy data products using FLORIS, OLCI, and SLSTR radiances cross-calibrated, geometrically co-registered, and ortho-rectified to a common 300 × 300 m^2 grid. Higher-level products include physiological response variables derived from temporal composites and spatial mosaics (e.g., activation/deactivation of photosynthesis; fluorescence quantum efficiency; and PSII and PSI contributions). These data are expected to improve estimation of GPP and surface fluxes at the local scale and to provide indicators of plant stresses that could reduce or compromise productivity and functional resilience. While the spatial resolution of FLEX exceeds existing satellite missions being used for SIF, it is not of the very high spatio-temporal granularity suited to small-scale farming. Also, the monthly repeat cycle (i.e., nadir view of the same area) at low latitude is not geared to applications requiring very frequent sampling – but at high latitudes, FLEX revisits (i.e., off-nadir view) will be more frequent, for example, 1–2 weeks in boreal areas, owing to orbital overlap, but also subject to viewing angle effects (Middleton et al., 2018; Wei et al., 2018). Studies currently underway for FLEX are investigating error analytics for mission products, and refinement of Cal/Val strategies, with fine-tuning of algorithms as required. The FLEX mission design and a conceptual framework for SIF applications have been described in detail elsewhere (e.g., Coppo et al., 2017; Drusch et al., 2017; ESA, 2018, 2015; Mohammed et al., 2014).

7.3. Atmospheric chemistry satellites used for SIF retrieval

Several global SIF datasets have been produced using spaceborne spectrometers that were originally designed for atmospheric chemistry applications (Table 3). In all cases, retrieval has been based on the utilization of FLs [Section 5.2.2].

The FL in-filling approach was pursued independently by Joiner et al. (2011), Frankenberg et al. (2011a, 2011b), and Guanter et al. (2012), with global application to the TANSO-FTS on the Japanese satellite, GOSAT. This high-spectral-resolution instrument has a channel covering the O_2-A band. The original purpose of the O_2-A band channel was to quantify the effects of aerosols and clouds on carbon dioxide (CO_2) and methane (CH_4) estimation. Several isolated FLs can be observed within this channel on either side of the O_2-A band, enabling retrieval of SIF. While the first global maps of SIF were generated from TANSO-FTS, its low SNR and relatively low sampling necessitated averaging the data over larger footprints (~2° latitude by 2° longitude) to obtain reliable contiguous coverage.

A similar channel in NASA's OCO-2 includes a high SR grating spectrometer designed to measure CO_2. Observations of SIF from OCO-2, have been compared with SIF results from the airborne CFIS instrument (Frankenberg et al., 2018; Sun et al., 2018, 2017). The OCO-2 ground footprint is much smaller than that of TANSO-FTS and it has denser sampling that enables more precise gridded measurements. But the higher spatial resolution of OCO-2 comes with a trade-off in that it does not provide contiguous orbital collections nor complete global coverage with its 10 km-wide swath. The higher repeat cycle (on the order of days) afforded by wide-swath satellite sensors designed for global analyses of atmospheric trace gases prompted Joiner et al. (2013) to examine whether those moderate-spectral-resolution sensors could be used reliably to quantify SIF. These include GOME-2 and similar sensors such as SCIAMACHY (which operated onboard the EnviSat satellite until contact was lost in 2012). They do have spectral coverage throughout the SIF emission range, but their ground footprints tend to be large. For example, SCIAMACHY's native footprint is approximately 30 km by 60 km for the nominal nadir mode that applies to red SIF, but due to onboard spectral averaging to reduce data volumes, the resolution is degraded to 30 km by 240 km for far-red SIF observations. GOME-2 spatial footprints are 40 km by 80 km in the nominal wide-swath mode, or 40 km by 40 km in a reduced-swath mode. There are currently two GOME-2 instruments in orbit: the GOME-2A (on the MetOp-A satellite), which operated in the nominal mode from January 2007 through mid-July 2013 and since then is

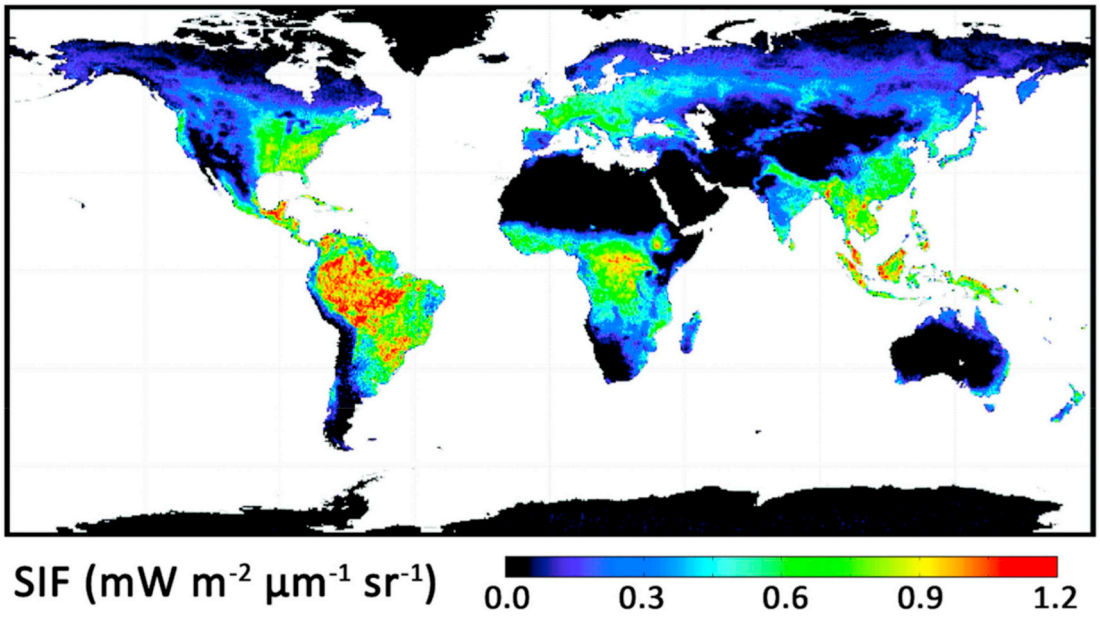

Fig. 13. Global map showing the 2009 annual average of observations for far-red SIF derived from the GOME-2 satellite sensor, utilizing observations acquired throughout 2009. (Source: Joiner et al., 2013.) (For interpretation of the references to colour in this figure legend, the reader is referred to the web version of this article.)

operating in the small-swath mode; and GOME-2B (on MetOp-B) which has operated in the nominal mode since mid-2013.

Joiner et al. (2013) showed that GOME-2 data could be used for discrimination of far-red SIF and that they produced higher fidelity global monthly maps of the far-red SIF emission as compared with GOSAT. A sample global map for annually integrated far-red SIF is shown in Fig. 13. Such retrieval is possible with GOME-2 due to its SR of ~0.5 nm in the SIF emission region, a high SNR (> ~1000), and a wider spectral coverage interval that surrounds the far-red peak (at 740 nm) and enables a fitting window between 712 and 775 nm. Monthly maps of far-red SIF have been produced at higher spatial resolution (typically ~0.5° latitude by 0.5° longitude) than was possible with GOSAT, and somewhat noisier maps could be made with similar spatial resolution at weekly time scales. [Note also that retrievals of the red SIF have been reported using GOME-2 and SCIAMACHY (Joiner et al., 2016; Wolanin et al., 2015; see also Section 5).]

Europe's S-5P satellite, carrying TROPOMI, was launched in late 2017 and flies in formation with NASA's Suomi National Polar Partnership satellite, timed for an early afternoon overpass. It provides daily SIF observations of similar or better quality as compared to those from GOME-2 and SCIAMACHY but at a much higher spatial resolution of 7 km × 7 km (Köhler et al., 2018a; Guanter et al., 2015). TROPOMI far-red SIF retrievals show that its mapping capabilities far surpass those of its predecessors, offering intriguing opportunities to map SIF at biome scales (Köhler et al., 2018a; Guanter et al., 2015).

Another advance will be from geostationary Earth orbit (GEO) spectrometers. Several planned GEO missions should provide a significant upgrade in temporal resolution of satellite-derived SIF as compared to currently available information, although at variable coarse spatial resolutions. The Tropospheric Emissions Monitoring of Pollution (TEMPO) mission will provide hourly scans over much of North America (Zoogman et al., 2016). Spectral coverage from the ultraviolet up to the near infrared (~740 nm) – with only one gap near 500 nm – should allow for determination of red and possibly far-red SIF as well as other vegetation indices. The Sentinel-4 GEO spectrometer on the Meteosat Third Generation-Sounder (MTG-S) satellite and the planned Geostationary Carbon Cycle Observatory (GeoCarb) instrument, like GOSAT and OCO-2, will have spectral coverage of the O_2-A band and its shoulders (Meijer et al., 2014; Moore III and Crowell, 2018; O'Brien et al., 2016) for Europe and the Americas, respectively. Their SRs of 0.05–0.12 nm are sufficient to retrieve far-red SIF using FL methodology, several times per day.

7.4. Factors affecting SIF retrieval accuracy of satellite data

Several issues complicate current satellite SIF retrievals. Large-footprint instruments in particular are affected by clouds and aerosols that contaminate the vast majority of observations. Since the atmosphere modifies the depth of atmospheric absorption features such as the O_2 bands used in SIF detection, one benefit of using FLs instead of O_2 bands for satellite SIF retrieval is that atmospheric effects do not modify the relative depth of the FLs (although the absolute depths are still attenuated by aerosol scattering). The impact of clouds when using far-red FLs has been studied by several research groups (Frankenberg et al., 2012; Köhler et al., 2015; Guanter et al., 2015) who have concluded that a sufficient amount of SIF emitted by the canopy is seen by the satellite even in the presence of optically thin or moderate amounts of broken clouds (optical thicknesses < ~5). However, this is an open topic that requires more study (W. Verhoef, personal communication). Compared to SIF, clouds and aerosols have a greater impact on

Table 4
Studies investigating remotely detected SIF in terrestrial vegetation for photosynthesis and stress detection. Tc: canopy temperature; Ta: air temperature. ***Vegetation:*** **C:** cropland; **F:** forest; **G:** grassland; **O:** orchard; **V:** various biomes. ***Scale:*** **G:** ground-based; **A:** airborne-based; **S:** satellite-based. ***SIF:*** **R:** red; **FR**: far-red; **PR:** R/FR fluorescence peak ratio; **F-SIF:** full SIF emission.

Objective	Vegetation	Scale	SIF	Publication examples
Photosynthesis and its estimation				
Absorbed PAR	C, F, O	G	FR	Cui et al., 2017a; Miao et al., 2018; Wagle et al., 2016; Yang et al., 2015; Zhang et al., 2016a
Diurnal dynamics	C, F	G, A	R, FR	Cogliati et al., 2015a; Damm et al., 2010; Middleton et al., 2017; Schickling et al., 2016; Sobrino et al., 2011
GPP (empirical)	C, F, G, V	G, A, S	R, FR	Alden et al., 2016; Berkelhammer et al., 2017; Chang et al., 2016; Gentine and Alemohammad, 2018; Goulas et al., 2017; Guan et al., 2015; Hu et al., 2018a; Guanter et al., 2014; Köhler et al., 2018b; Li et al., 2018a; Nichol et al., 2019; Sun et al., 2018, 2017; Wieneke et al., 2016
GPP (modelled)	V	S	FR	Luus et al., 2017; MacBean et al., 2018; Parazoo et al., 2014; Qiu et al., 2018; Thum et al., 2017; Verma et al., 2017; Wagle et al., 2016; Yoshida et al., 2015
Light use efficiency	C, F, G, V	G, S	R, FR	Cheng et al., 2013; Miao et al., 2018; Song et al., 2018; Walther et al., 2018; Verma et al., 2017; Yang et al., 2015
NPP	C	S	FR	Patel et al., 2018
Phenological stage	C	G	R, FR	Daumard et al., 2012; Miao et al., 2018
Seasonal dynamics	C, F, G, O, V	G, A, S	R, FR	Colombo et al., 2018; Koffi et al., 2015; Joiner et al., 2014; Meroni et al., 2011; Nichol et al., 2019; Parazoo et al., 2013; Rascher et al., 2015; Rossini et al., 2010; Smith et al., 2018; Wang et al., 2018; Wieneke et al., 2018; Wyber et al., 2017; Zarco-Tejada et al., 2013b
Vegetation type	C, F, G, V	G, A, S	R, FR	Damm et al., 2015a; Guan et al., 2016; Guanter et al., 2012; Li et al., 2018b; Liu et al., 2017; Madani et al., 2017; Rascher et al., 2009; Rossini et al., 2016; Sun et al., 2018
Stress detection				
Bacterial infection	O	A	FR	Zarco-Tejada et al., 2018
Fungal infection	C, F	A	FR	Calderón et al., 2015; Hernández-Clemente et al., 2017
Heat	C	S	FR	Guan et al., 2016; Song et al., 2018
Herbicide	C, G	G, A	R, FR	Pinto et al., 2016; Rossini et al., 2015
Nitrogen deficit	C	G	FR, PR	Cendrero-Mateo et al., 2016; Middleton et al., 2018 (review)
Transpiration	F	G	F-SIF	Lu et al., 2018b
Water deficit, drought	C, F, O, V	G, A, S	R, FR, PR	Daumard et al., 2010; Koren et al., 2018; Lee et al., 2013; Ma et al., 2016; Sanders et al., 2016; Sun et al., 2015; Wang et al., 2016; Wieneke et al., 2018, 2016; Xu et al., 2018; Yang et al., in press; Zarco-Tejada et al., 2012; Zuromski et al., 2018
Ancillary indices				
Chlorophyll content	C. O	G, A, S	R, FR	Panigada et al., 2014; Zhou et al., 2016; Zarco-Tejada et al., 2018, 2013b; Zhang et al., 2014
EVI	V	S	FR	Ma et al., 2016
MTCI	C	S	FR	Zhang et al., 2014
NDVI	C, F, G	G, A	R, FR	Garzonio et al., 2017; Rascher et al., 2009
PRI	C, G	G, A, S	FR, PR	Middleton et al., 2017; Paul-Limoges et al., 2018; Schickling et al., 2016; Verma et al., 2017
Tc-Ta; *or* Tc	C, F, O	A	FR	Calderón et al., 2015; Middleton et al., 2017; Zarco-Tejada et al., 2018, 2012

reflectance-based indices such as the Normalized Difference Vegetation Index (NDVI), as demonstrated with radiative transfer simulations by Guanter et al. (2015).

Another issue that affects all current coarse-spatial-scale sensors is systematic instrument errors. This was first found in GOSAT data, where it was coined 'zero-level offset'. The general problem is that non-zero values for SIF often get retrieved when zero values are expected (such as over the Sahara). These biases – which may have complex dependencies on radiance levels and may vary over time – must be accounted for in order to obtain accurate SIF estimates. [The causes of zero-level offset for different types of instrumentation and their mitigation strategies are discussed by Frankenberg et al. (2011b), Guanter et al., (2012), Köhler et al. (2015), Khosravi et al. (2015), and Joiner et al. (2016, 2012).]

Finally, overall sensor degradation occurs at greater or lesser rates in all satellite-based instruments and should be tracked and quantified. Degradation – which might be sudden or discontinuous – can be due to temperature changes, high radiation exposure, mechanical wear and tear, particles adhering to lenses, jolts from space debris, etc. This issue is particularly evident in data acquired by the very high-SR instruments used for atmospheric chemistry. Koren et al. (2018) and Zhang et al. (2018c) have identified possible artefacts in published GOME-2 SIF results that may have been due to sensor degradation. This underscores the need for consideration of such effects when using long-term records for analysis of SIF trends over time.

7.5. Challenges and future directions in satellite sensing of SIF

Earth observation from space provides a powerful way to assess and monitor the status of the biosphere. The potential of satellite-based SIF as an indicator of large-scale photosynthetic activity is evident from the growing body of literature examining global SIF patterns and dynamics (Frankenberg and Berry, 2018) [Section 8].

Although retrieval of SIF using space-based sensors offers an exciting new tool for studying vegetation dynamics, there are a number of challenges to basic understanding of carbon and water cycles at macroscales. The greatest challenge is to develop measurement and modelling approaches that bridge the SIF emission's vertical pathway and profile through the atmosphere, from vegetation at the surface to the observing satellite sensor above the Earth – in other words, we need reliable upscaling and downscaling capabilities in both temporal and spatial dimensions for SIF and carbon/water/energy processes. From basic science, it is known that chlorophyll fluorescence is influenced directly or indirectly by environmental and biological factors and this is not considered in a comprehensive way in the current satellite-based approaches. These factors often are manifested at the local scale, but tend to be overlooked or averaged out in large footprints and/or monthly aggregates (Magnani et al., 2014; Verrelst et al., 2016). Consequently, it is also essential that calibration and validation methods be developed to (i) prove conclusively whether satellite-retrieved SIF measures the same biological processes as ground-based instruments, and (ii) provide reliable quantitative results at local as well as global scales. The atmospheric chemistry satellites all have wide swaths to facilitate global coverage. Thus far, no corrections have been applied to account for the directional effects in the retrieved SIF values due to off-nadir viewing directions, and this definitely should be included in mature versions of the data processing chain for SIF. Also important will be consideration of the surface anisotropy of SIF (Middleton et al., 2018; Verhoef et al., 2018), which has received insufficient attention to date. Therefore, future retrieval schemes will likely be necessary to consider a number of factors not currently addressed, including surface anisotropy, surface reflectance, and aerosol type/amount.

While the atmospheric chemistry missions have provided novel and compelling large-scale information about SIF, the pressing societal applications in agriculture, food security, and forest ecology and management require high spatial resolution (≤ 0.5 km) as well as frequent observations, as prescribed by the application. With atmospheric chemistry missions, the observations are frequent but the footprints can be large. Future geostationary missions will provide moderate but variable spatial scale (e.g., 2–5 km^2) observations at several times of day (i.e., diurnally) for specific regions of the world. With FLEX, a higher spatial resolution will be possible globally, but observations will be less frequent. There is an obvious synergy between these different satellite SIF capabilities for achieving global mapping of vegetation health across the Earth's land surfaces. For future operational monitoring of the health of our ecosystems and food sources, we will want to have both aspects: frequent SIF measurements, at local scales.

8. Applications of remotely sensed SIF

Remotely detected SIF in terrestrial vegetation has been investigated for use in stress detection, estimation of photosynthesis and GPP, and tracking of temporal and phenological changes in different vegetation types. Table 4 shows examples from the last decade (see also reviews by Ač et al., 2015; Frankenberg and Berry, 2018; Malenovský et al., 2009; Meroni et al., 2009; Middleton et al., 2018). These investigations have been facilitated by advances in measurement technologies, retrieval methods, and modelling of physiological and radiative transfer processes.

8.1. Studies – and lessons learned

8.1.1. Ground-based canopy studies

Ground-based studies have shown the potential of SIF as an indicator of photosynthesis (Goulas et al., 2017; Pérez-Priego et al., 2015; Rascher et al., 2009; Rossini et al., 2010; Yang et al., 2015), transpiration (Lu et al., 2018b), and stress effects (Daumard et al., 2010; Xu et al., 2018) – and also its sensitivity to vegetation phenology (Daumard et al., 2012), and diurnal and seasonal dynamics (Meroni et al., 2011; Hu et al., 2018b; Rascher et al., 2009; Wyber et al., 2017). Further, they have provided insights into satellite-based findings of a relationship (sometimes even linear) between far-red SIF and GPP, and the factors that can complicate this relationship.

For SIF-GPP linkages, it is evident from the studies – and from modelling analyses [Section 4.6] – that far-red SIF is strongly associated with APAR (Cui et al., 2017a; Miao et al., 2018; Rossini et al., 2010; Wieneke et al., 2018; Yang et al., 2015; Zhang et al., 2016a). When APAR is constant, SIF might indicate LUE (Cheng et al., 2013; Yang et al., 2015; Zhang et al., 2016a). But Wohlfahrt et al. (2018) showed that even with constant APAR, the red or far-red SIF accounted for < 35% of the variability in GPP, whereas air temperature explained 77%. Empirical studies also point to a stronger association of far-red SIF to environmental conditions and structural effects than to GPP (Nichol et al., 2019; Paul-Limoges et al., 2018; Pérez-Priego et al., 2015). Sometimes corrections for such effects have helped to improve far-red SIF-GPP linkages (Nichol et al., 2019). Also normalization of fluorescence data by incident PAR, APAR, or APAR of photosynthetic components of the vegetation – to obtain quantum yield – has been done (Damm et al., 2010; Rascher et al., 2009; Rossini et al., 2010). In homogeneous crop canopies, Hu et al. (2018a) upscaled far-red SIF to a daily value using a PAR-based correction factor and obtained improved correlation with daily GPP.

Where a SIF-GPP relationship is found, its form can vary. In forest and crop sites, it was hyperbolic on stress-free days but linear under stressful conditions, possibly a result of reduced midday SIF values under stress (Paul-Limoges et al., 2018). Linearization was also seen with spatio-temporal scaling or aggregation of SIF data (e.g., Damm et al., 2015a, 2015b; Zhang et al., 2016a). Goulas et al. (2017) concluded for wheat that a simple linear SIF-GPP relationship might apply only in certain circumstances, such as when using far-red SIF and in the presence of a high dynamic range of green biomass and a low range of LUE variation. Studying crops and mixed forests, Liu et al. (2017)

suggested that the photosynthetic pathway (e.g., C_3, C_4) should be considered when analyzing far-red SIF-GPP correlations and diurnal patterns.

Ground-based studies confirm the influences of chlorophyll content, canopy structure and heterogeneity on remotely detected SIF, through effects on re-absorption and scattering within canopies. Stronger re-absorption of red than far-red SIF can be manifested as a decreased ratio of red to far-red SIF, as is observed when scaling from the leaf to the canopy, or with increasing leaf chlorophyll content, or with erectophile leaf inclination under high light (Daumard et al., 2012; Fournier et al., 2012). Also, the magnitude of the far-red SIF signal detected at TOC can be affected depending on the interplay of illumination geometry with leaf inclination and orientation, which can change during the day (Migliavacca et al., 2017b; Pinto et al., 2017). Such factors, in addition to inherent differences in SIF emission at the photosystem level, help to account for the variations seen among plant functional types or species, including higher SIF from some crop species than from broadleaf and needleleaf vegetation (Rossini et al., 2016).

Research into diurnal and inter-day changes in SIF have shown that far-red SIF measured across days was affected mainly by chlorophyll content, whereas diurnal changes reflect photosynthetic activity (Cogliati et al., 2015a; Pinto et al., 2016). A midday depression in far-red SIF during sunny days was associated with increased NPQ in mixed forest or crop canopies (Paul-Limoges et al., 2018). A more modest reduction in far-red SIF during early afternoon was found in winter wheat (Rascher et al., 2009), coincident with maximal light intensity, but red SIF closely tracked PPFD. Louis et al. (2005) saw a depression in fluorescence at the leaf level but not in the canopy of a pine forest, and suggested the cause may have been a canopy structural effect that moderated the intensity of light penetrating into deeper canopy layers, thereby reducing the need for NPQ.

Remotely detected SIF can indicate stress effects and transpiration status. The meta-analysis of Ač et al. (2015) concluded that canopy red or far-red SIF declines with water stress, while the ratio of red to far-red fluorescence increases with nitrogen deficit. Red and far-red SIF can also be early indicators of water stress and of recovery – but red SIF signals tend to be 'noisier' under stress (Daumard et al., 2010; Xu et al., 2018). Far-red SIF has been used to estimate transpiration during the growing season, but only in unstressed vegetation and when leaf area is not so high as to affect scattering and re-absorption of SIF (Lu et al., 2018b).

Consideration of NPQ is necessary for interpretation of SIF in the context of photosynthetic activity or stress effects (Atherton et al., 2016; Cheng et al., 2013; Daumard et al., 2010; Xu et al., 2018). Using PRI (or modified versions) as an indicator of NPQ has been effective for short-term assessments (i.e., over hours or a few days) when chlorophyll and structural traits are stable, and can help to improve estimation of gross productivity (e.g., Pérez-Priego et al., 2015; Rossini et al., 2010). Otherwise, PRI is subject to structural, anisotropic, and illumination effects that can confound links to NPQ behaviour (Schickling et al., 2016). Over longer timeframes, PRI in boreal evergreen conifers, has been shown to be more closely aligned with seasonally changing carotenoid-to-chlorophyll pigment ratios and shifting leaf albedo during periods of deep cold than with NPQ (Wong and Gamon, 2015). That is consistent with the findings of Wyber et al. (2017) who observed that, at seasonal scales, SIF was principally correlated with increased *constitutive* (rather than *regulated*) heat dissipation along with changes in leaf irradiance and electron transport rate.

SIF adjustments related to vegetation phenology have been found. Daumard et al. (2012) reported that during early growth in sorghum, the red SIF (687 nm) increased rapidly, then became saturated even as far-red SIF (760 nm) continued to increase. During growth, the ratio of red to far-red SIF was lower in the canopy than in leaves and decreased with increasing leaf chlorophyll content (likely due to re-absorption of red SIF). Meroni et al. (2011) found that in grassland, far-red SIF increased in spring, peaked in summer, then declined in late summer, responding primarily to the amount of chlorophyll in the canopy and the intensity of PPFD. The review by Middleton et al. (2018) of their studies with corn spoke to the combined effects of water stress, phenological state, and anisotropy on red and far-red SIF.

Ground-based and modelling studies have been informative on the respective utility of red and far-red SIF. Reviews by Ač et al. (2015) and Middleton et al. (2018) indicated the importance of the ratio of red to far-red SIF for identifying nitrogen deficiency, and modelling exercises using SCOPE (Verrelst et al., 2016, 2015b) identified benefits to retrieving both emissions – especially in heterogeneous canopies – for estimation of photosynthetic variables. In comparison, Goulas et al. (2017) found far-red SIF in wheat was more closely aligned to GPP. A complication for red SIF is its susceptibility to re-absorption, which can reduce TOC signals (Rascher et al., 2009).

Overall, ground-based canopy studies have revealed prospects for SIF in research and extended applications, but they also show that extraneous factors can make interpretation tricky.

8.1.2. Airborne-based studies

Studies using airborne techniques have demonstrated the added value of imaging and mapping of spatial distribution or spatio-temporal trends of SIF for stress detection (Rascher et al., 2015; Zarco-Tejada et al., 2013b). Also, hyperspectral imagery of canopies has revealed the influence of vegetation stand age on red SIF, surface anisotropic effects on far-red SIF, ecosystem-specific effects on far-red SIF-GPP relationships, and spatio-temporal scaling impacts on the linearization of far-red SIF-GPP linkages (Colombo et al., 2018; Damm et al., 2015a, 2015b; Zarco-Tejada et al., 2013b). Airborne-retrieved data have delineated natural quantitative ranges in SIF values for different vegetation types (Garzonio et al., 2017) and helped to clarify diurnal as well as canopy functional versus structural influences on SIF (Middleton et al., 2017; Rascher et al., 2015, 2009; Schickling et al., 2016; Sobrino et al., 2011).

In stress detection, SIF assessed via airborne approaches has been effective in detection of plant diseases (Calderón et al., 2015, 2013; Hernández-Clemente et al., 2017; Zarco-Tejada et al., 2018), water stress (Panigada et al., 2014; Wieneke et al., 2016; Zarco-Tejada et al., 2012), and herbicide stress (Rossini et al., 2015). Recently, Zarco-Tejada et al. (2018) were able to identify incipient infection in olive trees by the pathogen *Xylella fastidiosa* with prediction accuracies exceeding 80%. Their approach combined fluorescence, thermography, and spectral indicators of chlorophyll content and vegetation structural changes. They suggested the importance of defining a spectral bandset combination that enables retrieval of the most sensitive host-plant traits linked with a specific disease. For detection of *Phytophthora* infection, advanced modelling strategies have helped to decipher aggregated heterogeneous pixels of complex vegetation systems (Hernández-Clemente et al., 2017).

With respect to herbicide stress, red and far-red SIF were able to track variations in photosynthetic efficiency caused by a chemical known to inhibit photosynthesis and selectively intensify fluorescence, whereas surface reflectance was almost unaffected (Rossini et al., 2015). This trial demonstrated the capability of SIF to detect herbicide damage before the appearance of visual symptoms.

In the presence of water stress, a helpful index to support interpretation of SIF changes has been the difference in temperature between the plant canopy and the surrounding air (Calderón et al., 2015; Panigada et al., 2014; Zarco-Tejada et al., 2012). When stress induces stomatal closure, e.g., in the cases of water deficit or high vapour pressure deficit, evaporative cooling is restricted and foliage can warm to above air temperature, with a concomitant increase in NPQ and a decrease in SIF. The temperature differential can be an alternative or complementary index to PRI (Panigada et al., 2014; Schickling et al., 2016), assuming accurate canopy and air temperature data are obtainable.

As with ground-based and satellite studies, SIF retrieved from airborne sensors has been evaluated for estimation of GPP. Zarco-Tejada et al. (2013b) used UAVs to investigate spatio-temporal trends of far-red SIF and other narrow-band physiological and structural indices, and found that canopy SIF and indices related to chlorophyll content and LUE (i.e., PRI) had a similar seasonal trend as GPP assessed from EC towers at the time of the flights. Also, combinations of observational and modelling approaches have been used to improve forward modelling of GPP (Wieneke et al., 2016) and to depict linearization of SIF-GPP relationships with leaf-to-canopy and temporal scaling (Damm et al., 2015a).

To support future operational applications, Garzonio et al. (2017) studied far-red SIF in different vegetation types (crops, meadow, broadleaf species) using the HyUAS (UAV) system. They found diverse average SIF values which could have arisen due to strong species-related canopy directional effects. They further noted the existence of potentially complex overlaps and cross-effects among vegetation types. Finally, they anticipated valuable developments using integrative methods based on combined analysis of reflectance and SIF. Such developments have now been demonstrated using airborne (*HyPlant*) reflectance and SIF data acquired over agricultural crops (Yang et al., in press), wherein the combination of RTMs, TOC reflectance and TOC SIF were used to separate physiological effects from those of structure and other factors (pigments, dry matter, water).

In applications of SIF, age effects should be considered. In different even-aged stands of loblolly pine forest, young stands had a nearly two-fold higher red SIF yield than plantations older than 10–15 years, but the far-red SIF was constant (Colombo et al., 2018). This effect was interpreted as arising mainly from stomatal limitation in the older vegetation, with possible residual influences from canopy structure with aging and higher re-absorption of the red SIF. Middleton et al. (2017) assessed the same sites diurnally and found that temperature differences between the forest canopy and surrounding air had greater fluctuation in young versus older stands.

8.1.3. Satellite-based studies

Over the short lifetime of the global satellite SIF data era, a number of papers have reported that far-red SIF from current satellites has the potential to indicate large-scale photosynthetic activity. First trials with GOSAT showed a high correlation of retrieved SIF with data-driven GPP results at coarse global and annual scales (Frankenberg et al., 2011b), although a per-biome dependency in the SIF-to-GPP ratio was also identified (Guanter et al., 2012). Joiner et al. (2014) analyzed a time series of SIF retrievals and compared them with GPP estimates from data-driven and process-based models and measurements from eddy covariance flux towers. They found a good correspondence between the temporal trajectories of retrieved far-red SIF and GPP, which performed as well as remote sensing-based vegetation parameters. Initial indications are that far-red SIF might also contain information about LUE – as shown for tundra vegetation, and this aspect warrants further study (Walther et al., 2018).

Global SIF measurements retrieved from GOSAT and GOME-2 satellites for ecosystem-level monitoring applications have been published. Far-red SIF data from GOME-2 were shown to have a higher sensitivity to crop photosynthesis than reflectance-based vegetation indices and data-driven GPP models, the latter failing to capture the high GPP levels found in some areas of the US Corn Belt (Guanter et al., 2014). This finding was applied to produce estimates of crop photosynthetic capacity using SIF (Guan et al., 2016; Zhang et al., 2018a; Zhang et al., 2014). Zhang et al. (2014) tuned the maximal carboxylation capacity (V_{cmax}) in SCOPE to match simulated-to-satellite observed SIF, and found an improvement in GPP estimation compared to use of an a priori value for V_{cmax}. In their approach, the values of other parameters in SCOPE were obtained from ancillary satellite data. Guan et al. (2016) used a more direct empirical relation to derive the electron transport rate from observed SIF per unit of APAR. The estimates of GPP that they obtained – after multiplication of ETR by a photosynthetic-pathway-dependent electron use efficiency – were an improvement over other satellite-derived approaches considered.

Several satellite-based trials have reported the potential of far-red SIF to indicate drought and temperature stress at ecosystem scales (Berkelhammer et al., 2017; Koren et al., 2018; Song et al., 2018; Sun et al., 2015; Wang et al., 2018, 2016; Wu et al., 2018; Yoshida et al., 2015; Zuromski et al., 2018). Others have used far-red SIF to monitor the dynamics of photosynthesis, for example, in the Amazon forest (e.g., Alden et al., 2016; Guan et al., 2015; Köhler et al., 2018b; Koren et al., 2018; Lee et al., 2013; Parazoo et al., 2013; Yang et al., 2018a), high-latitude forests (Jeong et al., 2017; Walther et al., 2016), tundra ecosystems (Luus et al., 2017; Walther et al., 2018), dryland ecosystems of southwestern North America (Smith et al., 2018; Zhang et al., 2016c), and across Australia (Ma et al., 2016; Sanders et al., 2016). The links between large-scale far-red SIF and GPP (e.g., He et al., 2017; Koffi et al., 2015; Zhang et al., 2018b) have resulted in the use of SIF to analyze the coupling between carbon and water fluxes at regional to global scales (e.g., Alemohammad et al., 2017; Cui et al., 2017b; Green et al., 2017; Madani et al., 2017; Qiu et al., 2018; Wagle et al., 2016; Zhang et al., 2016b) and to benchmark GPP representations and other parameters in global models (e.g., Chang et al., 2016; Lee et al., 2015; MacBean et al., 2018; Parazoo et al., 2014; Thum et al., 2017; Walker et al., 2017).

Methods to downscale SIF spatially from large-pixel instruments such as GOME-2 to smaller scales using higher-resolution imager data also have been developed (Duveiller and Cescatti, 2016; Gentine and Alemohammad, 2018; Joiner et al., 2018). Lately, the advent of higher-spatial-resolution data from OCO-2 has enabled new possibilities (e.g., Lu et al., 2018a; Sun et al., 2018; Wei et al., 2018; Zhang et al., 2018d), including direct comparisons between far-red SIF retrievals and tower-based GPP for the understanding of SIF-GPP relationships (Sun et al., 2017). For instance, Verma et al. (2017) looked at the effect of environmental conditions on the relationship between far-red SIF and GPP at a grassland site and concluded that the linear relationship is more robust at ecosystem scale than the theory based on leaf-level processes might suggest, but that NPQ (besides APAR and LUE) might need to be explicitly factored into GPP estimations in future analyses. (Considering the results of ground-based and airborne studies, this is a definite requirement.) Wood et al. (2017) also took advantage of direct comparisons between SIF derived from OCO-2 observations and tower-based estimates of GPP to investigate the effect of different spatial and temporal scales on SIF-GPP relationships. They found a robust linear GPP-SIF scaling that is sensitive to plant physiology but insensitive to the spatial or temporal scale. Li et al. (2018a) performed similar comparisons between OCO-2 SIF retrievals and tower-level GPP to show a linear relationship between SIF and GPP in temperate forests. It was further shown, in a study of the Indo-Gangetic Plans of India, that far-red SIF is related to net primary productivity (NPP) and that SIF values for C_4-crop-dominated areas were higher than for C_3-crop districts during summer yet low during winter (Patel et al., 2018). In comparison, Zhang et al. (2018e) cautioned that identifying a near-universal linear relationship between OCO-2 SIF and GPP may be complicated by sun-sensor angle considerations related to OCO-2's three observation modes (nadir, glint, and target) and their different geometries. These types of studies are expected to become more comprehensive as further OCO-2 and also TROPOMI results become available (Li et al., 2018b).

8.2. Summary of SIF drivers and influential factors

Correct interpretation of SIF data is essential in applications, as multiple factors can influence SIF results. It is essential to understand sources of uncertainty in SIF-photosynthesis relationships at a range of scales (Ryu et al., 2019) and to keep those aspects in mind when

Table 5
Drivers of steady-state fluorescence, processes that may be affected, and ecological and temporal scales of influence. ***Process:*** **A:** absorption of incident light; **R:** re-absorption of fluorescence; **S:** fluorescence scattering; **PQ:** photochemical quenching; **NPQ:** non-photochemical quenching; **OP:** other photoprotection. ***Ecological scale:*** **L:** leaf; **C:** canopy; **E:** ecosystem; **B:** biome. ***Temporal scale:*** **ST** (short-term)**:** seconds, minutes, hours, diurnal; **MT** (medium-term)**:** days, weeks; **LT** (long-term)**:** months, years; **SV:** seasonal variation. **Definitions of ecological scales**: *Leaf*: a single leaf or leaf cluster on a single plant; *Canopy*: a single plant or monospecific closed canopy stand; *Ecosystem*: a mixed-species stand with closed or open heterogeneous structure; *Biome*: a major habitat (e.g., tundra, grassland, tropical rainforest) with multiple ecosystems and heterogeneous structure. (For interpretation of the references to colour in this table, the reader is referred to the web version of this article.)

Fluorescence driver	**Process potentially affected**						**Ecological scale**				**Temporal scale**			
Vegetation traits and processes	A	R	S	PQ	NPQ	OP	L	C	E	B	ST	MT	LT	SV
age [9, 41]	•	•	•	•	•	•	•	•				•	•	
carboxylation capacity (e.g. V_{cmax}) [1, 26]				•			•	•			•	•	•	•
chlorophyll content [8, 21, 36]	•	•	•	•			•	•				•	•	•
chloroplast movements [4, 11]	•	•	•			•	•				•			
electron transport rate [36, 39]				•			•	•			•	•	•	•
epicuticular wax [8, 13]	•		•			•	•	•				•	•	•
evapotranspiration [10]				•		•	•	•			•	•		•
fraction functional PSII reaction centres [28]				•			•				•	•	•	•
fraction open PSII reaction centres [36]				•			•				•			
leaf area index, LAI distribution [1, 37]	•	•	•					•				•	•	•
leaf inclination, heliotropism [26]	•	•	•	•		•		•			•			
leaf internal anatomy [8, 13, 20, 21, 49]	•	•	•	•			•	•				•	•	
leaf thickness [19]	•	•	•				•	•				•	•	
light use efficiency [25, 29, 36, 50]	•			•			•	•			•	•	•	•
mesophyll conductance [14, 32]				•		•	•	•			•	•	•	•
non-chlorophyll pigments [8, 17, 20]	•	•	•		•	•	•	•			•	•	•	•
non-foliar photosynthesis [20]	•			•				•			•	•	•	•
phenological stage [8, 18, 21, 25, 34]	•	•	•	•	•	•	•	•				•	•	•
photodamage [21, 36]				•			•	•				•	•	•
photoinhibition (reversible) [21, 36, 39]				•		•	•	•			•	•	•	•
photorespiration [5, 29, 36]				•		•	•	•			•	•	•	•
photosynthetic pathway (C_3, C_4) [29, 33, 52]	•			•		•	•	•				•	•	•
photosystem state transitions [36]	•	•		•		•	•				•			
photosystem stoichiometry (PSII:PSI) [36]	•			•		•	•	•				•	•	•
PSII efficiency (quantum yield) [36, 39]				•			•	•			•	•	•	•
species, plant functional type [20, 21, 23]	•	•	•	•	•	•		•	•	•		•	•	•
stomatal conductance [7, 24]				•		•	•				•	•	•	•
surface albedo [15, 28]	•		•	•				•	•	•	•	•	•	•
thermal dissipation – constitutive [36]						•	•	•				•	•	•
thermal dissipation – regulated [36]					•		•				•	•		
water content [21, 25]			•	•			•	•			•	•	•	•
vegetative competition [6, 27, 30]	•	•	•	•			•	•	•			•	•	•
Environmental, atmospheric, and stress factors														
air temperature; cold or heat stress [8, 21, 36]	•		•	•	•	•	•	•	•	•	•	•	•	•
atm. aerosols/pollutants/O_3 [5, 21, 35, 46, 47]	•		•	•		•	•	•	•	•	•	•	•	•
carbon dioxide concentration [2, 31]				•			•	•	•	•	•	•	•	•
cloud cover [45]	•	•	•	•				•	•		•	•		•
daylength [42]	•	•	•	•		•	•	•	•			•	•	•
herbicide stress [17, 21, 28, 39]	•			•	•	•	•	•	•		•	•		•
incident light intensity [20, 21, 39, 43, 44]	•			•	•	•	•	•	•		•	•	•	•
incident light spectral quality [8, 20, 21]	•	•	•	•		•	•	•	•		•	•	•	•
nutrient deficiency, toxicity [8, 21, 29]	•	•		•	•	•	•	•	•			•	•	•
oxygen concentration [40]	•	•	•	•		•	•	•	•		•	•	•	•
pathogen / pest stress [3, 8, 53]	•	•	•	•	•	•	•	•	•			•	•	•
relative humidity, VPD [12, 36]	•			•	•	•	•	•	•		•	•		•
solar zenith angle [51]	•	•	•	•		•	•	•	•		•	•	•	•
surface (atmospheric) pressure [48]	•		•	•	•	•		•	•		•	•	•	•
water stress [8, 21, 25, 38, 44]	•	•	•	•	•	•	•	•	•			•	•	•
wind stress [16, 22]	•	•	•	•	•	•		•	•		•	•		•

[1] Alton, 2018; **[2]** Barták et al., 1999; **[3]** Bauer et al., 2000; **[4]** Brugnoli and Bjorkman, 1992; **[5]** Bussotti et al., 2011; **[6]** Carter et al., 1989; **[7]** Cendrero-Mateo et al., 2016; **[8]** Cerovic et al., 1999; **[9]** Colombo et al., 2018; **[10]** Corp et al., 2003; **[11]** Dall'Osto et al., 2014; **[12]** De Mattos and Lüttge, 2001; **[13]** Donaldson and Williams, 2018; **[14]** Flexas et al., 2012; **[15]** Frankenberg et al., 2011a; **[16]** Furuuchi et al., 2013; **[17]** García-Plazaola et al., 2015; **[18]** Goulas et al., 2017; **[19]** Knapp and Carter, 1998; **[20]** Lagorio et al., 2015; **[21]** Lichtenthaler and Rinderle, 1988; **[22]** Lucieer et al., 2014; **[23]** Madani et al., 2017; **[24]** Magnani et al., 2009; **[25]** Middleton et al., 2018; **[26]** Migliavacca et al., 2017b; **[27]** Mohammed et al., 1998; **[28]** Moya and Cerovic, 2004; **[29]** Murchie and Lawson, 2013; **[30]** Musil et al., 2009; **[31]** Niinemets, 2010; **[32]** Niinemets et al., 2009; **[33]** Patel et al., 2018; **[34]** Pinto et al., 2016; **[35]** Pöhlker et al., 2012; **[36]** Porcar-Castell et al., 2014; **[37]** Rossini et al., 2016; **[38]** Sanders et al., 2016; **[39]** Schreiber, 2004; **[40]** Schreiber and Bilger, 1987; **[41]** Šesták and Šiffel, 1997; **[42]** Soukupová et al., 2008; **[43]** Sun et al., 2017; **[44]** Sun et al., 2015; **[45]** Thum et al., 2017; **[46]** Van Wittenberghe et al., 2014; **[47]** Van Wittenberghe et al., 2013; **[48]** Vasilkov et al., 2013; **[49]** Vogelmann et al., 1996; **[50]** Walther et al., 2018; **[51]** Wolanin et al., 2015; **[52]** Wu et al., 2018; **[53]** Zarco-Tejada et al., 2018.

planning and conducting SIF assessments. To that end, Table 5 summarizes factors and processes affecting chlorophyll fluorescence through their effects on light absorption, re-absorption, and scattering – as well as PQ, NPQ, and other photoprotective processes. The table is a synthesis of published papers and theoretical understanding from fundamental CF science, photosynthesis, ecophysiology, and remote sensing (updated from Mohammed et al., 2016). This information can support research planning, development of hypotheses, design of interpretative frameworks, and refinement of process-based models. In a given situation, not all aspects might be influential or equally important.

8.3. Challenges and future directions for applications

Several needs and future directions are indicated. First, planning should consider more deliberately the types of influential factors and drivers that could challenge interpretation in a given situation, so that photosynthetic functional information may be disentangled from extraneous effects. This will involve consideration of vegetation, site, and environmental factors; ancillary data at relevant spatial scales; and application of current modelling capabilities to analyze key drivers in a given situation and infer ancillary data needs (Verrelst et al., 2016, 2015a). A trend in satellite-based Earth Observation has been for acquisition of ancillary and complementary data from multiple sensors and missions, which could accelerate in the future as more technologies – operating at diverse spatial scales – become available (Lausch et al., 2017, 2016; Scholze et al., 2017). Geostationary satellite-based systems for SIF are a further helpful development to acquire high-temporal-resolution data from space.

Second, the capabilities of the remote sensor and the efficacy of retrieval algorithms must be critically appraised in light of the needs of the particular application and the drivers likely to be encountered. In practical or precision farming, for example, high spectral, spatial (~20 m), and temporal resolutions are desirable (Hank et al., 2018; Tremblay et al., 2012). In forestry, complex vegetation systems (i.e., multi-species, uneven-aged canopies with understory) are common and are among the most demanding situations for SIF retrieval and interpretation with respect to photosynthetic activity (Drusch et al., 2017; Paul-Limoges et al., 2018) – therefore, sufficient spatial and temporal resolution is needed to avoid representativeness errors. At high latitudes, SIF signals are inherently low and prone to systematic errors (Thum et al., 2017), so high SNR and radiometric stability are important for capturing changes in SIF accurately over space and time. The need to quantify NPQ is increasingly recognized, and for this purpose, reflectance in relevant spectral bands (e.g., for PRI and other indices) and determination of canopy/air temperature differentials may be informative (assuming stable leaf pigment pools and albedo for PRI use).

Validation of SIF retrievals began only recently for satellite-based data (e.g., Sun et al., 2017), and it is a key topic moving forward. Validation has been a challenge for sensors with limited spatial resolution, but prospects are improving with the newer generation of more-highly-resolved instruments (Frankenberg and Berry, 2018; Guanter et al., 2015). Development of some airborne sensors as demonstrators of satellite counterparts (e.g., *HyPlant* and CFIS, for the FLEX and OCO-2 missions, respectively) is a modern strategy that assists mission preparatory activities and post-launch validation and interpretation.

Third, there is a need for effective routines to ingest and convert SIF data into informative analytics for applications. SIF is already being incorporated into models addressing leaf and canopy SIF and photosynthesis (Van der Tol et al., 2016, 2014), re-absorption phenomena in leaves and canopies (Romero et al., 2018), and 3D vegetation architecture (Gastellu-Etchegorry et al., 2017). Downstream applications geared to decision-support service providers – and eventually non-expert users – would benefit from having automated procedures that seamlessly integrate, say, machine learning, neural networks, and model emulators (Rivera et al., 2015; Verrelst and Rivera, 2017) into accessible formats to enhance decision-making.

Finally, it is essential that future efforts continue to encompass the full suite of technological options allowing SIF measurement at different spatial and temporal scales. Hand-held devices, stationary and mobile field systems, UAVs and other airborne sensors, and satellite systems together afford versatility and flexibility for SIF analysis and validation activities. That capacity will help to address the needs of researchers for comprehensive or sophisticated analysis, and of practical users and resource managers needing 'on-the-go' and real-time assessments (Tremblay et al., 2012). Long-term baseline datasets are required to help benchmarking, and this type of work is underway (Nichol et al., 2019). To establish best practices and minimize risk of data artefacts, ongoing communication among sensor developers, researchers, and downstream users will be critical. It is an exciting undertaking for scientists and R&D professionals to navigate this new avenue of remote sensing with a diverse group of users from forestry, agriculture, and environmental domains.

This paper has focused on progress in remote sensing of fluorescence in terrestrial vegetation. But chlorophyll fluorescence has a long history of use with aquatic algal species (Duysens and Sweers, 1963), and there are established remote sensing applications in marine systems for quantifying chlorophyll and productivity (Blondeau-Patissier et al., 2014; Gower, 2016). Mouw et al. (2015) noted that until recently, satellite options for optical remote sensing of coastal and inland water bodies lagged behind those for open waters, and their paper underscored the need for orbital missions sampling on the scales of high variability encountered in these system while having the finer spectral, spatial and temporal detail needed for resampling in various applications. We anticipate that in optically complex waters, synergies will be possible across land and aquatic satellite missions suitable for analyzing SIF and related variables, such as with the Terra/Aqua (MODerate resolution Imaging Spectroradiometer, MODIS), Sentinel-5/5P (TROPOMI), and FLEX/Sentinel-3 missions.

9. Conclusion

Remote sensing of SIF is a promising optical indicator of photosynthetic status and related stress effects in terrestrial vegetation. The last few decades have seen great strides in measurement techniques, retrieval algorithms, and modelling of fluorescence-photosynthesis and radiative transfer processes. SIF measurement is now possible at all

biological, spatial, and temporal scales, with intriguing prospects for applications. These developments are noteworthy because SIF is not a simple phenomenon. To fully realize its potential, developments will be needed in all subject areas considered in this review so that researchers and applied users will be able to implement SIF technologies with confidence. Key topics for the coming years will be understanding and addressing confounding factors, validation of SIF retrievals and related products, provision of user-friendly options, and availability of technologies to meet the different needs of advanced and practical users. Encouraging results in satellite-based detection of SIF have been reported in the last decade which, in concert with ground-based and airborne methods, opens the door to studying actual photosynthetic dynamics in canopies, ecosystems, landscapes, and biomes. In the near future, there will be tailored space-based technologies for SIF, emphasizing quantifiable accuracy, availability of multiple SIF metrics, relevant ancillary data, and improved spectral, spatial and temporal resolutions. This will allow satellite-derived SIF to be used in local to landscape-scale applications – a benefit already evident with field and airborne-based SIF methods. The vision of the early proposers of satellite-based SIF detection was for optimized systems that would reduce uncertainties – and that vision remains strong today. As remote sensing of SIF matures, such systems will allow a more comprehensive appraisal of the capabilities of SIF and will help to shape the trajectory of the *next* 50 years.

Acronyms and abbreviations

APAR	Absorbed photosynthetically active radiation
ACGS	Atmospheric Carbon dioxide Grating Spectroradiometer
APEX	Airborne Prism EXperiment
BEPS	Boreal Ecosystems Productivity Simulator
BESS	Breathing Earth System Simulator
BOA	Bottom of atmosphere
BRDF	Bidirectional reflectance distribution function
CAM	Crassulacean acid metabolism
CASI	Compact Airborne Spectrographic Imager
CF	Chlorophyll fluorescence
CFIS	Chlorophyll Fluorescence Imaging Spectrometer
CLM	Community Land Model
DART	Discrete Anisotropic Radiative Transfer
EnviSat	Environmental Satellite
ESA	European Space Agency
EVI	Enhanced Vegetation Index
fAPAR	Fraction of photosynthetically active radiation absorbed
$fAPAR_{chl}$	Fraction of photosynthetically active radiation absorbed by chlorophyll
FL	Fraunhofer line
FLD	Fluorescence line depth
FLEX	FLuorescence EXplorer
FLORIS	FLuORescence Imaging Spectrometer
FluorWPS	Fluorescence model with Weighted Photon Spread
FRT	Fluorescence–Reflectance–Transmittance
F-SFM	Full-spectrum spectral fitting method
FWHM	Full width at half maximum
GEO	Geostationary Earth orbit
GeoCARB	Geostationary Carbon Cycle Observatory
GEP	Gross ecosystem productivity
GOSAT	Greenhouse gases Observing SATellite
GOME-2	Global Ozone Monitoring Experiment-2
GPP	Gross primary productivity
KMF	Kubelka-Munk Fluorescence
LEAF-NL	Laser Environmental Active Fluorosensor
LIF	Laser-induced fluorescence
LIFT	Laser-Induced (*or* Light-Induced) Fluorescence Transient
LSM	Land surface model
LUE	Light use efficiency
MERIS	MEdium Resolution Imaging Spectrometer
MetOp-A, -B	Meteorological Operational satellite-A or -B
MODIS	MODerate resolution Imaging Spectroradiometer
MODTRAN	MODerate resolution atmospheric TRANsmission
MTCI	MERIS Terrestrial Chlorophyll Index
MTG-S	Meteosat Third Generation-Sounder
NDVI	Normalized Difference Vegetation Index
NPP	Net primary productivity
NPQ	Non-photochemical quenching
OCO	Orbiting Carbon Observatory
OLCI	Ocean and Land Colour Imager
ORCHIDEE	ORganising Carbon and Hydrology In Dynamic EcosystEms
PAM	Pulse-amplitude modulation
PCA	Principal Component Analysis
PMFD	Passive Multi-wavelength Fluorescence Detector
PPFD	Photosynthetic photon flux density
PQ	Photochemical quenching
PRI	Photochemical Reflectance Index
PROSPECT	PROpriétés SPECTrales
PSII, PSI	Photosystem II or I
ROSIS	Reflective Optics System Imaging Spectrometer
RTM	Radiative transfer model
SAIL	Scattering of Arbitrarily Inclined Leaves
S-3	Sentinel-3
SCIAMACHY	SCanning Imaging Absorption spectroMeter for Atmospheric CHartographY
SCOPE	Soil-Canopy-Observation of Photosynthesis and Energy fluxes
SEN2FLEX	SENtinel-2 and FLuorescence EXperiment
S-5P	Sentinel-5 Precursor
SiB	Simple Biosphere Model
SVAT	Soil-Vegetation-Atmosphere-Transfer
SVD	Singular Value Decomposition
SFM	Spectral fitting methods
SLSTR	Sea and Land Surface Temperature Radiometer
SNR	Signal-to-noise ratio
SR	Spectral resolution
TanSat	Carbon Dioxide Observation Satellite
TANSO-FTS	Thermal And Near-infrared Sensor for carbon Observation – Fourier Transform Spectrometer
TEMPO	Tropospheric Emissions: Monitoring of Pollution
TOA	Top of atmosphere
TOC	Top of canopy
TROPOMI	TROPOspheric Monitoring Instrument
UAS	Unmanned aircraft system
UAV	Unmanned aerial vehicle
V_{cmax}	Maximal carboxylation capacity
VIRAF	Visible Infrared Reflectance Absorbance Fluorescence
VNIR	Visible and near-infrared

Acknowledgements

We are very grateful to individuals who provided helpful contributions during the preparation of this paper: Ralf Bock, Matthias Drusch, and Pedro José Jurado Lozano (European Space Agency), for providing information and the schematic Fig. 12 of the FLEX/S-3 tandem mission; David R. Landis (NASA/GSFC), for assistance with Table 3 on the satellite missions; and Dan Pernokis (P&M Technologies), for assistance in proofreading and editing the manuscript. In addition, we recognize the following funding: Zbyněk Malenovský was supported by the Australian Research Council Future Fellowship *Bridging Scales in Remote Sensing of Vegetation Stress* (FT160100477). Uwe Rascher acknowledges the SEN2Exp project funded by the European Space Agency in supporting part of this work.

References

Ač, A., Malenovský, Z., Olejníčková, J., Gallé, A., Rascher, U., Mohammed, G., 2015. Meta-analysis assessing potential of steady-state chlorophyll fluorescence for remote sensing detection of plant water, temperature and nitrogen stress. Remote Sens. Environ. 168, 420–436.

Agati, G., Mazzinghi, P., Fusi, F., Ambrosini, I., 1995. The F685/F730 chlorophyll fluorescence ratio as a tool in plant physiology: response to physiological and environmental factors. J. Plant Physiol. 145, 228–238.

Aldea, M., Frank, T.D., DeLucia, E.H., 2006. A method for quantitative analysis of spatially variable physiological processes across leaf surfaces. Photosynth. Res. 90, 161–172.

Alden, C.B., Miller, J.B., Gatti, L.V., Gloor, M.M., Guan, K., Michalak, A.M., Van der Laan-Luijkx, I.T., Touma, D., Andrews, A., Basso, L.S., Correia, C.S.C., Domingues, L.G., Joiner, J., Krol, M.C., Lyapustin, A.I., Peters, W., Shiga, Y.P., Thoning, K., Van der Velde, I., Van Leeuwen, T.T., Yadav, V., Diffenbaugh, N.S., 2016. Regional atmospheric CO_2 inversion reveals seasonal and geographic differences in Amazon net biome exchange. Glob. Change Biol. 22, 3427–3443.

Alemohammad, S.H., Fang, B., Konings, A.G., Aires, F., Green, J.K., Kolassa, J., Miralles, D., Prigent, C., Gentine, P., 2017. Water, energy, and carbon with artificial neural networks (WECANN): a statistically based estimate of global surface turbulent fluxes and gross primary productivity using solar-induced fluorescence. Biogeosciences 14, 4101–4124.

Allen, W.A., Gausman, H.W., Richardson, A.J., Thomas, J.R., 1969. Interaction of isotropic light with a compact plant leaf. J. Opt. Soc. Am. 59, 1376–1379.

Allen, W.A., Gayle, T.V., Richardson, A.J., 1970. Plant-canopy irradiance specified by the Duntley equations. J. Opt. Soc. Am. 60, 372–376.

Alonso, L., Gómez-Chova, L., Vila-Francés, J., Amorós-López, J., Guanter, L., Calpe, J., Moreno, J., 2008. Improved Fraunhofer line discrimination method for vegetation fluorescence quantification. IEEE Geosci. Remote Sens. Lett. 5, 620–624.

Alton, P.B., 2018. Decadal trends in photosynthetic capacity and leaf area index inferred from satellite remote sensing for global vegetation types. Agric. For. Meteorol. 250-251, 361–375.

Anderson, M.C., 1963. Studies of the woodland light climate: I. The photographic computation of light conditions. J. Ecol. 52, 27–41.

Atherton, J., Nichol, C.J., Porcar-Castell, A., 2016. Using spectral chlorophyll fluorescence and the photochemical reflectance index to predict physiological dynamics. Remote Sens. Environ. 176, 17–30.

Baker, N.R., Rosenqvist, E., 2004. Applications of chlorophyll fluorescence can improve crop production strategies: An examination of future possibilities. J. Exp. Bot. 55, 1607–1621.

Ball, J.T., Woodrow, I.E., Berry, J.A., 1987. A model predicting stomatal conductance and its contribution to the control of photosynthesis under different environmental conditions. In: Biggins, J. (Ed.), Progress in Photosynthesis Research. Martinus Nijhoff, Dordrecht, pp. 221–224.

Barón, M., Pineda, M., Pérez-Bueno, M.L., 2016. Picturing pathogen infection in plants. Z. Naturforsch. C 71, 355–368.

Barták, M., Raschi, A., Tognetti, R., 1999. Photosynthetic characteristics of sun and shade leaves in the canopy of *Arbutus unedo* L. trees exposed to *in situ* long-term elevated CO_2. Photosynthetica 37, 1–16.

Bauer, H., Plattner, K., Volgger, W., 2000. Photosynthesis in Norway spruce seedlings infected by the needle rust *Chrysomyxa rhododendri*. Tree Physiol. 20, 211–216.

Bendig, J., Gautam, D., Malenovský, Z., Lucieer, A., 2018. Influence of cosine corrector and UAS platform dynamics on airborne spectral irradiance measurements. In: Proc. IEEE International Geoscience and Remote Sensing Symposium (IGARSS), 22–27 July 2018, Valencia, Spain, pp. 8826–8829.

Benediktyová, Z., Nedbal, L., 2009. Imaging of multi-color fluorescence emission from leaf tissues. Photosynth. Res. 102, 169.

Bennett, D.I.G., Fleming, G.R., Amarnath, K., 2018. Energy-dependent quenching adjusts the excitation diffusion length to regulate photosynthetic light harvesting. Proc. Natl. Acad. Sci. U. S. A. 115, E9523–E9531.

Berk, A., Conforti, P., Kennett, R., Perkins, T., Hawes, F., Van den Bosch, J., 2014. MODTRAN6: A major upgrade of the MODTRAN radiative transfer code. In: Proc. SPIE 9088, Algorithms and Technologies for Multispectral, Hyperspectral, and Ultraspectral Imagery XX, 90880H, 13 June 2014.

Berkelhammer, M., Stefanescu, I.C., Joiner, J., Anderson, L., 2017. High sensitivity of gross primary production in the Rocky Mountains to summer rain. Geophys. Res. Lett. 44, 3643–3652.

Berni, J.A.J., Zarco-Tejada, P.J., Suárez, L., Fereres, E., 2009. Thermal and narrowband multispectral remote sensing for vegetation monitoring from an unmanned aerial vehicle. IEEE Trans. Geosci. Remote Sens. 47, 722–738.

Bilger, W., Björkman, O., 1990. Role of the xanthophyll cycle in photoprotection elucidated by measurements of light-induced absorbance changes, fluorescence and photosynthesis in leaves of *Hedera canariensis*. Photosynth. Res. 25, 173–185.

Blondeau-Patissier, D., Gower, J.F.R., Dekker, A.G., Phinn, S.R., Brando, V.E., 2014. A review of ocean color remote sensing methods and statistical techniques for the detection, mapping and analysis of phytoplankton blooms in coastal and open oceans. Prog. Oceanogr. 123, 123–144.

Boardman, N.K., Thorne, S.W., Anderson, J.M., 1966. Fluorescence properties of particles obtained by digitonin fragmentation of spinach chloroplasts. Proc. Natl. Acad. Sci. U. S. A. 56, 586–593.

Bolhàr-Nordenkampf, H.R., Long, S.P., Baker, N.R., Oquist, G., Schreiber, U., Lechner, E.G., 1989. Chlorophyll fluorescence as a probe of the photosynthetic competence of leaves in the field: a review of current instrumentation. Funct. Ecol. 3, 497–514.

Bonan, G.B., 1996. A land surface model (LSM version 1.0) for ecological, hydrological, and atmospheric studies: Technical description and user's guide. In: NCAR Technical Note NCAR/TN-417-STR. National Center for Atmospheric Research, Boulder, CO (United States). Climate and Global Dynamics Div. https://doi.org/10.5065/D6DF6P5X.

Bonan, G.B., Lawrence, P.J., Oleson, K.W., Levis, S., Jung, M., Reichstein, M., Lawrence, D.M., Swenson, S.C., 2011. Improving canopy processes in the community land model version 4 (CLM4) using global flux fields empirically inferred from FLUXNET data. J. Geophys. Res. Biogeosci. 116, G02014. https://doi.org/10.1029/2010JG001593.

Bornman, J.F., Vogelmann, T.C., Martin, G., 1991. Measurement of chlorophyll fluorescence within leaves using a fibreoptic microprobe. Plant Cell Environ. 14, 719–725.

Bradbury, M., Baker, N.R., 1981. Analysis of the slow phases of the *in vivo* chlorophyll fluorescence induction curve. Changes in redox state of photosystem II electron acceptors and fluorescence emission from photosystem I and II. Biochim. Biophys. Acta 635, 542–551.

Brewster, D., 1834. On the colours of natural bodies. Trans. R. Soc. Edinburgh 12, 538–545.

Brugnoli, E., Björkman, O., 1992. Chloroplast movements in leaves: influence on chlorophyll fluorescence and measurements of light-induced absorbance changes related to ΔpH and zeaxanthin formation. Photosynth. Res. 32, 23–35.

Burkart, A., Schickling, A., Cendrero Mateo, M.P., Wrobel, T.J., Rossini, M., Cogliati, S., Julitta, T., Rascher, U., 2015. A method for uncertainty assessment of passive sun-induced chlorophyll fluorescence retrieval using an infrared reference light. IEEE Sensors J. 15, 4603–4611.

Buschmann, C., 2007. Variability and application of the chlorophyll fluorescence emission ratio red/far-red of leaves. Photosynth. Res. 92, 261–271.

Buschmann, C., Lichtenthaler, H.K., 1988. Reflectance and chlorophyll fluorescence signatures in leaves. In: Lichtenthaler, H.K. (Ed.), Applications of Chlorophyll Fluorescence in Photosynthesis Research, Stress Physiology, Hydrobiology and Remote Sensing. Springer, Dordrecht, pp. 325–332.

Buschmann, C., Lichtenthaler, H.K., 1998. Principles and characteristics of multi-colour fluorescence imaging of plants. J. Plant Physiol. 152, 297–314.

Buschmann, C., Langsdorf, G., Lichtenthaler, H.K., 2000. Imaging of the blue, green, and red fluorescence emission of plants: an overview. Photosynthetica 38, 483–491.

Buschmann, C., Langsdorf, G., Lichtenthaler, H.K., 2009. Blue, green, red, and far-red fluorescence signatures of plant tissues, their multicolor fluorescence imaging, and application for agrofood assessment. In: Zude, M. (Ed.), Optical Monitoring of Fresh and Processed Agricultural Crops. Taylor & Francis / CRC Press, Boca Raton, pp. 272–319.

Bussotti, F., Desotgiu, R., Cascio, C., Pollastrini, M., Gravano, E., Gerosa, G., Marzuoli, R., Nali, C., Lorenzini, G., Salvatori, E., Manes, F., Schaub, M., Strasser, R.J., 2011. Ozone stress in woody plants assessed with chlorophyll a fluorescence. A critical reassessment of existing data. Environ. Exp. Bot. 73, 19–30.

Buurman, E.P., Sanders, R., Draaijer, A., Gerritsen, H.C., Van Veen, J.J.F., Houpt, P.M., Levine, Y.K., 1992. Fluorescence lifetime imaging using a confocal laser scanning microscope. Scanning 14, 155–159.

Calatayud, A., Roca, D., Martinez, P.F., 2006. Spatio-temporal variations in rose leaves under water stress conditions studied by chlorophyll fluorescence imaging. Plant Physiol. Biochem. 44, 564–573.

Calderón, R., Navas-Cortés, J.A., Lucena, C., Zarco-Tejada, P.J., 2013. High-resolution airborne hyperspectral and thermal imagery for early detection of *Verticillium* wilt of olive using fluorescence, temperature and narrow-band spectral indices. Remote Sens. Environ. 139, 231–245.

Calderón, R., Navas-Cortés, J.A., Zarco-Tejada, P.J., 2015. Early detection and quantification of *Verticillium* wilt in olive using hyperspectral and thermal imagery over large areas. Remote Sens. 7, 5584–5610.

Campbell, P.K.E., Middleton, E.M., McMurtrey, J.E., Corp, L.A., Chappelle, E.W., 2007. Assessment of vegetation stress using reflectance or fluorescence measurements. J. Environ. Qual. 36, 832–845.

Campbell, P.K.E., Middleton, E.M., Corp, L.A., Kim, M.S., 2008. Contribution of chlorophyll fluorescence to the apparent vegetation reflectance. Sci. Total Environ. 404, 433–439.

Carter, G.A., Paliwal, K., Pathre, U., Green, T.H., Mitchell, R.J., Gjerstad, D.H., 1989. Effect of competition and leaf age on visible and infrared reflectance in pine foliage. Plant Cell Environ. 12, 309–315.

Carter, G.A., Theisen, A.F., Mitchell, R.J., 1990. Chlorophyll fluorescence measured using the Fraunhofer line-depth principle and relationship to photosynthetic rate in the field. Plant Cell Environ. 13, 79–83.

Carter, G.A., Jones, J.H., Mitchell, R.J., Brewer, C.H., 1996. Detection of solar-excited chlorophyll *a* fluorescence and leaf photosynthetic capacity using a Fraunhofer line radiometer. Remote Sens. Environ. 55, 89–92.

Cecchi, G., Mazzinghi, P., Pantani, L., Valentini, R., Tirelli, D., De Angelis, P., 1994. Remote sensing of chlorophyll *a* fluorescence of vegetation canopies. 1. Near and far field measurement techniques. Remote Sens. Environ. 47, 18–28.

Celesti, M., Van der Tol, C., Cogliati, S., Panigada, C., Yang, P., Pinto, F., Rascher, U., Miglietta, F., Colombo, R., Rossini, M., 2018. Exploring the physiological information of sun-induced chlorophyll fluorescence through radiative transfer model inversion. Remote Sens. Environ. 215, 97–108.

Cendrero-Mateo, M.P., Moran, M.S., Papuga, S.A., Thorp, K.R., Alonso, L., Moreno, J., Ponce-Campos, G., Rascher, U., Wang, G., 2016. Plant chlorophyll fluorescence: active and passive measurements at canopy and leaf scales with different nitrogen treatments. J. Exp. Bot. 67, 275–286.

Cerovic, Z.G., Goulas, Y., Gorbunov, M., Briantais, J.-M., Camenen, L., Moya, I., 1996. Fluoresensing of water stress in plants: diurnal changes of the mean lifetime and yield of chlorophyll fluorescence, measured simultaneously and at a distance with a τ-LIDAR and a modified PAM-fluorimeter, in maize, sugar beet, and kalanchoë. Remote

Sens. Environ. 58, 311–321.
Cerovic, Z.G., Samson, G., Morales, F., Tremblay, N., Moya, I., 1999. Ultraviolet-induced fluorescence for plant monitoring: present state and prospects. Agronomie 19, 543–578.
Chaerle, L., Leinonen, I., Jones, H.G., Van der Straeten, D., 2007. Monitoring and screening plant populations with combined thermal and chlorophyll fluorescence imaging. J. Exp. Bot. 58, 773–784.
Chang, J., Ciais, P., Herrero, M., Havlik, P., Campioli, M., Zhang, X., Bai, Y., Viovy, N., Joiner, J., Wang, X., Peng, S., Yue, C., Piao, S., Wang, T., Hauglustaine, D.A., Soussana, J.-F., Peregon, A., Kosykh, N., Mironycheva-Tokareva, N., 2016. Combining livestock production information in a process-based vegetation model to reconstruct the history of grassland management. Biogeosciences 13, 3757–3776.
Chappelle, E.W., Williams, D.L., 1987. Laser-induced fluorescence (LIF) from plant foliage. IEEE Trans. Geosci. Remote Sens. GE-25, 726–736.
Chekalyuk, A.M., Hoge, F.E., Wright, C.W., Swift, R.N., 2000. Short-pulse pump-and-probe technique for airborne laser assessment of photosystem II photochemical characteristics. Photosynth. Res. 66, 33–44.
Chen, J.M., Leblanc, S.G., 1997. A four-scale bidirectional reflectance model based on canopy architecture. IEEE Trans. Geosci. Remote Sens. 35, 1316–1337.
Chen, J.M., Liu, J., Cihlar, J., Goulden, M.L., 1999. Daily canopy photosynthesis model through temporal and spatial scaling for remote sensing applications. Ecol. Model. 124, 99–119.
Cheng, Y.-B., Middleton, E.M., Zhang, Q., Huemmrich, K.F., Campbell, P.K.E., Corp, L.A., Cook, B.D., Kustas, W.P., Daughtry, C.S., 2013. Integrating solar induced fluorescence and the photochemical reflectance index for estimating gross primary production in a cornfield. Remote Sens. 5, 6857–6879.
Cogliati, S., Rossini, M., Julitta, T., Meroni, M., Schickling, A., Burkart, A., Pinto, F., Rascher, U., Colombo, R., 2015a. Continuous and long-term measurements of reflectance and sun-induced chlorophyll fluorescence by using novel automated field spectroscopy systems. Remote Sens. Environ. 164, 270–281.
Cogliati, S., Verhoef, W., Kraft, S., Sabater, N., Alonso, L., Vicent, J., Moreno, J., Drusch, M., Colombo, R., 2015b. Retrieval of sun-induced fluorescence using advanced spectral fitting methods. Remote Sens. Environ. 169, 344–357.
Cogliati, S., Colombo, R., Celesti, M., Tagliabue, G., Rascher, U., Schickling, A., Rademske, P., Alonso, L., Sabater, N., Schuettemeyer, D., Drusch, M., 2018. Red and far-red fluorescence emission retrieval from airborne high-resolution spectra collected by the Hyplant-Fluo sensor. In: Proc. IEEE International Geoscience and Remote Sensing Symposium (IGARSS), 22–27 July 2018, Valencia, Spain, pp. 3935–3938.
Collatz, G.J., Ball, J.T., Grivet, C., Berry, J.A., 1991. Physiological and environmental regulation of stomatal conductance, photosynthesis and transpiration: a model that includes a laminar boundary layer. Agric. For. Meteorol. 54, 107–136.
Colombo, R., Celesti, M., Bianchi, R., Campbell, P.K.E., Cogliati, S., Cook, B.D., Corp, L.A., Damm, A., Domec, J.-C., Guanter, L., Julitta, T., Middleton, E.M., Noormets, A., Panigada, C., Pinto, F., Rascher, U., Rossini, M., Schickling, A., 2018. Variability of sun-induced chlorophyll fluorescence according to stand age-related processes in a managed loblolly pine forest. Glob. Chang. Biol. 24, 2980–2996.
Coppo, P., Taiti, A., Pettinato, L., Francois, M., Taccola, M., Drusch, M., 2017. Fluorescence imaging spectrometer (FLORIS) for ESA FLEX mission. Remote Sens. 9, 649.
Corp, L.A., McMurtrey, J.E., Middleton, E.M., Mulchi, C.L., Chappelle, E.W., Daughtry, C.S.T., 2003. Fluorescence sensing systems: in vivo detection of biophysical variations in field corn due to nitrogen supply. Remote Sens. Environ. 86, 470–479.
Cui, T., Sun, R., Qiao, C., Zhang, Q., Yu, T., Liu, G., Liu, Z., 2017a. Estimating diurnal courses of gross primary production for maize: a comparison of sun-induced chlorophyll fluorescence, light-use efficiency and process-based models. Remote Sens. 9, 1267.
Cui, Y., Xiao, X., Zhang, Y., Dong, J., Qin, Y., Doughty, R.B., Zhang, G., Wang, J., Wu, X., Qin, Y., Zhou, S., Joiner, J., Moore III, B., 2017b. Temporal consistency between gross primary production and solar-induced chlorophyll fluorescence in the ten most populous megacity areas over years. Sci. Rep. 7, 14963.
Dai, Y., Dickinson, R.E., Wang, Y.-P., 2004. A two-big-leaf model for canopy temperature, photosynthesis, and stomatal conductance. J. Clim. 17, 2281–2299.
Dall'Osto, L., Cazzaniga, S., Wada, M., Bassi, R., 2014. On the origin of a slowly reversible fluorescence decay component in the *Arabidopsis npq4* mutant. Phil. Trans. R. Soc. B 369, 20130221.
Damm, A., Elbers, J.A., Erler, A., Giolis, B., Hamdi, K., Hutjes, R.W.A., Kosvancova, M., Meroni, M., Miglietta, F., Moersch, A., Moreno, J., Schickling, A., Sonnenschein, R., Udelhoven, T., Van der Linden, S., Hostert, P., Rascher, U., 2010. Remote sensing of sun-induced fluorescence to improve modeling of diurnal courses of gross primary production (GPP). Glob. Chang. Biol. 16, 171–186.
Damm, A., Erler, A., Hillen, W., Meroni, M., Schaepman, M.E., Verhoef, W., Rascher, U., 2011. Modeling the impact of spectral sensor configurations on the FLD retrieval accuracy of sun-induced chlorophyll fluorescence. Remote Sens. Environ. 115, 1882–1892.
Damm, A., Guanter, L., Laurent, V.C.E., Schaepman, M.E., Schickling, A., Rascher, U., 2014. FLD-based retrieval of sun-induced chlorophyll fluorescence from medium spectral resolution airborne spectroscopy data. Remote Sens. Environ. 147, 256–266.
Damm, A., Guanter, L., Paul-Limoges, E., Van der Tol, C., Hueni, A., Buchmann, N., Eugster, W., Ammann, C., Schaepman, M.E., 2015a. Far-red sun-induced chlorophyll fluorescence shows ecosystem-specific relationships to gross primary production: An assessment based on observational and modeling approaches. Remote Sens. Environ. 166, 91–105.
Damm, A., Guanter, L., Verhoef, W., Schläpfer, D., Garbari, S., Schaepman, M.E., 2015b. Impact of varying irradiance on vegetation indices and chlorophyll fluorescence derived from spectroscopy data. Remote Sens. Environ. 156, 202–215.
Daumard, F., Champagne, S., Fournier, A., Goulas, Y., Ounis, A., Hanocq, J.-F., Moya, I., 2010. A field platform for continuous measurement of canopy fluorescence. IEEE Trans. Geosci. Remote Sens. 48, 3358–3368.
Daumard, F., Goulas, Y., Champagne, S., Fournier, A., Ounis, A., Olioso, A., Moya, I., 2012. Continuous monitoring of canopy level sun-induced chlorophyll fluorescence during the growth of a sorghum field. IEEE Trans. Geosci. Remote Sens. 50, 4292–4300.
De Mattos, E.A., Lüttge, U., 2001. Chlorophyll fluorescence and organic acid oscillation during transition from CAM to C_3-photosynthesis in *Clusia minor* L. (Clusiaceae). Ann. Bot. 88, 457–463.
De Pury, D.G.G., Farquhar, G.D., 1997. Simple scaling of photosynthesis from leaves to canopies without the errors of big-leaf models. Plant Cell Environ. 20, 537–557.
De Wit, C.T., 1965. Photosynthesis of leaf canopies. In: Agricultural Research Report No. 663. PUDOC, Wageningen.
DeEll, J.R., Toivonen, P.M.A. (Eds.), 2003. Practical Applications of Chlorophyll Fluorescence in Plant Biology. Kluwer/Springer, Dordrecht.
Demmig-Adams, B., 1990. Carotenoids and photoprotection in plants: a role for the xanthophyll zeaxanthin. Biochim. Biophys. Acta 1020, 1–24.
Demmig-Adams, B., Adams III, W.W., Heber, U., Neimanis, S., Winter, K., Krüger, A., Czygan, F.-C., Bilger, W., Björkman, O., 1990. Inhibition of zeaxanthin formation and of rapid changes in radiationless energy dissipation by dithiothreitol in spinach leaves and chloroplasts. Plant Physiol. 92, 293–301.
Demmig-Adams, B., Cohu, C.M., Muller, O., Adams III, W.W., 2012. Modulation of photosynthetic energy conversion efficiency in nature: from seconds to seasons. Photosynth. Res. 113, 75–88.
Disney, M., 2016. Remote sensing of vegetation: potentials, limitations, developments and applications. In: Hikosaka, K., Niinemets, Ü., Anten, N.P.R. (Eds.), Canopy Photosynthesis: From Basics to Applications. Springer, Dordrecht, pp. 289–331.
Disney, M.I., Lewis, P., North, P.R.J., 2000. Monte Carlo ray tracing in optical canopy reflectance modelling. Remote Sens. Rev. 18, 163–196.
Dobrowski, S.Z., Pushnik, J.C., Zarco-Tejada, P.J., Ustin, S.L., 2005. Simple reflectance indices track heat and water stress-induced changes in steady-state chlorophyll fluorescence at the canopy scale. Remote Sens. Environ. 97, 403–414.
D'Odorico, P., Alberti, E., Schaepman, M.E., 2010. In-flight spectral performance monitoring of the Airborne Prism Experiment. Appl. Opt. 49, 3082–3091.
Donaldson, L., Williams, N., 2018. Imaging and spectroscopy of natural fluorophores in pine needles. Plants 7, 10.
Drusch, M., Moreno, J., Del Bello, U., Franco, R., Goulas, Y., Huth, A., Kraft, S., Middleton, E.M., Miglietta, F., Mohammed, G., Nedbal, L., Rascher, U., Schüttemeyer, D., Verhoef, W., 2017. The FLuorescence EXplorer mission concept - ESA's Earth Explorer 8. IEEE Trans. Geosci. Remote Sens. 55, 1273–1284.
Du, S., Liu, L., Liu, X., Zhang, X., Zhang, X., Bi, Y., Zhang, L., 2018. Retrieval of global terrestrial solar-induced chlorophyll fluorescence from TanSat satellite. Sci. Bull. 63, 1502–1512.
Duveiller, G., Cescatti, A., 2016. Spatially downscaling sun-induced chlorophyll fluorescence leads to an improved temporal correlation with gross primary productivity. Remote Sens. Environ. 182, 72–89.
Duysens, L.N.M., 1963. Role of two photosynthetic pigment systems in cytochrome oxidation, pyridine nucleotide reduction, and fluorescence. Proc. R. Soc. Lond. B 157, 301–313.
Duysens, L.N.M., Sweers, H.E., 1963. Mechanism of two photochemical reactions in algae as studied by means of fluorescence. In: Japanese Society of Plant Physiologists (Ed.), Studies on Microalgae and Photosynthetic Bacteria. A Collection of Papers. University of Tokyo Press, Tokyo, Japan, pp. 353–372.
ESA (European Space Agency), 2015. Report for Mission Selection: FLEX. ESA SP-1330/2 (2 Volume Series). 197 pp., Noordwijk (The Netherlands). https://esamultimedia.esa.int/docs/EarthObservation/SP1330-2_FLEX.pdf.
ESA (European Space Agency), 2018. FLEX Earth Explorer 8 Mission Requirements Document, Version 3.0, Issue Date 05/06/2018, ESA Earth and Mission Science Division, Ref: ESAEOP-SM/2221/MDru-md.
Evain, S., Camenen, L., Moya, I., 2001. Three channels detector for remote sensing of chlorophyll fluorescence and reflectance from vegetation. In: Proc. 8th International Symposium: Physical Measurements and Signatures in Remote Sensing, 8–12 January 2001, Aussois, France, pp. 395–400.
Farquhar, G.D., Von Caemmerer, S., Berry, J.A., 1980. A biochemical model of photosynthetic CO_2 assimilation in leaves of C_3 species. Planta 149, 78–90.
Fawcett, D., Verhoef, W., Schläpfer, D., Schneider, F.D., Schaepman, M.E., Damm, A., 2018. Advancing retrievals of surface reflectance and vegetation indices over forest ecosystems by combining imaging spectroscopy, digital object models, and 3D canopy modelling. Remote Sens. Environ. 204, 583–595.
Fernandez-Jaramillo, A.A., Duarte-Galvan, C., Contreras-Medina, L.M., Torres-Pacheco, I., Romero-Troncoso, R.J., Guevara-Gonzalez, R.G., Millan-Almaraz, J.R., 2012. Instrumentation in developing chlorophyll fluorescence biosensing: a review. Sensors 12, 11853–11869.
Flexas, J., Briantais, J.-M., Cerovic, Z., Medrano, H., Moya, I., 2000. Steady-state and maximum chlorophyll fluorescence responses to water stress in grapevine leaves: a new remote sensing system. Remote Sens. Environ. 73, 283–297.
Flexas, J., Escalona, J.M., Evain, S., Gulías, J., Moya, I., Osmond, C.B., Medrano, H., 2002. Steady-state chlorophyll fluorescence (Fs) measurements as a tool to follow variations of net CO_2 assimilation and stomatal conductance during water-stress in C_3 plants. Physiol. Plant. 114, 231–240.
Flexas, J., Barbour, M.M., Brendel, O., Cabrera, H.M., Carriqui, M., Díaz-Espejo, A., Douthe, C., Dreyer, E., Ferrio, J.P., Gago, J., Gallé, A., Galmés, J., Kodama, N., Medrano, H., Niinemets, Ü., Peguero-Pina, J.J., Pou, A., Ribas-Carbó, M., Tomás, M., Tosens, T., Warren, C.R., 2012. Mesophyll diffusion conductance to CO_2: An unappreciated central player in photosynthesis. Plant Sci. 193-194, 70–84.

Fournier, A., Daumard, F., Champagne, S., Ounis, A., Goulas, Y., Moya, I., 2012. Effect of canopy structure on sun-induced chlorophyll fluorescence. ISPRS J. Photogramm. Remote Sens. 68, 112–120.
Fournier, A., Daumard, F., Champagne, S., Ounis, A., Moya, I., Goulas, Y., 2014. Effects of vegetation directional reflectance on sun-induced fluorescence retrieval in the oxygen absorption bands. In: Proc. 5th International Workshop on Remote Sensing of Vegetation Fluorescence, 22–24 April 2014, Paris, France.
Franck, J., Herzfeld, K.F., 1941. Contribution to a theory of photosynthesis. J. Phys. Chem. 45, 978–1025.
Franck, J., French, C.S., Puck, T.T., 1941. The fluorescence of chlorophyll and photosynthesis. J. Phys. Chem. 45, 1268–1300.
Franck, F., Juneau, P., Popovic, R., 2002. Resolution of the photosystem I and photosystem II contributions to chlorophyll fluorescence of intact leaves at room temperature. Biochim. Biophys. Acta 1556, 239–246.
Frankenberg, C., Berry, J., 2018. Solar induced chlorophyll fluorescence: Origins, relation to photosynthesis and retrieval. In: Reference Module in Earth Systems and Environmental Sciences. vol. 3. Elsevier, pp. 143–162. https://doi.org/10.1016/B978-0-12-409548-9.10632-3.
Frankenberg, C., Butz, A., Toon, G.C., 2011a. Disentangling chlorophyll fluorescence from atmospheric scattering effects in O_2 A-band spectra of reflected sun-light. Geophys. Res. Lett. 38, L03801.
Frankenberg, C., Fisher, J.B., Worden, J., Badgley, G., Saatchi, S.S., Lee, J.-E., Toon, G.C., Butz, A., Jung, M., Kuze, A., Yokota, T., 2011b. New global observations of the terrestrial carbon cycle from GOSAT: patterns of plant fluorescence with gross primary productivity. Geophys. Res. Lett. 38, L17706.
Frankenberg, C., O'Dell, C., Guanter, L., McDuffie, J., 2012. Remote sensing of near-infrared chlorophyll fluorescence from space in scattering atmospheres: implications for its retrieval and interferences with atmospheric CO_2 retrievals. Atmos. Meas. Tech. 5, 2081–2094.
Frankenberg, C., O'Dell, C., Berry, J., Guanter, L., Joiner, J., Köhler, P., Pollack, R., Taylor, T.E., 2014. Prospects for chlorophyll fluorescence remote sensing from the Orbiting Carbon Observatory-2. Remote Sens. Environ. 147, 1–12.
Frankenberg, C., Köhler, P., Magney, T.S., Geier, S., Lawson, P., Schwochert, M., McDuffie, J., Drewry, D.T., Pavlick, R., Kuhnert, A., 2018. The chlorophyll fluorescence imaging spectrometer (CFIS), mapping far red fluorescence from aircraft. Remote Sens. Environ. 217, 523–536.
Freedman, A., Cavender-Bares, J., Kebabian, P.L., Bhaskar, R., Scott, H., Bazzaz, F.A., 2002. Remote sensing of solar-excited plant fluorescence as a measure of photosynthetic rate. Photosynthetica 40, 127–132.
Furuuchi, H., Jenkins, M.W., Senock, R.S., Houpis, J.L.J., Pushnik, J.C., 2013. Estimating plant crown transpiration and water use efficiency by vegetative reflectance indices associated with chlorophyll fluorescence. Open Journal of Ecology 3, 122–132.
Gamon, J.A., Surfus, J.S., 1999. Assessing leaf pigment content and activity with a reflectometer. New Phytol. 143, 105–117.
Gamon, J.A., Field, C.B., Bilger, W., Björkman, O., Fredeen, A.L., Peñuelas, J., 1990. Remote sensing of the xanthophyll cycle and chlorophyll fluorescence in sunflower leaves and canopies. Oecol 85, 1–7.
Gamon, J.A., Peñuelas, J., Field, C.B., 1992. A narrow-waveband spectral index that tracks diurnal changes in photosynthetic efficiency. Remote Sens. Environ. 41, 35–44.
Gamon, J.A., Serrano, L., Surfus, J.S., 1997. The photochemical reflectance index: An optical indicator of photosynthetic radiation use efficiency across species, functional types, and nutrient levels. Oecol. 112, 492–501.
Garbulsky, M.F., Filella, I., Peñuelas, J., 2014a. Recent advances in the estimation of photosynthetic stress for terrestrial ecosystem services related to carbon uptake. In: Alcaraz-Segura, D., Di Bella, C.M., Straschnoy, J.V. (Eds.), Earth Observation of Ecosystem Services. CRC Press, Boca Raton, pp. 39–62.
Garbulsky, M.F., Filella, I., Verger, A., Peñuelas, J., 2014b. Photosynthetic light use efficiency from satellite sensors: from global to Mediterranean vegetation. Environ. Exp. Bot. 103, 3–11.
García-Plazaola, J.I., Esteban, R., Fernández-Marín, B., Kranner, I., Porcar-Castell, A., 2012. Thermal energy dissipation and xanthophyll cycles beyond the *Arabidopsis* model. Photosynth. Res. 113, 89–103.
García-Plazaola, J.I., Fernández-Marín, B., Duke, S.O., Hernández, A., López-Arbeloa, F., Becerril, J.M., 2015. Autofluorescence: biological functions and technical applications. Plant Sci. 236, 136–145.
Garzonio, R., Di Mauro, B., Colombo, R., Cogliati, S., 2017. Surface reflectance and sun-induced fluorescence spectroscopy measurements using a small hyperspectral UAS. Remote Sens. 9, 472.
Gastellu-Etchegorry, J.P., Demarez, V., Pinel, V., Zagolski, F., 1996. Modeling radiative transfer in heterogeneous 3-D vegetation canopies. Remote Sens. Environ. 58, 131–156.
Gastellu-Etchegorry, J.-P., Yin, T., Lauret, N., Cajgfinger, T., Gregoire, T., Grau, E., Feret, J.-B., Lopes, M., Guilleux, J., Dedieu, G., Malenovský, Z., Cook, B.D., Morton, D., Rubio, J., Durrieu, S., Cazanave, G., Martin, E., Ristorcelli, T., 2015. Discrete anisotropic radiative transfer (DART 5) for modeling airborne and satellite spectroradiometer and LIDAR acquisitions of natural and urban landscapes. Remote Sens. 7, 1667–1701.
Gastellu-Etchegorry, J.-P., Lauret, N., Yin, T., Landier, L., Kallel, A., Malenovský, Z., Al Bitar, A., Aval, J., Benhmida, S., Qi, J., Medjdoub, G., Guilleux, J., Chavanon, E., Cook, B., Morton, D., Chrysoulakis, N., Mitraka, Z., 2017. DART: recent advances in remote sensing data modeling with atmosphere, polarization, and chlorophyll fluorescence. IEEE J. Sel. Top. Appl. Earth Obs. Remote Sens. 10, 2640–2649.
Gautam, D., Watson, C., Lucieer, A., Malenovský, Z., 2018. Error budget for geolocation of spectroradiometer point observations from an unmanned aircraft system. Sensors 18, 3465.
Gentine, P., Alemohammad, S.H., 2018. Reconstructed solar-induced fluorescence: a machine learning vegetation product based on MODIS surface reflectance to reproduce GOME-2 solar-induced fluorescence. Geophys. Res. Lett. 45, 3136–3146.
Genty, B., Meyer, S., 1995. Quantitative mapping of leaf photosynthesis using chlorophyll fluorescence imaging. Aust. J. Plant Physiol. 22, 277–284.
Genty, B., Briantais, J.-M., Baker, N.R., 1989. The relationship between the quantum yield of photosynthetic electron transport and quenching of chlorophyll fluorescence. Biochim. Biophys. Acta 990, 87–92.
Genty, B., Wonders, J., Baker, N.R., 1990. Non-photochemical quenching of F_0 in leaves is emission wavelength dependent: consequences for quenching analysis and its interpretation. Photosynth. Res. 26, 133–139.
Gerhards, M., Schlerf, M., Rascher, U., Udelhoven, T., Juszczak, R., Alberti, G., Miglietta, F., Inoue, Y., 2018. Analysis of airborne optical and thermal imagery for detection of water stress symptoms. Remote Sens. 10, 1139.
Gitelson, A.A., Buschmann, C., Lichtenthaler, H.K., 1998. Leaf chlorophyll fluorescence corrected for re-absorption by means of absorption and reflectance measurements. J. Plant Physiol. 152, 283–296.
Gitelson, A.A., Buschmann, C., Lichtenthaler, H.K., 1999. The chlorophyll fluorescence ratio F_{735}/F_{700} as an accurate measure of the chlorophyll content in plants. Remote Sens. Environ. 69, 296–302.
Gómez-Chova, L., Alonso-Chorda, L., Amoros-Lopez, J., Vila-Frances, J., Del Valle-Tascon, S., Calpe, J., Moreno, J., 2006. Solar induced fluorescence measurements using a field spectroradiometer. AIP Conf. Proc. 852, 274–281.
Gorbe, E., Calatayud, A., 2012. Applications of chlorophyll fluorescence imaging technique in horticultural research: a review. Sci. Hortic. 138, 24–35.
Goss, R., Lepetit, B., 2015. Biodiversity of NPQ. J. Plant Physiol. 172, 13–32.
Goudriaan, J., 1977. Crop micrometeorology: a simulation study. In: Simulation Monograph. PUDOC, Wageningen.
Goulas, Y., Fournier, A., Daumard, F., Champagne, S., Ounis, A., Marloie, O., Moya, I., 2017. Gross primary production of a wheat canopy relates stronger to far red than to red solar-induced chlorophyll fluorescence. Remote Sens. 9, 97.
Govindjee, 1995. Sixty-three years since Kautsky: chlorophyll *a* fluorescence. Aust. J. Plant Physiol. 22, 131–160.
Govindjee, 2004. Chlorophyll *a* fluorescence: A bit of basics and history. In: Papageorgiou, G.C., Govindjee (Eds.), Chlorophyll Fluorescence: A Signature of Photosynthesis. Kluwer, Dordrecht, pp. 1–41.
Gower, J., 2016. On the use of satellite-measured chlorophyll fluorescence for monitoring coastal waters. Int. J. Remote Sens. 37, 2077–2086.
Gower, J.F.R., Borstad, G.A., 1990. Mapping of phytoplankton by solar-stimulated fluorescence using an imaging spectrometer. Int. J. Remote Sens. 11, 313–320.
Green, J.K., Konings, A.G., Alemohammad, S.H., Berry, J., Entekhabi, D., Kolassa, J., Lee, J.-E., Gentine, P., 2017. Regionally strong feedbacks between the atmosphere and terrestrial biosphere. Nat. Geosci. 10, 410–414.
Grossmann, K., Frankenberg, C., Magney, T.S., Hurlock, S.C., Seibt, U., Stutz, J., 2018. PhotoSpec: a new instrument to measure spatially distributed red and far-red solar-induced chlorophyll fluorescence. Remote Sens. Environ. 216, 311–327.
Guan, K., Pan, M., Li, H., Wolf, A., Wu, J., Medvigy, D., Caylor, K.K., Sheffield, J., Wood, E.F., Malhi, Y., Liang, M., Kimball, J.S., Saleska, S.R., Berry, J., Joiner, J., Lyapustin, A.I., 2015. Photosynthetic seasonality of global tropical forests constrained by hydroclimate. Nat. Geosci. 8, 284–289.
Guan, K., Berry, J.A., Zhang, Y., Joiner, J., Guanter, L., Badgley, G., Lobell, D.B., 2016. Improving the monitoring of crop productivity using spaceborne solar-induced fluorescence. Glob. Change Biol. 22, 716–726.
Guanter, L., Alonso, L., Gómez-Chova, L., Amorós-López, J., Vila, J., Moreno, J., 2007. Estimation of solar-induced vegetation fluorescence from space measurements. Geophys. Res. Lett. 34, L08401.
Guanter, L., Alonso, L., Gómez-Chova, L., Meroni, M., Preusker, R., Fischer, J., Moreno, J., 2010. Developments for vegetation fluorescence retrieval from spaceborne high-resolution spectrometry in the O_2-A and O_2-B absorption bands. J. Geophys. Res. Atmos. 115 (D19), 303. https://doi.org/10.1029/2009JD013716. (D19303).
Guanter, L., Frankenberg, C., Dudhia, A., Lewis, P.E., Gómez-Dans, J., Kuze, A., Suto, H., Grainger, R.G., 2012. Retrieval and global assessment of terrestrial chlorophyll fluorescence from GOSAT space measurements. Remote Sens. Environ. 121, 236–251.
Guanter, L., Zhang, Y., Jung, M., Joiner, J., Voigt, M., Berry, J.A., Frankenberg, C., Huete, A.R., Zarco-Tejada, P., Lee, J.-E., Moran, M.S., Ponce-Campos, G., Beer, C., Camps-Valls, G., Buchmann, N., Dianelle, D., Klumpp, K., Cescatti, A., Baker, J.M., Griffis, T.J., 2014. Global and time-resolved monitoring of crop photosynthesis with chlorophyll fluorescence. Proc. Natl. Acad. Sci. U. S. A. 111, E1327–E1333.
Guanter, L., Aben, I., Tol, P., Krijger, J.M., Hollstein, A., Köhler, P., Damm, A., Joiner, J., Frankenberg, C., Landgraf, J., 2015. Potential of the TROPOspheric Monitoring Instrument (TROPOMI) onboard the Sentinel-5 Precursor for the monitoring of terrestrial chlorophyll fluorescence. Atmos. Meas. Tech. 8, 1337–1352.
Hank, T.B., Berger, K., Bach, H., Clevers, J.G.P.W., Gitelson, A., Zarco-Tejada, P., Mauser, W., 2018. Spaceborne imaging spectroscopy for sustainable agriculture: contributions and challenges. Surv. Geophys. https://doi.org/10.1007/s10712-018-9492-0.
He, L., Chen, J.M., Liu, J., Mo, G., Joiner, J., 2017. Angular normalization of GOME-2 sun-induced chlorophyll fluorescence observation as a better proxy of vegetation productivity. Geophys. Res. Lett. 44, 5691–5699.
Hemphill, W.R., Watson, R.D., Bigelow, R.C., Hessen, T.D., 1977. Measurement of luminescence of geochemically stressed trees and other materials. U.S. Geological Survey Professional Paper 1015, 93–112.
Hendrickson, L., Chow, W.S., Furbank, R.T., 2004. A simple alternative approach to assessing the fate of absorbed light energy using chlorophyll fluorescence. Photosynth. Res. 82, 73–81.
Hernández-Clemente, R., North, P.R.J., Hornero, A., Zarco-Tejada, P.J., 2017. Assessing the effects of forest health on sun-induced chlorophyll fluorescence using the

FluorFLIGHT 3-D radiative transfer model to account for forest structure. Remote Sens. Environ. 193, 165–179.
Herwitz, S.R., Johnson, L.F., Dunagan, S.E., Higgins, R.G., Sullivan, D.V., Zheng, J., Lobitz, B.M., Leung, J.G., Gallmeyer, B.A., Aoyagi, M., Slye, R.E., Brass, J.A., 2004. Imaging from an unmanned aerial vehicle: agricultural surveillance and decision support. Comput. Electron. Agric. 44, 49–61.
Hoge, F.E., Swift, R.N., 1981. Airborne simultaneous spectroscopic detection of laser-induced water Raman backscatter and fluorescence from chlorophyll *a* and other naturally-occurring pigments. Appl. Opt. 20, 3197–3205.
Hu, J., Liu, L., Guo, J., Du, S., Liu, X., 2018a. Upscaling solar-induced chlorophyll fluorescence from an instantaneous to daily scale gives an improved estimation of the gross primary productivity. Remote Sens. 10, 1663.
Hu, J., Liu, X., Liu, L., Guan, L., 2018b. Evaluating the performance of the SCOPE model in simulating canopy solar-induced chlorophyll fluorescence. Remote Sens. 10, 250.
Ireland, C.R., Long, S.P., Baker, N.R., 1984. The relationship between carbon dioxide fixation and chlorophyll *a* fluorescence during induction of photosynthesis in maize leaves at different temperatures and carbon dioxide concentrations. Planta 160, 550–558.
Jacquemoud, S., 1993. Inversion of the PROSPECT + SAIL canopy reflectance model from AVIRIS equivalent spectra: theoretical study. Remote Sens. Environ. 44, 281–292.
Jacquemoud, S., Baret, F., 1990. PROSPECT: a model of leaf optical properties spectra. Remote Sens. Environ. 34, 75–91.
Jacquemoud, S., Verhoef, W., Baret, F., Bacour, C., Zarco-Tejada, P.J., Asner, G.P., François, C., Ustin, S.L., 2009. PROSPECT + SAIL models: a review of use for vegetation characterization. Remote Sens. Environ. 113 (Suppl. 1), S56–S66.
Jeong, S.-J., Schimel, D., Frankenberg, C., Drewry, D.T., Fisher, J.B., Verma, M., Berry, J.A., Lee, J.-E., Joiner, J., 2017. Application of satellite solar-induced chlorophyll fluorescence to understanding large-scale variations in vegetation phenology and function over northern high latitude forests. Remote Sens. Environ. 190, 178–187.
Johnson, L.F., Herwitz, S., Dunagan, S., Lobitz, B., Sullivan, D., Slye, R., 2003. Collection of ultra high spatial and spectral resolution image data over California vineyards with a small UAV. In: Proc. 30th International Symposium on Remote Sensing of Environment, 10–14 November 2003, Honolulu (HI), USA, pp. 663–665.
Joiner, J., Yoshida, Y., Vasilkov, A.P., Yoshida, Y., Corp, L.A., Middleton, E.M., 2011. First observations of global and seasonal terrestrial chlorophyll fluorescence from space. Biogeosciences 8, 637–651.
Joiner, J., Yoshida, Y., Vasilkov, A.P., Middleton, E.M., Campbell, P.K.E., Yoshida, Y., Kuze, A., Corp, L.A., 2012. Filling-in of near-infrared solar lines by terrestrial fluorescence and other geophysical effects: simulations and space-based observations from SCIAMACHY and GOSAT. Atmos. Meas. Tech. 5, 809–829.
Joiner, J., Guanter, L., Lindstrot, R., Voigt, M., Vasilkov, A.P., Middleton, E.M., Huemmrich, K.F., Yoshida, Y., Frankenberg, C., 2013. Global monitoring of terrestrial chlorophyll fluorescence from moderate spectral resolution near-infrared satellite measurements: methodology, simulations, and application to GOME-2. Atmos. Meas. Tech. 6, 2803–2823.
Joiner, J., Yoshida, Y., Vasilkov, A.P., Schaefer, K., Jung, M., Guanter, L., Zhang, Y., Garrity, S., Middleton, E.M., Huemmrich, K.F., Gu, L., Belelli Marchesini, L., 2014. The seasonal cycle of satellite chlorophyll fluorescence observations and its relationship to vegetation phenology and ecosystem atmosphere carbon exchange. Remote Sens. Environ. 152, 375–391.
Joiner, J., Yoshida, Y., Guanter, L., Middleton, E.M., 2016. New methods for retrieval of chlorophyll red fluorescence from hyperspectral satellite instruments: simulations and application to GOME-2 and SCIAMACHY. Atmos. Meas. Tech. 9, 3939–3967.
Joiner, J., Yoshida, Y., Zhang, Y., Duveiller, G., Jung, M., Lyapustin, A., Wang, Y., Tucker, C.J., 2018. Estimation of terrestrial global gross primary production (GPP) with satellite data-driven models and eddy covariance flux data. Remote Sens. 10, 1346.
Julitta, T., Corp, L.A., Rossini, M., Burkart, A., Cogliati, S., Davies, N., Hom, M., Mac Arthur, A., Middleton, E.M., Rascher, U., Schickling, A., Colombo, R., 2016. Comparison of sun-induced chlorophyll fluorescence estimates obtained from four portable field spectroradiometers. Remote Sens. 8, 122.
Julitta, T., Burkart, A., Colombo, R., Rossini, M., Schickling, A., Migliavacca, M., Cogliati, S., Wutzler, T., Rascher, U., 2017. Accurate measurements of fluorescence in the O_2A and O_2B band using the FloX spectroscopy system - results and prospects. In: Proc. Potsdam GHG Flux Workshop: From Photosystems to Ecosystems, 24–26 October 2017, Potsdam, Germany. https://www.potsdam-flux-workshop.eu/.
Kalaji, H.M., Goltsev, V., Bosa, K., Allakhverdiev, S.I., Strasser, R.J., 2012. Experimental *in vivo* measurements of light emission in plants: a perspective dedicated to David Walker. Photosynth. Res. 114, 69–96.
Kalaji, H.M., Schansker, G., Ladle, R.J., Goltsev, V., Bosa, K., Allakhverdiev, S.I., Brestic, M., Bussotti, F., Calatayud, A., Dabrowski, P., Elsheery, N.I., Ferroni, L., Guidi, L., Hogewoning, S.W., Jajoo, A., Misra, A.N., Nebauer, S.G., Pancaldi, S., Penella, C., Poli, D., Pollastrini, M., Romanowska-Duda, Z.B., Rutkowska, B., Serôdio, J., Suresh, K., Szulc, W., Tambussi, E., Yanniccari, M., Zivcak, M., 2014. Frequently asked questions about *in vivo* chlorophyll fluorescence: practical issues. Photosynth. Res. 122, 121–158.
Kalma, J.D., McVicar, T.R., McCabe, M.F., 2008. Estimating land surface evaporation: a review of methods using remotely sensed surface temperature data. Surv. Geophys. 29, 421–469.
Kancheva, R., Borisova, D., Iliev, I., Yonova, P., 2007. Chlorophyll fluorescence as a quantitative measure of plant stress. In: Bochenek, Z. (Ed.), New Developments and Challenges in Remote Sensing. Millpress, Rotterdam, pp. 37–43.
Kautsky, H., Hirsch, A., 1931. Neue versuche zur kohlensäureassimilation. Die Naturwissenschaften 19, 964.
Kebabian, P.L., Theisen, A.F., Kallelis, S., Freedman, A., 1999. A passive two-band sensor of sunlight-excited plant fluorescence. Rev. Sci. Instrum. 70, 4386–4393.
Keller, B., Vass, I., Matsubara, S., Paul, K., Jedmowski, C., Pieruschka, R., Nedbal, L., Rascher, U., Muller, O., 2019. Maximum fluorescence and electron transport kinetics determined by light induced fluorescence transients (LIFT) for photosynthesis phenotyping. Photosynth. Res. https://doi.org/10.1007/s11120-018-0594-9.
Khosravi, N., Vountas, M., Rozanov, V.V., Bracher, A., Wolanin, A., Burrows, J.P., 2015. Retrieval of terrestrial plant fluorescence based on the in-filling of far-red Fraunhofer lines using SCIAMACHY observations. Front. Environ. Sci. 3. https://doi.org/10.3389/fenvs.2015.00078.
Kim, H.H., 1973. New algae mapping technique by the use of an airborne laser fluorosensor. Appl. Opt. 12, 1454–1459.
Kitajima, M., Butler, W.L., 1975. Quenching of chlorophyll fluorescence and primary photochemistry in chloroplasts by dibromothymoquinone. Biochim. Biophys. Acta 376, 105–115.
Knapp, A.K., Carter, G.A., 1998. Variability in leaf optical properties among 26 species from a broad range of habitats. Am. J. Bot. 85, 940–946.
Koffi, E.N., Rayner, P.J., Norton, A.J., Frankenberg, C., Scholze, M., 2015. Investigating the usefulness of satellite-derived fluorescence data in inferring gross primary productivity within the carbon cycle data assimilation system. Biogeosciences 12, 4067–4084.
Köhler, P., Guanter, L., Joiner, J., 2015. A linear method for the retrieval of sun-induced chlorophyll fluorescence from GOME-2 and SCIAMACHY data. Atmos. Meas. Tech. 8, 2589–2608.
Köhler, P., Frankenberg, C., Magney, T.S., Guanter, L., Joiner, J., Landgraf, J., 2018a. Global retrievals of solar-induced chlorophyll fluorescence with TROPOMI: first results and intersensor comparison to OCO-2. Geophys. Res. Lett. https://doi.org/10.1029/2018GL079031.
Köhler, P., Guanter, L., Kobayashi, H., Walther, S., Yang, W., 2018b. Assessing the potential of sun-induced fluorescence and the canopy scattering coefficient to track large-scale vegetation dynamics in Amazon forests. Remote Sens. Environ. 204, 769–785.
Kolber, Z., Falkowski, P.G., 1993. Use of active fluorescence to estimate phytoplankton photosynthesis *in situ*. Limnol. Oceanogr. 38, 1646–1665.
Kolber, Z.S., Prášil, O., Falkowski, P.G., 1998. Measurements of variable chlorophyll fluorescence using fast repetition rate techniques: defining methodology and experimental protocols. Biochim. Biophys. Acta 1367, 88–106.
Kolber, Z., Klimov, D., Ananyev, G., Rascher, U., Berry, J., Osmond, B., 2005. Measuring photosynthetic parameters at a distance: laser induced fluorescence transient (LIFT) method for remote measurements of photosynthesis in terrestrial vegetation. Photosynth. Res. 84, 121–129.
Koren, G., Van Schaik, E., Araújo, A.C., Boersma, K.F., Gärtner, A., Killaars, L., Kooreman, M.L., Kruijt, B., Van der Laan-Luijkx, I.T., Von Randow, C., Smith, N.E., Peters, W., 2018. Widespread reduction in sun-induced fluorescence from the Amazon during the 2015/2016 El Niño. Phil. Trans. R. Soc. B. 373, 20170408.
Kotchenova, S.Y., Vermote, E.F., Levy, R., Lyapustin, A., 2008. Radiative transfer codes for atmospheric correction and aerosol retrieval: intercomparison study. Appl. Opt. 47, 2215–2226.
Krause, G.H., Weis, E., 1984. Chlorophyll fluorescence as a tool in plant physiology. II. Interpretation of fluorescence signals. Photosynth. Res. 5, 139–157.
Krause, G.H., Weis, E., 1991. Chlorophyll fluorescence and photosynthesis: the basics. Annu. Rev. Plant Physiol. Plant Mol. Biol. 42, 313–349.
Krinner, G., Viovy, N., De Noblet-Ducoudré, N., Ogée, J., Polcher, J., Friedlingstein, P., Ciais, P., Sitch, S., Prentice, I.C., 2005. A dynamic global vegetation model for studies of the coupled atmosphere-biosphere system. Glob. Biogeochem. Cycles 19, GB1015.
Kubelka, P., Munk, F., 1931. An article on optics of paint layers. Z. Tech. Phys. 12, 593–601.
Kuckenberg, J., Tartachnyk, I., Noga, G., 2009. Detection and differentiation of nitrogen-deficiency, powdery mildew and leaf rust at wheat leaf and canopy level by laser-induced chlorophyll fluorescence. Biosyst. Eng. 103, 121–128.
Kückenbrink, D., Hueni, A., Schneider, F., Damm, A., Gastellu-Etchegorry, J.P., Schaepman, M.E., Morsdorf, F., 2019. Mapping the irradiance field of a single tree: quantifying vegetation induced adjacency effects. IEEE Trans. Geosci. Remote Sens. https://doi.org/10.1109/TGRS.2019.2895211.
Lagorio, M.G., Cordon, G.B., Iriel, A., 2015. Reviewing the relevance of fluorescence in biological systems. Photochem. Photobiol. Sci. 14, 1538–1559.
Lang, M., Lichtenthaler, H.K., Sowinska, M., Heisel, F., Miehé, J.A., 1996. Fluorescence imaging of water and temperature stress in plant leaves. J. Plant Physiol. 148, 613–621.
Lausch, A., Bannehr, L., Beckmann, M., Boehm, C., Feilhauer, H., Hacker, J.M., Heurich, M., Jung, A., Klenke, R., Neumann, C., Pause, M., Rocchini, D., Schaepman, M.E., Schmidtlein, S., Schulz, K., Selsam, P., Settele, J., Skidmore, A.K., Cord, A.F., 2016. Linking earth observation and taxonomic, structural and functional biodiversity: local to ecosystem perspectives. Ecol. Indic. 70, 317–339.
Lausch, A., Erasmi, S., King, D.J., Magdon, P., Heurich, M., 2017. Understanding forest health with remote sensing-part II–A review of approaches and data models. Remote Sens. 9, 129.
Lawson, T., 2009. Guard cell photosynthesis and stomatal function. New Phytol. 181, 13–34.
Lee, J.-E., Frankenberg, C., Van der Tol, C., Berry, J.A., Guanter, L., Boyce, C.K., Fisher, J.B., Morrow, E., Worden, J.R., Asefi, S., Badgley, G., Saatchi, S., 2013. Forest productivity and water stress in Amazonia: observations from GOSAT chlorophyll fluorescence. Proc. R. Soc. London B Biol. Sci. 280, 20130171.
Lee, J.-E., Berry, J.A., Van der Tol, C., Yang, X., Guanter, L., Damm, A., Baker, I., Frankenberg, C., 2015. Simulations of chlorophyll fluorescence incorporated into the community land model version 4. Glob. Chang. Biol. 21, 3469–3477.
Leuning, R., 1995. A critical appraisal of a combined stomatal-photosynthesis model for C_3 plants. Plant Cell Environ. 18, 339–355.

Li, X., Xiao, J., He, B., 2018a. Chlorophyll fluorescence observed by OCO-2 is strongly related to gross primary productivity estimated from flux towers in temperate forests. Remote Sens. Environ. 204, 659–671.
Li, X., Xiao, J., He, B., Arain, M.A., Beringer, J., Desai, A.R., Emmel, C., Hollinger, D.Y., Krasnova, A., Mammarella, I., Noe, S.M., Ortiz, P.S., Rey-Sanchez, A.C., Rocha, A.V., Varlagin, A., 2018b. Solar-induced chlorophyll fluorescence is strongly correlated with terrestrial photosynthesis for a wide variety of biomes: first global analysis based on OCO-2 and flux tower observations. Glob. Chang. Biol. 24, 3990–4008.
Lichtenthaler, H.K. (Ed.), 1989. Applications of Chlorophyll Fluorescence in Photosynthesis Research, Stress Physiology, Hydrobiology and Remote Sensing. Kluwer, Dordrecht.
Lichtenthaler, H.K., Rinderle, U., 1988. The role of chlorophyll fluorescence in the detection of stress conditions in plants. Crit. Rev. Anal. Chem. 19 (Suppl. 1), S29–S85.
Liu, X., Liu, L., 2018. Influence of the canopy BRDF characteristics and illumination conditions on the retrieval of solar-induced chlorophyll fluorescence. Int. J. Remote Sens. 39, 1782–1799.
Liu, J., Chen, J.M., Cihlar, J., Park, W.M., 1997. A process-based boreal ecosystem productivity simulator using remote sensing inputs. Remote Sens. Environ. 62, 158–175.
Liu, L., Zhang, Y., Wang, J., Zhao, C., 2005. Detecting solar-induced chlorophyll fluorescence from field radiance spectra based on the Fraunhofer line principle. IEEE Trans. Geosci. Remote Sens. 43, 827–832.
Liu, X., Liu, L., Zhang, S., Zhou, X., 2015. New spectral fitting method for full-spectrum solar-induced chlorophyll fluorescence retrieval based on principal components analysis. Remote Sens. 7, 10626–10645.
Liu, L., Guan, L., Liu, X., 2017. Directly estimating diurnal changes in GPP for C3 and C4 crops using far-red sun-induced chlorophyll fluorescence. Agric. For. Meteorol. 232, 1–9.
Liu, X., Guanter, L., Liu, L., Damm, A., Malenovský, Z., Rascher, U., Peng, D., Du, S., Gastellu-Etchegorry, J.-P., 2018. Downscaling of solar-induced chlorophyll fluorescence from canopy level to photosystem level using a random forest model. Remote Sens. Environ. https://doi.org/10.1016/j.rse.2018.05.035.
Louis, J., Ounis, A., Ducruet, J.-M., Evain, S., Laurila, T., Thum, T., Aurela, M., Wingsle, G., Alonso, L., Pedros, R., Moya, I., 2005. Remote sensing of sunlight-induced chlorophyll fluorescence and reflectance of Scots pine in the boreal forest during spring recovery. Remote Sens. Environ. 96, 37–48.
Louis, J., Cerovic, Z.G., Moya, I., 2006. Quantitative study of fluorescence excitation and emission spectra of bean leaves. J. Photochem. Photobiol. 85, 65–71.
Lu, X., Cheng, X., Li, X., Tang, J., 2018a. Opportunities and challenges of applications of satellite-derived sun-induced fluorescence at relatively high spatial resolution. Sci. Total Environ. 619-620, 649–653.
Lu, X., Liu, Z., An, S., Miralles, D.G., Maes, W., Liu, Y., Tang, J., 2018b. Potential of solar-induced chlorophyll fluorescence to estimate transpiration in a temperate forest. Agric. For. Meteorol. 252, 75–87.
Lucieer, A., Malenovský, Z., Veness, T., Wallace, L., 2014. HyperUAS—imaging spectroscopy from a multirotor unmanned aircraft system. J. Field Robot. 31, 571–590.
Luus, K.A., Commane, R., Parazoo, N.C., Benmergui, J., Euskirchen, E.S., Frankenberg, C., Joiner, J., Lindaas, J., Miller, C.E., Oechel, W.C., Zona, D., Wofsy, S., Lin, J.C., 2017. Tundra photosynthesis captured by satellite-observed solar-induced chlorophyll fluorescence. Geophys. Res. Lett. 44, 1564–1573.
Ma, X., Huete, A., Cleverly, J., Eamus, D., Chevallier, F., Joiner, J., Poulter, B., Zhang, Y., Guanter, L., Meyer, W., Xie, Z., Ponce-Campos, G., 2016. Drought rapidly diminishes the large net CO_2 uptake in 2011 over semi-arid Australia. Sci. Rep. 6, 37747.
Mac Arthur, A., Robinson, I., Rossini, M., Davies, N., McDonald, K., 2014. A dual-field-of-view spectrometer system for reflectance and fluorescence measurements (Piccolo Doppio) and correction of etaloning. In: Proc. 5th International Workshop on Remote Sensing of Vegetation Fluorescence, 22–24 April 2014, Paris, France.
MacBean, N., Maignan, F., Bacour, C., Lewis, P., Peylin, P., Guanter, L., Köhler, P., Gomez-Dans, J., Disney, M., 2018. Strong constraint on modelled global carbon uptake using solar-induced chlorophyll fluorescence data. Sci. Rep. 8, 1973.
Madani, N., Kimball, J.S., Jones, L.A., Parazoo, N.C., Guan, K., 2017. Global analysis of bioclimatic controls on ecosystem productivity using satellite observations of solar-induced chlorophyll fluorescence. Remote Sens. 9, 530.
Magnani, F., Olioso, A., Demarty, J., Germain, V., Verhoef, W., Moya, I., Goulas, Y., Cecchi, G., Agati, G., Zarco-Tejada, P., Mohammed, G., Van der Tol, C., 2009. Assessment of Vegetation Photosynthesis through Observation of Solar Induced Fluorescence from Space, Final Report. ESA/ESTEC Contract No. 20678/07/NL/HE. (256 p).
Magnani, F., Raddi, S., Mohammed, G., Middleton, E.M., 2014. Let's exploit available knowledge on vegetation fluorescence. Proc. Natl. Acad. Sci. U. S. A. 111, E2510.
Magney, T.S., Frankenberg, C., Fisher, J.B., Sun, Y., North, G.B., Davis, T.S., Kornfeld, A., Siebke, K., 2017. Connecting active to passive fluorescence with photosynthesis: a method for evaluating remote sensing measurements of Chl fluorescence. New Phytol. 215, 1594–1608.
Maier, S.W., 2002. Remote sensing and modelling of solar induced fluorescence. In: Proc. FLEX Workshop, 19–20 June 2002, Noordwijk, Netherlands. European Space Agency, (Special Publication) ESA SP, Issue 527.
Maier, S.W., Günther, K.P., Stellmes, M., 2003. Sun-induced fluorescence: a new tool for precision farming. In: Schepers, J., VanToai, T. (Eds.), Digital Imaging and Spectral Techniques: Applications to Precision Agriculture and Crop Physiology. ASA Spec. Publ. 66. ASA, CSSA, and SSSA, Madison (Wisconsin), USA, pp. 209–222.
Malenovský, Z., Mishra, K.B., Zemek, F., Rascher, U., Nedbal, L., 2009. Scientific and technical challenges in remote sensing of plant canopy reflectance and fluorescence. J. Exp. Bot. 60, 2987–3004.
Malenovský, Z., Lucieer, A., King, D.H., Turnbull, J.D., Robinson, S.A., 2017. Unmanned aircraft system advances health mapping of fragile polar vegetation. Methods Ecol. Evol. 8, 1842–1857.
Matsubara, S., Morosinotto, T., Osmond, C.B., Bassi, R., 2007. Short- and long-term operation of the lutein-epoxide cycle in light-harvesting antenna complexes. Plant Physiol. 144, 926–941.
Maxwell, K., Johnson, G.N., 2000. Chlorophyll fluorescence — a practical guide. J. Exp. Bot. 51, 659–668.
Mazzoni, M., Falorni, P., Del Bianco, S., 2008. Sun-induced leaf fluorescence retrieval in the O_2-B atmospheric absorption band. Opt. Express 16, 7014–7022.
Mazzoni, M., Falorni, P., Verhoef, W., 2010. High-resolution methods for fluorescence retrieval from space. Opt. Express 18, 15643–15663.
Mazzoni, M., Meroni, M., Fortunato, C., Colombo, R., Verhoef, W., 2012. Retrieval of maize canopy fluorescence and reflectance by spectral fitting in the O_2-A absorption band. Remote Sens. Environ. 124, 72–82.
McAlister, E.D., Myers, J., 1940. Time course of photosynthesis and fluorescence. Science 92, 241–243.
McFarlane, J.C., Watson, R.D., Theisen, A.F., Jackson, R.D., Ehrler, W.L., Pinter, P.J., Idso, S.B., Reginato, R.J., 1980. Plant stress detection by remote measurement of fluorescence. Appl. Opt. 19, 3287–3289.
Meijer, Y., Ingmann, P., Langen, J., Veihelmann, B., Zehner, C., 2014. Potential of current and future Copernicus satellite missions for low spatial resolution fluorescence monitoring. In: Proceedings 5th International Workshop on Remote Sensing of Vegetation Fluorescence, 22–24 April 2014, Paris, France. http://www.congrexprojects.com/2014-events/14c04/proceedings.
Meroni, M., Colombo, R., 2006. Leaf level detection of solar induced chlorophyll fluorescence by means of a subnanometer resolution spectroradiometer. Remote Sens. Environ. 103, 438–448.
Meroni, M., Rossini, M., Picchi, V., Panigada, C., Cogliati, S., Nali, C., Colombo, R., 2008. Assessing steady-state fluorescence and PRI from hyperspectral proximal sensing as early indicators of plant stress: the case of ozone exposure. Sensors 8, 1740–1754.
Meroni, M., Rossini, M., Guanter, L., Alonso, L., Rascher, U., Colombo, R., Moreno, J., 2009. Remote sensing of solar-induced chlorophyll fluorescence: review of methods and applications. Remote Sens. Environ. 113, 2037–2051.
Meroni, M., Busetto, L., Colombo, R., Guanter, L., Moreno, J., Verhoef, W., 2010. Performance of spectral fitting methods for vegetation fluorescence quantification. Remote Sens. Environ. 114, 363–374.
Meroni, M., Barducci, A., Cogliati, S., Castagnoli, F., Rossini, M., Busetto, L., Migliavacca, M., Cremonese, E., Galvagno, M., Colombo, R., Morra di Cella, U., 2011. The hyperspectral irradiometer, a new instrument for long-term and unattended field spectroscopy measurements. Rev. Sci. Instrum. 82, 043106.
Miao, G., Guan, K., Yang, X., Bernacchi, C.J., Berry, J.A., DeLucia, E.H., Wu, J., Moore, C.E., Meacham, K., Cai, Y., Peng, B., Kimm, H., Masters, M.D., 2018. Sun-induced chlorophyll fluorescence, photosynthesis, and light use efficiency of a soybean field from seasonally continuous measurements. J. Geophys. Res. Biogeosci. 123, 610–623.
Middleton, E.M., Chappelle, E.W., Cannon, T.A., Adamse, P., Britz, S.J., 1996. Initial assessment of physiological response to UV-B irradiation using fluorescence measurements. J. Plant Physiol. 148, 69–77.
Middleton, E.M., Kim, M.S., Krizek, D.T., Bajwa, R.K., 2005. Evaluating UV-B effects and EDU protection in soybean leaves using fluorescence. Photochem. Photobiol. 81, 1075–1085.
Middleton, E.M., Corp, L.A., Campbell, P.K.E., 2008. Comparison of measurements and FluorMOD simulations for solar-induced chlorophyll fluorescence and reflectance of a corn crop under nitrogen treatments. Int. J. Remote Sens. 29, 5193–5213.
Middleton, E.M., Huemmrich, K.F., Zhang, Q., Campbell, P.K.E., Landis, D.R., 2018. Spectral bio-indicators of photosynthetic efficiency and vegetation stress, chap. 5. In: Thenkabail, P.S., Lyon, J.G., Huete, A. (Eds.), Hyperspectral Remote Sensing of Vegetation, 2nd edition. Vol. III: Biophysical and Biochemical Characterization and Plant Species Studies Taylor & Francis, New York, pp. 133–179.
Middleton, E.M., Rascher, U., Corp, L.A., Huemmrich, K.F., Cook, B.D., Noormets, A., Schickling, A., Pinto, F., Alonso, L., Damm, A., Guanter, L., Colombo, R., Campbell, P.K.E., Landis, D.R., Zhang, Q., Rossini, M., Schuettemeyer, D., Bianchi, R., 2017. The 2013 FLEX–US airborne campaign at the Parker Tract loblolly pine plantation in North Carolina, USA. Remote Sens. 9, 612.
Migliavacca, M., El Madany, T., Perez-Priego, O., Carrara, A., Hammer, T., Henkel, K., Kolle, O., Luo, Y., Moreno, G., Morris, K., Nair, R., Schrumpf, M., Wutzler, T., Reichstein, M., 2017a. Effects of a large scale nitrogen and phosphorus fertilization on the ecosystem functioning of a Mediterranean tree-grass ecosystem. In: Proc. 19th EGU General Assembly, EGU2017, 23–28 April 2017, Vienna, Austria, pp. 11586.
Migliavacca, M., Perez-Priego, O., Rossini, M., El-Madany, T.S., Moreno, G., Van der Tol, C., Rascher, U., Berninger, A., Bessenbacher, V., Burkart, A., Carrara, A., Fava, F., Guan, J.-H., Hammer, T.W., Henkel, K., Juarez-Alcalde, E., Julitta, T., Kolle, O., Martín, M.P., Musavi, T., Pacheco-Labrador, J., Pérez-Burgueño, A., Wutzler, T., Zaehle, S., Reichstein, M., 2017b. Plant functional traits and canopy structure control the relationship between photosynthetic CO_2 uptake and far-red sun-induced fluorescence in a Mediterranean grassland under different nutrient availability. New Phytol. 214, 1078–1091.
Miller, J., Berger, M., Goulas, Y., Jacquemoud, S., Louis, J., Mohammed, G., Noise, N., Moreno, J., Moya, I., Pédros, R., Verhoef, W., Zarco-Tejada, P., 2005. Development of a Vegetation Fluorescence Canopy Model, Final Report. ESA/ESTEC Contract No. 16365/02/NL/FF. (138 p).
Mohammed, G.H., Binder, W.D., Gillies, S.L., 1995. Chlorophyll fluorescence: a review of its practical forestry applications and instrumentation. Scand. J. For. Res. 10, 383–410.
Mohammed, G.H., Noland, T.L., Wagner, R.G., 1998. Physiological perturbation in jack pine (*Pinus banksiana* Lamb.) in the presence of competing herbaceous vegetation. For. Ecol. Manag. 103, 77–85.
Mohammed, G.H., Zarco-Tejada, P., Miller, J.R., 2003. Applications of chlorophyll fluorescence in forestry and ecophysiology. In: DeEll, J.R., Toivonen, P.M.A. (Eds.),

Practical Applications of Chlorophyll Fluorescence in Plant Biology. Kluwer/Springer, Dordrecht, pp. 79–124.
Mohammed, G.H., Goulas, Y., Magnani, F., Moreno, J., Olejníčková, J., Rascher, U., Van der Tol, C., Verhoef, W., Ač, A., Daumard, F., Gallé, A., Malenovský, Z., Pernokis, D., Rivera, J.P., Verrelst, J., Drusch, M., 2014. FLEX/Sentinel-3 Tandem Mission Photosynthesis Study, Final Report. ESA/ESTEC Contract No. 4000106396/12/NL/AF. (159 p).
Mohammed, G.H., Colombo, R., Moreno, J., Van der Tol, C., Rascher, U., Ač, A., Alonso, L., Celesti, M., Cogliati, S., Damm, A., Fawcett, D., Gomez-Dans, J., Henry, C., Lewis, P., MacBean, N., Magnani, F., Malaprade, J., Matveeva, M., Olejníčková, J., Pernokis, D., Pinto, F., Raddi, S., Rajh Vilfan, N., Rivera, J.P., Rossini, M., Sabater, N., Schickling, A., Tenjo, C., Verhoef, W., Verrelst, J., Vicent Servera, J., Drusch, M., 2016. FLEX Bridge Study, Final Report. ESA/ESTEC Contract No. 4000112341/14/NL/FF/gp. (187 p).
Mohanty, P., Braun, B.Z., Govindjee, Thornber, J.P., 1972. Chlorophyll fluorescence characteristics of system I chlorophyll *a*-protein complex and system II particles at room and liquid nitrogen temperatures. Plant Cell Physiol. 13, 81–91.
Moore III, B., Crowell, S., 2018. The GeoCarb mission. In: Proc. 98th Amer. Meteor. Soc. Annual Meeting, 7–11 January 2018, Austin, TX.
Moreno, J., Asner, G.P., Bach, H., Belenguer, T., Bell, A., Buschmann, C., Calera, A., Calpe, J., Campbell, P., Cecchi, G., Colombo, R., Corp, L.A., Court, A., Cutter, M.A., Disney, M., Dudelzak, A., D'Urso, G., Fernandes, R., Flexas, J., Gege, P., Gielen, B., Gitelson, A., Gloor, E.U., Gower, J., Green, R.O., Hill, J., Jacquemoud, S., Jia, L., Kneubühler, M., Laurila, T., Lewis, P., Lobb, D., Magnani, F., Maier, S.W., Marek, M.V., Martinez, A., Martinez-Cobo, P., Mazzinghi, P., Menenti, M., Merton, R., Middleton, E., De Miguel, E., Miller, J., Mohammed, G., Milton, E.J., Morales, F., Moya, I., Nedbal, L., Knorr, W., Ottlé, C., Olioso, A., Pace, S., Palucci, A., Pedros, R., Peltoniemi, J., Peñuelas, J., Plaza, A., Polcher, J., Rascher, U., Reuter, R., Rosema, A., Roujean, J.-L., Saito, Y., Saugier, B., Schaepman, M., Serrano, J.B., Settle, J.J., Sierra, M., Sobrino, J., Stoll, M.-P., Su, Z.B., Tobehn, C., Tremblay, N., Valcke, R., Verhoef, W., Veroustraete, F., Verstraete, M., Zarco-Tejada, P., 2006. FLuorescence EXplorer (FLEX): An optimised payload to map vegetation photosynthesis from space. In: Proc. 57th International Astronautical Congress, 2–6 October 2006, Valencia, Spain.
Moreno, J., Rascher, U., Goulas, Y., Colombo, R., Verhoef, W., Damm, A., Alonso, L., Cogliati, S., Daumard, F., Rivera, J.P., Sabater, N., Schickling, A., Tenjo, C., Timmermans, J., Verrelst, J., Drusch, M., 2014. FLEX/S3 Tandem Mission Performance Analysis and Requirements Consolidation Study (PARCS), Final Report. ESA/ESTEC Contract No. 4000105078/11/NL/AF. (141 p).
Morris, J.M., Fleming, G.R., 2018. Quantitative modeling of energy dissipation in *Arabidopsis thaliana*. Environ. Exp. Bot. 154, 99–109.
Mouw, C.B., Greb, S., Aurin, D., DiGiacomo, P.M., Lee, Z., Twardowski, M., Binding, C., Hu, C., Ma, R., Moore, T., Moses, W., Craig, S.E., 2015. Aquatic color radiometry remote sensing of coastal and inland waters: challenges and recommendations for future satellite missions. Remote Sens. Environ. 160, 15–30.
Moya, I., Cerovic, Z.G., 2004. Remote sensing of chlorophyll fluorescence: Instrumentation and analysis. In: Papageorgiou, G.C., Govindjee (Eds.), Chlorophyll *a* Fluorescence: A Signature of Photosynthesis. Springer, Dordrecht, pp. 429–445.
Moya, I., Guyot, G., Goulas, Y., 1992. Remotely sensed blue and red fluorescence emission for monitoring vegetation. ISPRS J. Photogram. Remote Sens. 47, 205–231.
Moya, I., Goulas, Y., Morales, F., Camenen, L., Guyot, G., Schmuck, G., 1995. Remote sensing of time-resolved chlorophyll fluorescence and back-scattering of the laser excitation by vegetation. EARSeL Adv. Remote Sens. 3, 188–197.
Moya, I., Camenen, L., Evain, S., Goulas, Y., Cerovic, Z.G., Latouche, G., Flexas, J., Ounis, A., 2004. A new instrument for passive remote sensing. 1. Measurements of sunlight-induced chlorophyll fluorescence. Remote Sens. Environ. 91, 186–197.
Moya, I., Daumard, F., Moise, N., Ounis, A., Goulas, Y., 2006. First airborne multi-wavelength passive chlorophyll fluorescence measurements over La Mancha (Spain) fields. In: Proc. 2nd International Symposium on Recent Advances in Quantitative Remote Sensing, 25–29 September 2006, Torrent (Valencia), Spain, pp. 820–825.
Müller, N.J.C., 1874. Beziehungen zwischen assimilation, absorption und fluoreszenz im chlorophyll des lebenden blattes. Jahrbücher für Wissenchaftliche Botanik 9, 42–49.
Murata, N., Nishimura, M., Tamiya, A., 1966. Fluorescence of chlorophyll in photosynthetic systems. III. Emission and action spectra of fluorescence—three emission bands of chlorophyll *a* and the energy transfer between two pigment systems. Biochim. Biophys. Acta 126, 234–243.
Murchie, E.H., Lawson, T., 2013. Chlorophyll fluorescence analysis: a guide to good practice and understanding some new applications. J. Exp. Bot. 64, 3983–3998.
Musil, C.F., Arnolds, J.L., Van Heerden, P.D.R., Kgope, B.S., 2009. Mechanisms of photosynthetic and growth inhibition of a southern African geophyte *Tritonia crocata* (L.) Ker. Gawl. by an invasive European annual grass *Lolium multiflorum* Lam. Environ. Exp. Bot. 66, 38–45.
Nedbal, L., Whitmarsh, J., 2004. Chlorophyll fluorescence imaging of leaves and fruits. In: Papageorgiou, G.C., Govindjee (Eds.), Chlorophyll *a* Fluorescence: A Signature of Photosynthesis. Springer, Dordrecht, pp. 389–407.
Nedbal, L., Trtílek, M., Kaftan, D., 1999. Flash fluorescence induction: a novel method to study regulation of photosystem II. J. Photochem. Photobiol. B 48, 154–157.
Nedbal, L., Soukupová, J., Kaftan, D., Whitmarsh, J., Trtílek, M., 2000. Kinetic imaging of chlorophyll fluorescence using modulated light. Photosynth. Res. 66, 3–12.
Neville, R.A., Gower, J.F.R., 1977. Passive remote-sensing of phytoplankton via chlorophyll *a* fluorescence. J. Geophys. Res. 82, 3487–3493.
Nichol, C.J., Drolet, G., Porcar-Castell, A., Wade, T., Sabater, N., Middleton, E.M., MacLellan, C., Levula, J., Mammarella, I., Vesala, T., Atherton, J., 2019. Diurnal and seasonal solar induced chlorophyll fluorescence and photosynthesis in a boreal Scots pine canopy. Remote Sens. 11, 273.
Niinemets, Ü., 2010. Responses of forest trees to single and multiple environmental stresses from seedlings to mature plants: past stress history, stress interactions, tolerance and acclimation. For. Ecol. Manag. 260, 1623–1639.
Niinemets, Ü., Wright, I.J., Evans, J.R., 2009. Leaf mesophyll diffusion conductance in 35 Australian sclerophylls covering a broad range of foliage structural and physiological variation. J. Exp. Bot. 60, 2433–2449.
Ni-Meister, W., Yang, W., Kiang, N.Y., 2010. A clumped-foliage canopy radiative transfer model for a global dynamic terrestrial ecosystem model. I: theory. Agric. For. Meteorol. 150, 881–894.
Norman, J.M., 1979. Modeling the complete crop canopy. In: Barfield, B.J., Gerber, J.F. (Eds.), Modification of the Aerial Environment of Plants. Am. Soc. Agric. Eng., St Joseph, MI, pp. 249–277.
North, P.R.J., 1996. Three-dimensional forest light interaction model using a Monte Carlo method. IEEE Trans. Geosci. Remote Sens. 34, 946–956.
Norton, A.J., Rayner, P.J., Koffi, E.N., Scholze, M., 2018. Assimilating solar-induced chlorophyll fluorescence into the terrestrial biosphere model BETHY-SCOPE v1.0: model description and information content. Geosci. Model Dev. 11, 1517–1536.
O'Brien, D.M., Polonsky, I.N., Utembe, S.R., Rayner, P.J., 2016. Potential of a geostationary geoCARB mission to estimate surface emissions of CO_2, CH_4 and CO in a polluted urban environment: case study Shanghai. Atmos. Meas. Tech. 9, 4633–4654.
Omasa, K., Hosoi, F., Konishi, A., 2007. 3D lidar imaging for detecting and understanding plant responses and canopy structure. J. Exp. Bot. 58, 881–898.
Öquist, G., Wass, R., 1988. A portable, microprocessor operated instrument for measuring chlorophyll fluorescence kinetics in stress physiology. Physiol. Plant. 73, 211–217.
Osmond, B., Schwartz, O., Gunning, B., 1999. Photoinhibitory printing on leaves, visualised by chlorophyll fluorescence imaging and confocal microscopy, is due to diminished fluorescence from grana. Aust. J. Plant Physiol. 26, 717–724.
Ounis, A., Cerovic, Z.G., Briantais, J.M., Moya, I., 2001. Dual-excitation FLIDAR for the estimation of epidermal UV absorption in leaves and canopies. Remote Sens. Environ. 76, 33–48.
Ounis, A., Bach, J., Mahjoub, A., Daumard, F., Moya, I., Goulas, Y., 2016. Combined use of LIDAR and hyperspectral measurements for remote sensing of fluorescence and vertical profile of canopies. Revista de Teledetección 45 (Special Issue), 87–94.
Oxborough, K., 2004. Imaging of chlorophyll *a* fluorescence: theoretical and practical aspects of an emerging technique for the monitoring of photosynthetic performance. J. Exp. Bot. 55, 1195–1205.
Palombi, L., Cecchi, G., Lognoli, D., Raimondi, V., Toci, G., Agati, G., 2011. A retrieval algorithm to evaluate the photosystem I and photosystem II spectral contributions to leaf chlorophyll fluorescence at physiological temperatures. Photosynth. Res. 108, 225–239.
Panigada, C., Rossini, M., Meroni, M., Cilia, C., Busetto, L., Amaducci, S., Boschetti, M., Cogliati, S., Picchi, V., Pinto, F., Marchesi, A., Colombo, R., 2014. Fluorescence, PRI and canopy temperature for water stress detection in cereal crops. Int. J. Appl. Earth Obs. Geoinf. 30, 167–178.
Papageorgiou, G., 1975. Chlorophyll fluorescence: An intrinsic probe of photosynthesis. In: Govindjee (Ed.), Bioenergetics of Photosynthesis. Academic Press, New York, pp. 319–371.
Papageorgiou, G., Govindjee (Eds.), 2004. Chlorophyll *a* Fluorescence: A Signature of Photosynthesis. Springer, Dordrecht.
Parazoo, N.C., Bowman, K., Frankenberg, C., Lee, J.-E., Fisher, J.B., Worden, J., Jones, D.B.A., Berry, J., Collatz, G.J., Baker, I.T., Jung, M., Liu, J., Osterman, G., O'Dell, C., Sparks, A., Butz, A., Guerlet, S., Yoshida, Y., Chen, H., Gerbig, C., 2013. Interpreting seasonal changes in the carbon balance of southern Amazonia using measurements of XCO_2 and chlorophyll fluorescence from GOSAT. Remote Sens. Environ. 40, 2829–2833.
Parazoo, N.C., Bowman, K., Fisher, J.B., Frankenberg, C., Jones, D.B.A., Cescatti, A., Pérez-Priego, O., Wohlfahrt, G., Montagnani, L., 2014. Terrestrial gross primary production inferred from satellite fluorescence and vegetation models. Glob. Chang. Biol. 20, 3103–3121.
Patel, N.R., Padalia, H., Devadas, R., Huete, A., Kumar, A.S., Krishna Murthy, Y.V.N., 2018. Estimating net primary productivity of croplands in Indo-Gangetic Plains using GOME-2 sun-induced fluorescence and MODIS NDVI. Curr. Sci. 114, 1333–1337.
Paul-Limoges, E., Damm, A., Hueni, A., Liebische, F., Eugster, W., Schaepman, M.E., Buchmann, N., 2018. Effect of environmental conditions on sun-induced fluorescence in a mixed forest and a cropland. Remote Sens. Environ. 219, 310–323.
Pedrós, R., Moya, I., Goulas, Y., Jacquemoud, S., 2008. Chlorophyll fluorescence emission spectrum inside a leaf. Photochem. Photobiol. Sci. 7, 498–502.
Pedrós, R., Goulas, Y., Jacquemoud, S., Louis, J., Moya, I., 2010. FluorMODleaf: a new leaf fluorescence emission model based on the PROSPECT model. Remote Sens. Environ. 114, 155–167.
Peñuelas, J., Llusia, J., Piñol, J., Filella, I., 1997. Photochemical reflectance index and leaf photosynthetic radiation-use-efficiency assessment in Mediterranean trees. Int. J. Remote Sens. 18, 2863–2868.
Peñuelas, J., Filella, I., Llusià, J., Siscart, D., Piñol, J., 1998. Comparative field study of spring and summer leaf gas exchange and photobiology of the Mediterranean trees *Quercus ilex* and *Phillyrea latifolia*. J. Exp. Bot. 49, 229–238.
Pérez-Priego, O., Zarco-Tejada, P.J., Miller, J.R., Sepulcre-Cantó, G., Fereres, E., 2005. Detection of water stress in orchard trees with a high-resolution spectrometer through chlorophyll fluorescence *in-filling* of the O_2-A band. IEEE Trans. Geosci. Remote Sens. 43, 2860–2869.
Pérez-Priego, O., Guan, J., Rossini, M., Fava, F., Wutzler, T., Moreno, G., Carvalhais, N., Carrara, A., Kolle, O., Julitta, T., Schrumpf, M., Reichstein, M., Migliavacca, M., 2015. Sun-induced chlorophyll fluorescence and photochemical reflectance index improve remote-sensing gross primary production estimates under varying nutrient availability in a typical Mediterranean savanna ecosystem. Biogeosciences 12, 6351–6367.
Pfündel, E., 1998. Estimating the contribution of photosystem I to total leaf chlorophyll fluorescence. Photosynth. Res. 56, 185–195.

Pinto, F., Damm, A., Schickling, A., Panigada, C., Cogliati, S., Müller-Linow, M., Balvora, A., Rascher, U., 2016. Sun-induced chlorophyll fluorescence from high-resolution imaging spectroscopy data to quantify spatio-temporal patterns of photosynthetic function in crop canopies. Plant Cell Environ. 39, 1500–1512.
Pinto, F., Müller-Linow, M., Schickling, A., Cendrero-Mateo, M.P., Ballvora, A., Rascher, U., 2017. Multiangular observation of canopy sun-induced chlorophyll fluorescence by combining imaging spectroscopy and stereoscopy. Remote Sens. 9, 415.
Pitman, A.J., 2003. The evolution of, and revolution in, land surface schemes designed for climate models. Int. J. Climatol. 23, 479–510.
Plascyk, J.A., 1975. The MK II Fraunhofer line discriminator (FLD-II) for airborne and orbital remote sensing of solar-stimulated luminescence. Opt. Eng. 14, 144339.
Plascyk, J.A., Gabriel, F.C., 1975. The Fraunhofer Line Discriminator MKII – an airborne instrument for precise and standardized ecological luminescence measurement. IEEE Trans. Instrum. Meas. 24, 306–313.
Pöhlker, C., Huffman, J.A., Pöschl, U., 2012. Autofluorescence of atmospheric bioaerosols - fluorescent biomolecules and potential interferences. Atmos. Meas. Tech. 5, 37–71.
Porcar-Castell, A., Tyystjärvi, E., Atherton, J., Van der Tol, C., Flexas, J., Pfündel, E.E., Moreno, J., Frankenberg, C., Berry, J.A., 2014. Linking chlorophyll *a* fluorescence to photosynthesis for remote sensing applications: mechanisms and challenges. J. Exp. Bot. 65, 4065–4095.
Qiu, B., Xue, Y., Fisher, J.B., Guo, W., Berry, J.A., Zhang, Y., 2018. Satellite chlorophyll fluorescence and soil moisture observations lead to advances in the predictive understanding of global terrestrial coupled carbon-water cycles. Glob. Biogeochem. Cycles 32, 360–375.
Rascher, U., Lüttge, U., 2002. High-resolution chlorophyll fluorescence imaging serves as a non-invasive indicator to monitor the spatio-temporal variations of metabolism during the day-night cycle and during the endogenous rhythm in continuous light in the CAM plant *Kalanchoë daigremontiana*. Plant Biol. 4, 671–681.
Rascher, U., Hütt, M.-T., Siebke, K., Osmond, B., Beck, F., Lüttge, U., 2001. Spatiotemporal variation of metabolism in a plant circadian rhythm: the biological clock as an assembly of coupled individual oscillators. Proc. Natl. Acad. Sci. U. S. A. 98, 11801–11805.
Rascher, U., Gioli, B., Miglietta, F., 2008. FLEX – Fluorescence Explorer: A remote sensing approach to quantify spatio-temporal variations of photosynthetic efficiency from space. In: Allen, J.F., Gantt, E., Golbeck, J.H., Osmond, B. (Eds.), Photosynthesis. Energy from the Sun. Springer, Dordrecht, pp. 1387–1390.
Rascher, U., Agati, G., Alonso, L., Cecchi, G., Champagne, S., Colombo, R., Damm, A., Daumard, F., De Miguel, E., Fernandez, G., Franch, B., Franke, J., Gerbig, C., Gioli, B., Gómez, J.A., Goulas, Y., Guanter, L., Gutiérrez-de-la-Cámara, Ó., Hamdi, K., Hostert, P., Jiménez, M., Kosvancova, M., Lognoli, D., Meroni, M., Miglietta, F., Moersch, A., Moreno, J., Moya, I., Neininger, B., Okujeni, A., Ounis, A., Palombi, L., Raimondi, V., Schickling, A., Sobrino, J.A., Stellmes, M., Toci, G., Toscano, P., Udelhoven, T., Van der Linden, S., Zaldei, A., 2009. CEFLES2: the remote sensing component to quantify photosynthetic efficiency from the leaf to the region by measuring sun-induced fluorescence in the oxygen absorption bands. Biogeosciences 6, 1181–1198.
Rascher, U., Alonso, L., Burkart, A., Cilia, C., Cogliati, S., Colombo, R., Damm, A., Drusch, M., Guanter, L., Hanus, J., Hyvärinen, T., Julitta, T., Jussila, J., Kataja, K., Kokkalis, P., Kraft, S., Kraska, T., Matveeva, M., Moreno, J., Muller, O., Panigada, C., Pikl, M., Pinto, F., Prey, L., Pude, R., Rossini, M., Schickling, A., Schurr, U., Schüttemeyer, D., Verrelst, J., Zemek, F., 2015. Sun-induced fluorescence - a new probe of photosynthesis: first maps from the imaging spectrometer *HyPlant*. Glob. Chang. Biol. 21, 4673–4684.
Rivera, J.P., Verrelst, J., Gómez-Dans, J., Muñoz-Marí, J., Moreno, J., Camps-Valls, G., 2015. An emulator toolbox to approximate radiative transfer models with statistical learning. Remote Sens. 7, 9347–9370.
Roháček, K., Soukupová, J., Barták, M., 2008. Chlorophyll fluorescence: a wonderful tool to study plant physiology and plant stress. In: Schoefs, B. (Ed.), Plant Cell Compartments – Selected Topics. Kerala India, Research Signpost, pp. 41–104.
Romero, J.M., Cordon, G.B., Lagorio, M.G., 2018. Modeling re-absorption of fluorescence from the leaf to the canopy level. Remote Sens. Environ. 204, 138–146.
Rosema, A., Verhoef, W., Schroote, J., Snel, J.F.H., 1991. Simulating fluorescence light-canopy interaction in support of laser-induced fluorescence measurements. Remote Sens. Environ. 37, 117–130.
Rosema, A., Verhoef, W., Noorbergen, H., Borgesius, J.J., 1992. A new forest light interaction model in support of forest monitoring. Remote Sens. Environ. 42, 23–41.
Rosema, A., Snel, J.F.H., Zahn, H., Buurmeijer, W.F., Van Hove, L.W.A., 1998. The relation between laser-induced chlorophyll fluorescence and photosynthesis. Remote Sens. Environ. 65, 143–154.
Rossini, M., Meroni, M., Migliavacca, M., Manca, G., Cogliati, S., Busetto, L., Picchi, V., Cescatti, A., Seufert, G., Colombo, R., 2010. High resolution field spectroscopy measurements for estimating gross ecosystem production in a rice field. Agric. For. Meteorol. 150, 1283–1296.
Rossini, M., Nedbal, L., Guanter, L., Ač, A., Alonso, L., Burkart, A., Cogliati, S., Colombo, R., Damm, A., Drusch, M., Hanus, J., Janoutova, R., Julitta, T., Kokkalis, P., Moreno, J., Novotny, J., Panigada, C., Pinto, F., Schickling, A., Schüttemeyer, D., Zemek, F., Rascher, U., 2015. Red and far-red sun-induced chlorophyll fluorescence as a measure of plant photosynthesis. Geophys. Res. Lett. 42, 1632–1639.
Rossini, M., Meroni, M., Celesti, M., Cogliati, S., Julitta, T., Panigada, C., Rascher, U., Van der Tol, C., Colombo, R., 2016. Analysis of red and far-red sun-induced chlorophyll fluorescence and their ratio in different canopies based on observed and modeled data. Remote Sens. 8, 412.
Ryu, Y., Baldocchi, D.D., Kobayashi, H., van Ingen, C., Li, J., Black, T.A., Beringer, J., van Gorsel, E., Knohl, A., Law, B.E., Roupsard, O., 2011. Integration of MODIS land and atmosphere products with a coupled-process model to estimate gross primary productivity and evapotranspiration from 1 km to global scales. Glob. Biogeochem. Cycles 25. https://doi.org/10.1029/2011GB004053.
Ryu, Y., Berry, J.A., Baldocchi, D.D., 2019. What is global photosynthesis? History, uncertainties and opportunities. Remote Sens. Environ. 223, 95–114.
Sabater, N., Alonso, L., Cogliati, S., Vicent, J., Tenjo, C., Verrelst, J., Moreno, J., 2015. A sun-induced vegetation fluorescence retrieval method from top of atmosphere radiance for the FLEX/Sentinel-3 tandem mission. In: Proc. IEEE International Geoscience and Remote Sensing Symposium (IGARSS), 26–31 July 2015, Milan, Italy, pp. 2669–2672.
Sabater, N., Vicent, J., Alonso, L., Cogliati, S., Verrelst, J., Moreno, J., 2017. Impact of atmospheric inversion effects on solar-induced chlorophyll fluorescence: exploitation of the apparent reflectance as a quality indicator. Remote Sens. 9, 622.
Sabater, N., Vicent, J., Alonso, L., Verrelst, J., Middleton, E.M., Porcar–Castell, A., Moreno, J., 2018. Compensation of oxygen transmittance effects for proximal sensing retrieval of canopy-leaving sun-induced chlorophyll fluorescence. Remote Sens. 10, 1551.
Sanders, A.F.J., Verstraeten, W.W., Kooreman, M.L., Van Leth, T.C., Beringer, C., Joiner, J., 2016. Spaceborne sun-induced vegetation fluorescence time series from 2007 to 2015 evaluated with Australian flux tower measurements. Remote Sens. 8, 895.
Schickling, A., Matveeva, M., Damm, A., Schween, J.H., Wahner, A., Graf, A., Crewell, S., Rascher, U., 2016. Combining sun-induced chlorophyll fluorescence and photochemical reflectance index improves diurnal modeling of gross primary productivity. Remote Sens. 8, 574.
Schlapfer, D., Nieke, J., Itten, K.I., 2007. Spatial PSF nonuniformity effects in airborne pushbroom imaging spectrometry data. IEEE Trans. Geosci. Remote Sens. 45, 458–468.
Schmuck, G., Moya, I., 1994. Time-resolved chlorophyll fluorescence spectra of intact leaves. Remote Sens. Environ. 47, 72–76.
Scholze, M., Buchwitz, M., Dorigo, W., Guanter, L., Quegan, S., 2017. Reviews and syntheses: systematic earth observations for use in terrestrial carbon cycle data assimilation systems. Biogeosciences 14, 3401–3429.
Schreiber, U., 2004. Pulse-amplitude-modulation (PAM) fluorometry and saturation pulse method: an overview. In: Papageorgiou, G.C., Govindjee (Eds.), Chlorophyll *a* Fluorescence: A Signature of Photosynthesis. Springer, Dordrecht, pp. 279–319.
Schreiber, U., Bilger, W., 1987. Rapid assessment of stress effects on plant leaves by chlorophyll fluorescence measurements. In: Tenhunen, G.D. (Ed.), Plant Response to Stress. Springer-Verlag, Berlin, pp. 27–53.
Schreiber, U., Schliwa, U., Bilger, W., 1986. Continuous recording of photochemical and non-photochemical chlorophyll fluorescence quenching with a new type of modulation fluorometer. Photosynth. Res. 10, 51–62.
Schreiber, U., Bilger, W., Neubauer, C., 1995. Chlorophyll fluorescence as a nonintrusive indicator for rapid assessment of *in vivo* photosynthesis. In: Schulze, E.-D., Caldwell, M.M. (Eds.), Ecophysiology of Photosynthesis. Springer, Berlin/Heidelberg, pp. 49–70.
Sellers, P.J., Tucker, C.J., Collatz, G.J., Los, S.O., Justice, C.O., Dazlich, D.A., Randall, D.A., 1996. A revised land surface parameterization (SiB2) for atmospheric GCMs. Part II: the generation of global fields of terrestrial biophysical parameters from satellite data. J. Clim. 9, 706–737.
Šesták, Z., Šiffel, P., 1997. Leaf-age related differences in chlorophyll fluorescence. Photosynthetica 33, 347–369.
Simmer, C., Thiele-Eich, I., Masbou, M., Amelung, W., Bogena, H., Crewell, S., Diekkrüger, B., Ewert, F., Hendricks Franssen, H.-J., Huisman, J.A., Kemna, A., Klitzsch, N., Kollet, S., Langensiepen, M., Löhnert, U., Rahman, A.S.M.M., Rascher, U., Schneider, K., Schween, J., Shao, Y., Shrestha, P., Stiebler, M., Sulis, M., Vanderborght, J., Vereecken, H., Van der Kruk, J., Waldhoff, G., Zerenner, T., 2015. Monitoring and modeling the terrestrial system from pores to catchments: the transregional collaborative research center on patterns in the soil–vegetation–atmosphere system. Bull. Am. Meteorol. Soc. 96, 1765–1787.
Smith, W.K., Biederman, J.A., Scott, R.L., Moore, D.J.P., He, M., Kimball, J.S., Yan, D., Hudson, A., Barnes, M.L., MacBean, N., Fox, A.M., Litvak, M.E., 2018. Chlorophyll fluorescence better captures seasonal and interannual gross primary productivity dynamics across dryland ecosystems of southwestern North America. Geophys. Res. Lett. 45, 748–757.
Sobrino, J.A., Franch, B., Jimenez-Muñoz, J.C., Hidalgo, V., Soria, G., Julien, Y., Oltra-Carrio, R., Mattar, C., Ruescas, A., Daumard, F., Champagne, S., Fournier, A., Goulas, Y., Ounis, A., Moya, I., 2011. Fluorescence estimation in the framework of the CEFLES2 campaign. Int. J. Remote Sens. 32, 5875–5889.
Song, L., Guanter, L., Guan, K., You, L., Huete, A., Ju, W., Zhang, Y., 2018. Satellite sun-induced chlorophyll fluorescence detects early response of winter wheat to heat stress in the Indian Indo-Gangetic Plains. Glob. Change Biol. 2018, 1–15.
Soukupová, J., Cséfalvay, L., Urban, O., Košvancová, M., Marek, M., Rascher, U., Nedbal, L., 2008. Annual variation of the steady-state chlorophyll fluorescence emission of evergreen plants in temperate zone. Funct. Plant Biol. 35, 63–76.
Srivastava, P., Pandey, J., 2012. LICF spectrum as a fast detector of chlorophyll damage in safflower growing under mutagenic stress. World J. Agric. Sci. 8, 322–325.
Stober, F., Lang, M., Lichtenthaler, H.K., 1994. Blue, green, and red fluorescence emission signatures of green, etiolated, and white leaves. Remote Sens. Environ. 47, 65–71.
Stokes, G.G., 1852. On the change of refrangibility of light. Trans. R. Soc. Lond. 142,

463–562.
Stoll, M.-P., Laurila, T., Cunin, B., Gitelson, A.A., Lichtenthaler, H.K., Häme, T., 1999. FLEX: Fluorescence Explorer – a space mission for screening vegetated areas in the Fraunhofer lines. In: Proc. SPIE 3868, Remote Sensing for Earth Science, Ocean, and Sea Ice Applications, 20–24 September 1999, Florence, Italy, pp. 108–119.
Strand, M., Öquist, G., 1988. Effects of frost hardening, dehardening and freezing stress on *in vivo* chlorophyll fluorescence of seedlings of Scots pine (*Pinus sylvestris* L.). Plant Cell Environ. 11, 231–238.
Strasser, R.J., Srivastava, A., Govindjee, 1995. Polyphasic chlorophyll *a* fluorescence transient in plants and cyanobacteria. Photochem. Photobiol. 61, 32–42.
Subhash, N., 1995. Detection of vegetation stress from laser-induced fluorescence signatures. In: International Centre for Theoretical Physics (Trieste, Italy). LAMP Series Report, LAMP/95/4, June.
Subhash, N., Mohanan, C.N., 1997. Curve-fit analysis of chlorophyll fluorescence spectra: application to nutrient stress detection in sunflower. Remote Sens. Environ. 60, 347–356.
Suits, G.H., 1972. The calculation of the directional reflectance of a vegetative canopy. Remote Sens. Environ. 2, 117–125.
Sun, Y., Fu, R., Dickinson, R., Joiner, J., Frankenberg, C., Gu, L., Xia, Y., Fernando, N., 2015. Drought onset mechanisms revealed by satellite solar-induced chlorophyll fluorescence: insights from two contrasting extreme events. J. Geophys. Res. Biogeosci. 120, 2427–2440.
Sun, Y., Frankenberg, C., Wood, J.D., Schimel, D.S., Jung, M., Guanter, L., Drewry, D.T., Verma, M., Porcar-Castell, A., Griffis, T.J., Gu, L., Magney, T.S., Köhler, P., Evans, B., Yuen, K., 2017. OCO-2 advances photosynthesis observation from space via solar-induced chlorophyll fluorescence. Science 358, eaam5747. https://doi.org/10.1126/science.aam5747.
Sun, Y., Frankenberg, C., Jung, M., Joiner, J., Guanter, L., Köhler, P., Magney, T.S., 2018. Overview of solar-induced chlorophyll fluorescence (SIF) from the orbiting carbon observatory-2: retrieval, cross-mission comparison, and global monitoring for GPP. Remote Sens. Environ. 209, 808–823.
Sylak-Glassman, E.J., Zaks, J., Amarnath, K., Leuenberger, M., Fleming, G.R., 2016. Characterizing non-photochemical quenching in leaves through fluorescence lifetime snapshots. Photosynth. Res. 127, 69–76.
Szabó, K., Lichtenthaler, H.K., Kocsányi, L., Richter, P., 1992. A CCD-OMA device for the measurement of complete chlorophyll fluorescence emission spectra of leaves during the fluorescence induction kinetics. Radiat. Environ. Biophys. 31, 153–160.
Takahashi, S., Badger, M.R., 2011. Photoprotection in plants: a new light on photosystem II damage. Trends Plant Sci. 16, 53–60.
Terjung, F., 1998. Reabsorption of chlorophyll fluorescence and its effects on the spectral distribution and the picosecond decay of higher plant leaves. Z. Naturforsch. C 53, 924–926.
Thum, T., Zaehle, S., Köhler, P., Aalto, T., Aurela, M., Guanter, L., Kolari, P., Laurila, T., Lohila, A., Magnani, F., Van Der Tol, C., Markkanen, T., 2017. Modelling sun-induced fluorescence and photosynthesis with a land surface model at local and regional scales in northern Europe. Biogeosciences 14, 1969–1987.
Toivonen, P., Vidaver, W., 1984. Integrating fluorometer for the measurement of chlorophyll fluorescence induction in intact plants. Rev. Sci. Instrum. 55, 1687–1690.
Tremblay, N., Wang, Z., Cerovic, Z.G., 2012. Sensing crop nitrogen status with fluorescence indicators. A review. Agron. Sustain. Dev. 32, 451–464.
Turner, D., Lucieer, A., Malenovský, Z., King, D.H., Robinson, S.A., 2014. Spatial co-registration of ultra-high resolution visible, multispectral and thermal images acquired with a micro-UAV over Antarctic moss beds. Remote Sens. 6, 4003–4024.
Vácha, F., Sarafis, V., Benediktyová, Z., Bumba, L., Valenta, J., Vácha, M., Sheue, Ch.-R., Nedbal, L., 2007. Identification of photosystem I and photosystem II enriched regions of thylakoid membrane by optical microimaging of cryo-fluorescence emission spectra and of variable fluorescence. Micron 38, 170–175.
Valentini, R., Cecchi, G., Mazzinghi, P., Scarascia Mungnozza, G., Agati, G., Bazzani, M., De Angelis, P., Fusi, F., Matteucci, G., Raimondi, V., 1994. Remote sensing of chlorophyll *a* fluorescence of vegetation canopies: 2. Physiological significance of fluorescence signal in response to environmental stresses. Remote Sens. Environ. 47, 29–35.
Van de Hulst, H.C., 1957. Light Scattering by Small Particles. John Wiley & Sons, New York.
Van de Hulst, H.C., 1981. Light Scattering by Small Particles. Dover Publications, New York.
Van der Tol, C., Verhoef, W., Rosema, A., 2009a. A model for chlorophyll fluorescence and photosynthesis at leaf scale. Agric. For. Meteorol. 149, 96–105.
Van der Tol, C., Verhoef, W., Timmermans, J., Verhoef, A., Su, Z., 2009b. An integrated model of soil-canopy spectral radiances, photosynthesis, fluorescence, temperature and energy balance. Biogeosciences 6, 3109–3129.
Van der Tol, C., Berry, J.A., Campbell, P.K.E., Rascher, U., 2014. Models of fluorescence and photosynthesis for interpreting measurements of solar-induced chlorophyll fluorescence. J. Geophys. Res. Biogeosci. 119, 2312–2327.
Van der Tol, C., Rossini, M., Cogliati, S., Verhoef, W., Colombo, R., Rascher, U., Mohammed, G., 2016. A model and measurement comparison of diurnal cycles of sun-induced chlorophyll fluorescence of crops. Remote Sens. Environ. 186, 663–677.
Van Kooten, O., Snel, J.F.H., 1990. The use of chlorophyll fluorescence nomenclature in plant stress physiology. Photosynth. Res. 25, 147–150.
Van Wittenberghe, S., Alonso, L., Verrelst, J., Hermans, I., Delegido, J., Veroustraete, F., Valcke, R., Moreno, J., Samson, R., 2013. Upward and downward solar-induced chlorophyll fluorescence yield indices of four tree species as indicators of traffic pollution in Valencia. Environ. Pollut. 173, 29–37.
Van Wittenberghe, S., Alonso, L., Verrelst, J., Hermans, I., Valcke, R., Veroustraete, F., Moreno, J., Samson, R., 2014. A field study on solar-induced chlorophyll fluorescence and pigment parameters along a vertical canopy gradient of four tree species in an urban environment. Sci. Total Environ. 466-467, 185–194.
Van Wittenberghe, S., Alonso, L., Verrelst, J., Moreno, J., Samson, R., 2015. Bidirectional sun-induced chlorophyll fluorescence emission is influenced by leaf structure and light scattering properties – a bottom-up approach. Remote Sens. Environ. 158, 169–179.
Vasilkov, A., Joiner, J., Spurr, R., 2013. Note on rotational-Raman scattering in the O_2 A- and B-bands. Atmos. Meas. Tech. 6, 981–990.
Verhoef, W., 1984. Light scattering by leaf layers with application to canopy reflectance modeling: the SAIL model. Remote Sens. Environ. 16, 125–141.
Verhoef, W., 1985. Earth observation modeling based on layer scattering matrices. Remote Sens. Environ. 17, 165–178.
Verhoef, W., Van der Tol, C., Middleton, E.M., 2014. Vegetation canopy fluorescence and reflectance retrieval by model inversion using optimization. In: Proc. 5th International Workshop on Remote Sensing of Vegetation Fluorescence, 22–24 April 2014, Paris, France.
Verhoef, W., Van der Tol, C., Middleton, E.M., 2018. Hyperspectral radiative transfer modeling to explore the combined retrieval of biophysical parameters and canopy fluorescence from FLEX – Sentinel-3 tandem mission multi-sensor data. Remote Sens. Environ. 204, 942–963.
Verma, M., Schimel, D., Evans, B., Frankenberg, C., Beringer, J., Drewry, D.T., Magney, T., Marang, I., Hutley, L., Moore, C., Eldering, A., 2017. Effect of environmental conditions on the relationship between solar-induced fluorescence and gross primary productivity at an OzFlux grassland site. J. Geophys. Res. Biogeosci. 122, 716–733.
Verrelst, J., Rivera, J.P., 2017. A global sensitivity analysis toolbox to quantify drivers of vegetation radiative transfer models. In: Petropoulos, G., Srivastava, P. (Eds.), Sensitivity Analysis in Earth Observation Modelling. Elsevier, pp. 319–339.
Verrelst, J., Camps-Valls, G., Muñoz-Marí, J., Rivera, J.P., Veroustraete, F., Clevers, J.G.P.W., Moreno, J., 2015a. Optical remote sensing and the retrieval of terrestrial vegetation bio-geophysical properties – a review. ISPRS J. Photogramm. Remote Sens. 108, 273–290.
Verrelst, J., Rivera, J.P., Van der Tol, C., Magnani, F., Mohammed, G., Moreno, J., 2015b. Global sensitivity analysis of the SCOPE model: what drives simulated canopy-leaving sun-induced fluorescence? Remote Sens. Environ. 166, 8–21.
Verrelst, J., Van der Tol, C., Magnani, F., Sabater, N., Rivera, J.P., Mohammed, G., Moreno, J., 2016. Evaluating the predictive power of sun-induced chlorophyll fluorescence to estimate net photosynthesis of vegetation canopies: a SCOPE modeling study. Remote Sens. Environ. 176, 139–151.
Vicent, J., Sabater, N., Tenjo, C., Acarreta, J.R., Manzano, M., Rivera, J.P., Jurado, P., Franco, R., Alonso, L., Verrelst, J., Moreno, J., 2016. FLEX end-to-end mission performance simulator. IEEE Trans. Geosci. Remote Sens. 54, 4215–4223.
Vilfan, N., Van der Tol, C., Muller, O., Rascher, U., Verhoef, W., 2016. Fluspect-B: a model for leaf fluorescence, reflectance and transmittance spectra. Remote Sens. Environ. 186, 596–615.
Vilfan, N., Van der Tol, C., Yang, P., Wyber, R., Malenovský, Z., Robinson, S.A., Verhoef, W., 2018. Extending Fluspect to simulate xanthophyll driven leaf reflectance dynamics. Remote Sens. Environ. 211, 345–356.
Vogelmann, T.C., Evans, J.R., 2002. Profiles of light absorption and chlorophyll within spinach leaves from chlorophyll fluorescence. Plant Cell Environ. 25, 1313–1323.
Vogelmann, T.C., Bornman, J.F., Yates, D.J., 1996. Focusing of light by leaf epidermal cells. Physiol. Plant. 98, 43–56.
Von Hebel, C., Matveeva, M., Verweij, E., Rademske, P., Kaufmann, M.S., Brogi, C., Vereecken, H., Rascher, U., Van der Kruk, J., 2018. Understanding soil and plant interaction by combining ground-based quantitative electromagnetic induction and airborne hyperspectral data. Geophys. Res. Lett. 45, 7571–7579.
Wagle, P., Zhang, Y., Jin, C., Xiao, X., 2016. Comparison of solar-induced chlorophyll fluorescence, light-use efficiency, and process-based GPP models in maize. Ecol. Appl. 26, 1211–1222.
Walker, A.P., Quaife, T., Van Bodegom, P.M., De Kauwe, M.G., Keenan, T.F., Joiner, J., Lomas, M.R., MacBean, N., Xu, C., Yang, X., Woodward, F.I., 2017. The impact of alternative trait-scaling hypotheses for the maximum photosynthetic carboxylation rate (V_{cmax}) on global gross primary production. New Phytol. 215, 1370–1386.
Walther, S., Voigt, M., Thum, T., Gonsamo, A., Zhang, Y., Köhler, P., Jung, M., Varlagin, A., Guanter, L., 2016. Satellite chlorophyll fluorescence measurements reveal large-scale decoupling of photosynthesis and greenness dynamics in boreal evergreen forests. Glob. Chang. Biol. 22, 2979–2996.
Walther, S., Guanter, L., Heim, B., Jung, M., Duveiller, G., Wolanin, A., Sachs, T., 2018. Assessing the dynamics of vegetation productivity in circumpolar regions with different satellite indicators of greenness and photosynthesis. Biogeosciences 15, 6221–6255.
Wang, S., Huang, C., Zhang, L., Lin, Y., Cen, Y., Wu, T., 2016. Monitoring and assessing the 2012 drought in the Great Plains: analyzing satellite-retrieved solar-induced chlorophyll fluorescence, drought indices, and gross primary production. Remote Sens. 8, 61.
Wang, J., Xiao, X., Zhang, Y., Qin, Y., Doughty, R.B., Wu, X., Bajgain, R., Du, L., 2018. Enhanced gross primary production and evapotranspiration in juniper-encroached grasslands. Glob. Change Biol. 24, 5655–5667.
Watson, R.D., Hemphill, W.R., 1976. Use of an airborne Fraunhofer line discriminator for the detection of solar stimulated luminescence. In: U.S. Geological Survey Open-File

Report 76–202, pp. 109. https://doi.org/10.3133/ofr76202.
Wei, X., Wang, X., Wei, W., Wan, W., 2018. Use of sun-induced chlorophyll fluorescence obtained by OCO-2 and GOME-2 for GPP estimates of the Heihe River basin, China. Remote Sens. 10, 2039.
Weis, E., Berry, J.A., 1987. Quantum efficiency of photosystem II in relation to 'energy'-dependent quenching of chlorophyll fluorescence. Biochim. Biophys. Acta 894, 198–208.
Wieneke, S., Ahrends, H., Damm, A., Pinto, F., Stadler, A., Rossini, M., Rascher, U., 2016. Airborne based spectroscopy of red and far-red sun-induced chlorophyll fluorescence: implications for improved estimates of gross primary productivity. Remote Sens. Environ. 184, 654–667.
Wieneke, S., Burkart, A., Cendrero-Mateo, M.P., Julitta, T., Rossini, M., Schickling, A., Schmidt, M., Rascher, U., 2018. Linking photosynthesis and sun-induced fluorescence at sub-daily to seasonal scales. Remote Sens. Environ. 219, 247–258.
Wohlfahrt, G., Gerdel, K., Migliavacca, M., Rotenberg, E., Tatarinov, F., Müller, J., Hammerle, A., Julitta, T., Spielmann, F.M., Yakir, D., 2018. Sun-induced fluorescence and gross primary productivity during a heat wave. Sci. Rep. 8, 14169.
Wolanin, A., Rozanov, V.V., Dinter, T., Nöel, S., Vountas, M., Burrows, J.P., Bracher, A., 2015. Global retrieval of marine and terrestrial chlorophyll fluorescence at its red peak using hyperspectral top of atmosphere radiance measurements: feasibility study and first results. Remote Sens. Environ. 166, 243–261.
Wong, C.Y., Gamon, J.A., 2015. Three causes of variation in the photochemical reflectance index (PRI) in evergreen conifers. New Phytol. 206, 187–195.
Wood, J.D., Griffis, T.J., Baker, J.M., Frankenberg, C., Verma, M., Yuen, K., 2017. Multiscale analyses of solar-induced fluorescence and gross primary production. Geophys. Res. Lett. 44, 533–541.
Wu, X., Xiao, X., Zhang, Y., He, W., Wolf, S., Chen, J., He, M., Gough, C.M., Qin, Y., Zhou, Y., Doughty, R., Blanken, P.D., 2018. Spatiotemporal consistency of four gross primary production products and solar-induced chlorophyll fluorescence in response to climate extremes across CONUS in 2012. J. Geophys. Res. Biogeosci. 123. https://doi.org/10.1029/2018JG004484.
Wyber, R., Malenovský, Z., Ashcroft, M.B., Osmond, B., Robinson, S.A., 2017. Do daily and seasonal trends in leaf solar induced fluorescence reflect changes in photosynthesis, growth or light exposure? Remote Sens. 9, 604.
Xu, S., Liu, Z., Zhao, L., Zhao, H., Ren, S., 2018. Diurnal response of sun-induced fluorescence and PRI to water stress in maize using a near-surface remote sensing platform. Remote Sens. 10, 1510.
Yang, P., Van der Tol, C., 2018. Linking canopy scattering of far-red sun-induced chlorophyll fluorescence with reflectance. Remote Sens. Environ. 209, 456–467.
Yang, X., Tang, J., Mustard, J.F., Lee, J.-E., Rossini, M., Joiner, J., Munger, J.W., Kornfeld, A., Richardson, A.D., 2015. Solar-induced chlorophyll fluorescence that correlates with canopy photosynthesis on diurnal and seasonal scales in a temperate deciduous forest. Geophys. Res. Lett. 42, 2977–2987.
Yang, P., Verhoef, W., Van der Tol, C., 2017. The mSCOPE model: a simple adaptation to the SCOPE model to describe reflectance, fluorescence and photosynthesis of vertically heterogeneous canopies. Remote Sens. Environ. 201, 1–11.
Yang, J., Tian, H., Pan, S., Chen, G., Zhang, B., Dangal, S., 2018a. Amazon drought and forest response: largely reduced forest photosynthesis but slightly increased canopy greenness during the extreme drought of 2015/2016. Glob. Chang. Biol. 24, 1919–1934.
Yang, K., Ryu, Y., Dechant, B., Berry, J.A., Hwang, Y., Jiang, C., Kang, M., Kim, J., Kimm, H., Kornfeld, A., Yang, X., 2018b. Sun-induced chlorophyll fluorescence is more strongly related to absorbed light than to photosynthesis at half-hourly resolution in a rice paddy. Remote Sens. Environ. 216, 658–673.
Yang, X., Shi, H., Stovall, A., Guan, K., Miao, G., Zhang, Y., Zhang, Y., Xiao, X., Ryu, Y., Lee, J.-E., 2018c. FluoSpec 2—an automated field spectroscopy system to monitor canopy solar-induced fluorescence. Sensors 18, 2063.
Yang, P., Van der Tol, C., Verhoef, W., Damm, A., Schickling, A., Kraska, T., Muller, O., Rascher, U., 2019. Using reflectance to explain vegetation biochemical and structural effects on sun-induced chlorophyll fluorescence. Remote Sens. Environ. https://doi.org/10.1016/j.rse.2018.11.039. (In press).
Yoshida, Y., Joiner, J., Tucker, C., Berry, J., Lee, J.-E., Walker, G., Reichle, R., Koster, R., Lyapustin, A., Wang, Y., 2015. The 2010 Russian drought impact on satellite measurements of solar-induced chlorophyll fluorescence: insights from modeling and comparisons with parameters derived from satellite reflectances. Remote Sens. Environ. 166, 163–177.
Zaks, J., Amarnath, K., Kramer, D.M., Niyogi, K.K., Fleming, G.R., 2012. A kinetic model of rapidly reversible nonphotochemical quenching. Proc. Natl. Acad. Sci. U. S. A. 109, 15757–15762.
Zarco-Tejada, P.J., Miller, J.R., Mohammed, G.H., Noland, T.L., Sampson, P.H., 1999a. Canopy optical indices from infinite reflectance and canopy reflectance models for forest condition monitoring: Application to hyperspectral CASI data. In: Proc. IEEE International Geoscience and Remote Sensing Symposium (IGARSS), 28 June-2 July 1999, Hamburg, Germany. vol. 3. pp. 1878–1881.
Zarco-Tejada, P.J., Miller, J.R., Mohammed, G.H., Noland, T.L., Sampson, P.H., 1999b. Optical indices as bioindicators of forest condition from hyperspectral CASI data, in: Proceedings 19th EARSeL Symposium on Remote Sensing in the 21st Century, 31 May-2 June 1999, Valladolid, Spain.
Zarco-Tejada, P.J., Miller, J.R., Mohammed, G.H., Noland, T.L., 2000a. Chlorophyll fluorescence effects on vegetation apparent reflectance: I. Leaf-level measurements and model simulation. Remote Sens. Environ. 74, 582–595.
Zarco-Tejada, P.J., Miller, J.R., Mohammed, G.H., Noland, T.L., Sampson, P.H., 2000b. Chlorophyll fluorescence effects on vegetation apparent reflectance: II. Laboratory and airborne canopy-level measurements with hyperspectral data. Remote Sens. Environ. 74, 596–608.
Zarco-Tejada, P.J., Miller, J.R., Mohammed, G.H., Noland, T.L., Sampson, P.H., 2001. Estimation of chlorophyll fluorescence under natural illumination from hyperspectral data. Int. J. Appl. Earth Obs. Geoinf. (Special Issue on Applications of Imaging Spectroscopy) 3, 321–327.
Zarco-Tejada, P.J., Miller, J.R., Mohammed, G.H., Noland, T.L., Sampson, P.H., 2002. Vegetation stress detection through chlorophyll a + b estimation and fluorescence effects on hyperspectral imagery. J. Environ. Qual. 31, 1433–1441.
Zarco-Tejada, P.J., Pushnik, J.C., Dobrowski, S., Ustin, S.L., 2003. Steady-state chlorophyll *a* fluorescence detection from canopy derivative reflectance and *double-peak* red-edge effects. Remote Sens. Environ. 84, 283–294.
Zarco-Tejada, P.J., Miller, J.R., Pedrós, R., Verhoef, W., Berger, M., 2006. FluorMODgui V3.0: a graphic user interface for the spectral simulation of leaf and canopy chlorophyll fluorescence. Comput. Geosci. 32, 577–591.
Zarco-Tejada, P.J., Berni, J.A.J., Suárez, L., Sepulcre-Cantó, G., Morales, F., Miller, J.R., 2009. Imaging chlorophyll fluorescence with an airborne narrow-band multispectral camera for vegetation stress detection. Remote Sens. Environ. 113, 1262–1275.
Zarco-Tejada, P.J., González-Dugo, V., Berni, J.A.J., 2012. Fluorescence, temperature and narrow-band indices acquired from a UAV platform for water stress detection using a micro-hyperspectral imager and a thermal camera. Remote Sens. Environ. 117, 322–337.
Zarco-Tejada, P.J., Catalina, A., González, M.R., Martín, P., 2013a. Relationships between net photosynthesis and steady-state chlorophyll fluorescence retrieved from airborne hyperspectral imagery. Remote Sens. Environ. 136, 247–258.
Zarco-Tejada, P.J., Morales, A., Testi, L., Villalobos, F.J., 2013b. Spatio-temporal patterns of chlorophyll fluorescence and physiological and structural indices acquired from hyperspectral imagery as compared with carbon fluxes measured with eddy covariance. Remote Sens. Environ. 133, 102–115.
Zarco-Tejada, P.J., Camino, C., Beck, P.S.A., Calderon, R., Hornero, A., Hernández-Clemente, R., Kattenborn, T., Montes-Borrego, M., Susca, L., Morelli, M., Gonzalez-Dugo, V., North, P.R.J., Landa, B.B., Boscia, D., Saponari, M., Navas-Cortes, J.A., 2018. Previsual symptoms of *Xylella fastidiosa* infection revealed in spectral plant-trait alterations. Nat. Plants 4, 432–439.
Zhang, Y.J., Liu, L.Y., Hou, M.Y., Liu, L.T., Li, C.D., 2009. Progress in remote sensing of vegetation chlorophyll fluorescence. J. Remote Sens. 13, 963–978.
Zhang, Y., Guanter, L., Berry, J.A., Joiner, J., Van der Tol, C., Huete, A., Gitelson, A., Voigt, M., Köhler, P., 2014. Estimation of vegetation photosynthetic capacity from space-based measurements of chlorophyll fluorescence for terrestrial biosphere models. Glob. Chang. Biol. 20, 3727–3742.
Zhang, Y., Guanter, L., Berry, J.A., Van der Tol, C., Yang, X., Tang, J., Zhang, F., 2016a. Model-based analysis of the relationship between sun-induced chlorophyll fluorescence and gross primary production for remote sensing applications. Remote Sens. Environ. 187, 145–155.
Zhang, Y., Xiao, X., Guanter, L., Zhou, S., Ciais, P., Joiner, J., Sitch, S., Wu, X., Nabel, J., Dong, J., Kato, E., Jain, A.K., Wiltshire, A., Stocker, B.D., 2016b. Precipitation and carbon-water coupling jointly control the interannual variability of global land gross primary production. Sci. Rep. 6, 39748.
Zhang, Y., Xiao, X., Jin, C., Dong, J., Zhou, S., Wagle, P., Joiner, J., Guanter, L., Zhang, Y., Zhang, G., Qin, Y., Wang, J., Moore III, B., 2016c. Consistency between sun-induced chlorophyll fluorescence and gross primary production of vegetation in North America. Remote Sens. Environ. 183, 154–169.
Zhang, Y., Guanter, L., Joiner, J., Song, L., Guan, K., 2018a. Spatially-explicit monitoring of crop photosynthetic capacity through the use of space-based chlorophyll fluorescence data. Remote Sens. Environ. 210, 362–374.
Zhang, Y., Joiner, J., Alemohammad, S.H., Zhou, S., Gentine, P., 2018b. A global spatially continuous solar induced fluorescence (CSIF) dataset using neural networks. Biogeosciences 15, 5779–5800.
Zhang, Y., Joiner, J., Gentine, P., Zhou, S., 2018c. Reduced solar-induced chlorophyll fluorescence from GOME-2 during Amazon drought caused by dataset artifacts. Glob. Chang. Biol. 24. https://doi.org/10.1111/gcb.14134.
Zhang, Y., Xiao, X., Zhang, Y., Wolf, S., Zhou, S., Joiner, J., Guanter, L., Verma, M., Sun, Y., Yang, X., Paul-Limoges, E., Gough, C.M., Wohlfahrt, G., Gioli, B., Van der Tol, C., Yann, N., Lund, M., De Grandcourt, A., 2018d. On the relationship between sub-daily instantaneous and daily total gross primary production: implications for interpreting satellite-based SIF retrievals. Remote Sens. Environ. 205, 276–289.
Zhang, Z., Zhang, Y., Joiner, J., Migliavacca, M., 2018e. Angle matters: bidirectional effects impact the slope of relationship between gross primary productivity and sun-induced chlorophyll fluorescence from Orbiting Carbon Observatory-2 across biomes. Glob. Chang. Biol. 24, 5017–5020.
Zhao, F., Guo, Y., Verhoef, W., Gu, X., Liu, L., Yang, G., 2014. A method to reconstruct the solar-induced canopy fluorescence spectrum from hyperspectral measurements. Remote Sens. 6, 10171–10192.
Zhao, F., Dai, X., Verhoef, W., Guo, Y., Van der Tol, C., Li, Y., Huang, Y., 2016. FluorWPS: a Monte Carlo ray-tracing model to compute sun-induced chlorophyll fluorescence of three-dimensional canopy. Remote Sens. Environ. 187, 385–399.
Zhao, F., Li, R., Verhoef, W., Cogliati, S., Liu, X., Huang, Y., Guo, Y., Huang, J., 2018. Reconstruction of the full spectrum of solar-induced chlorophyll fluorescence: intercomparison study for a novel method. Remote Sens. Environ. 219, 233–246.

Zhou, X., Liu, Z., Xu, S., Zhang, W., Wu, J., 2016. An automated comparative observation system for sun-induced chlorophyll fluorescence of vegetation canopies. Sensors 16, 775.

Zoogman, P., Liu, X., Suleiman, R.M., Pennington, W.F., Flittner, D.E., Al-Saadi, J.A., Hilton, B.B., Nicks, D.K., Newchurch, M.J., Carr, J.L., Janz, S.J., Andraschko, M.R., Arola, A., Baker, B.D., Canova, B.P., Miller, C.C., Cohen, R.C., Davis, J.E., Dussault, M.E., Edwards, D.P., Fishman, J., Ghulam, A., González Abad, G., Grutter, M., Herman, J.R., Houck, J., Jacob, D.J., Joiner, J., Kerridge, B.J., Kim, J., Krotkov, N.A., Lamsal, L., Li, C., Lindfors, A., Martin, R.V., McElroy, C.T., McLinden, C., Natraj, V., Neil, D.O., Nowlan, C.R., O'Sullivan, E.J., Palmer, P.I., Pierce, R.B., Pippin, M.R., Saiz-Lopez, A., Spurr, R.J.D., Szykman, J.J., Torres, O., Veefkind, J.P., Veihelmann, B., Wang, H., Wang, J., Chance, K., 2016. Tropospheric emissions: monitoring of pollution (TEMPO). J. Quant. Spectrosc. Radiat. Transf. 186, 17–39.

Zuromski, L.M., Bowling, D.R., Köhler, P., Frankenberg, C., Goulden, M.L., Blanken, P.D., Lin, J.C., 2018. Solar-induced fluorescence detects interannual variation in gross primary production of coniferous forests in the western United States. Geophys. Res. Lett. 45, 7184–7193.